ASCE

Liquefaction Susceptibility and Cyclic Response of Intact Nonplastic and Plastic Silts

Armin W. Stuedlein, M.ASCE[1]; Ali Dadashiserej[2]; Amalesh Jana, M.ASCE[3]; and T. Matthew Evans, M.ASCE[4]

Abstract: This study presents the results of a laboratory test program that serves to improve the understanding of the liquefaction susceptibility and cyclic response of intact silts that span sand- and clay-like behaviors. Specimens were prepared from samples characterized with a plasticity index (PI) ranging from 0 to 39, fines content (FC) ranging from 29% to 100%, and overconsolidation ratio (OCR) ranging from 1.0 to 4.2, retrieved from five silt deposits in Western Oregon and Southwest Washington. The roles of PI, FC, and OCR on the 1D compression and monotonic and cyclic strength of nonplastic to plastic silts are identified. Hysteretic metrics proposed to quantify cyclic behavior provided an objective means to distinguish between qualitative judgments of sand-like, intermediate, and clay-like behavior. Prior soil index test-based liquefaction susceptibility criteria exhibited good to poor accuracy; modifications to existing criteria aligned with quantified hysteretic behavior, which together indicate that sand- and clay-like behavior is subject to the intensity and duration of cyclic loading. The variation of cyclic resistance ratio (CRR) and cyclic strength ratio, $\tau_{cyc}/s_{u,DSS}$, with the number of loading cycles, N, to reach single amplitude shear strain, γ, of 3% and 3.75% is presented. The $\tau_{cyc}/s_{u,DSS}$ for $N_{\gamma=3\%} = 10$ and 30 appeared constant for PI $\leq$ 11 and PI $\geq$ 18 and equal to 0.63 and 0.54, and 0.82 and 0.76, respectively, with an apparent linear trend for 11 < PI < 18. Despite higher void ratios, intact overconsolidated specimens exhibited greater CRR than their mechanically normally consolidated counterparts, highlighting the effects of OCR and natural soil fabric on cyclic resistance. Cyclic tests conducted on specimens consolidated using a quasi-stress history and normalized soil engineering properties (SHANSEP) method exhibited larger CRR than those tested using the recompression method, which is attributed to the smaller void ratios and potentially greater lateral stresses. The recompression technique is preferred for establishing the cyclic response to capture in-situ conditions when testing high-quality samples and where quantification of the preconsolidation stress is uncertain.
DOI: 10.1061/(ASCE)GT.1943-5606.0002935.

Introduction

Understanding of liquefaction triggering of coarse-grained, granular soils, and the corresponding consequences has been dramatically improved over the past decade. However, understanding of the liquefaction susceptibility, triggering, and resulting consequences of low and medium plasticity silt soils remains poor in comparison (Dahl et al. 2018). Many natural fine-grained soil deposits with characteristics intermediate to those associated with sands and clays, termed "transitional soils" (i.e., sandy silt, clayey sand, silt, and clayey silt), are prevalent in earthquake-prone areas (e.g., China: Haicheng 1975, Tangshen 1976; Turkey: Kocaeli 1999; New Zealand: Canterbury Earthquake Sequence 2010–2011) and do not fit neatly into the binary sand-like and clay-like paradigm (Boulanger and Idriss 2004; Erken and Ulker 2007; Idriss and Boulanger 2008; Kaya and Erken 2015). For example, under sufficient cyclic shear stresses and loading cycles, sand-like soils may generate an excess pore pressure ratio, r_u, nearly or equal to 100% associated with narrow stress-strain hysteresis and transient zero or near-zero shear stiffness. In contrast, clay-like soils exhibit broad stress-strain hysteresis with transient, nonzero shear stiffness and limited r_u. Intermediate soils exhibit hysteretic behaviors that lie between those of sand- and clay-like soils; however, clear quantitative means to distinguish between these behaviors continue to be elusive.

Several studies have demonstrated the importance of soil fabric (Wijewickreme et al. 2019; Jana and Stuedlein 2021), stress history (Dahl et al. 2014, 2018; Jana and Stuedlein 2021), fines content (Hazirbaba and Rathje 2009; Polito and Sibley 2020), mineralogy (Sanin and Wijewickreme 2006), and the depositional environment (Beyzaei et al. 2018, 2020) contributing to cyclic resistance of silt soils. Dahl et al. (2018) compiled the results of monotonic and cyclic test data for intact, intermediate soils to establish trends in their response with respect to plasticity index (PI), fines content (FC), and overconsolidation ratio (OCR). However, there remains uncertainty in the variation of cyclic resistance and hysteretic behavior (e.g., sand-like versus clay-like) with stress history and soil indices. Various index-based liquefaction susceptibility criteria for fine-grained soils have been proposed based on information from case histories where earthquakes have occurred (Bray et al. 2004; Cubrinovski et al. 2012). For example, the criteria proposed by Bray and Sancio (2006) suggests that the liquid limit (LL), PI, and natural water content, w_n, can be used to screen for liquefaction susceptibility. The criterion proposed by Boulanger and Idriss (2006) focuses solely on PI to identify engineering procedures

[1]Professor, School of Civil and Construction Engineering, Oregon State Univ., 101 Kearney Hall, Corvallis, OR 97331 (corresponding author). ORCID: https://orcid.org/0000-0002-6265-9906. Email: armin.stuedlein@oregonstate.edu

[2]Graduate Research Assistant, School of Civil and Construction Engineering, Oregon State Univ., 101 Kearney Hall, Corvallis, OR 97331.

[3]Postdoctoral Researcher, School of Civil and Construction Engineering, Oregon State Univ., 101 Kearney Hall, Corvallis, OR 97331.

[4]Professor, School of Civil and Construction Engineering, Oregon State Univ., 101 Kearney Hall, Corvallis, OR 97331. ORCID: https://orcid.org/0000-0002-8457-7602

Note. This manuscript was submitted on February 7, 2022; approved on August 22, 2022; published online on November 15, 2022. Discussion period open until April 15, 2023; separate discussions must be submitted for individual papers. This paper is part of the ***Journal of Geotechnical and Geoenvironmental Engineering***, © ASCE, ISSN 1090-0241.

for assessing anticipated cyclic resistance. In many cases, engineering judgment is required to interpret the differences between the observed and predicted responses of silty soils (Bray and Sancio 2006; Beyzaei et al. 2018, 2020).

The primary objective of the present study is to improve the understanding of the factors governing the cyclic response of intact transitional silty soils from five different sites in Western Oregon and Southwest Washington, located adjacent to the Columbia and Willamette rivers. The cyclic response of these silt deposits was investigated through a systematic laboratory testing program, including evaluation of index properties, specimen quality, compressibility, and monotonic and cyclic responses using monotonic direct simple shear (DSS) and cyclic DSS tests. The results of this study present a comprehensive database that aims to answer pertinent and outstanding questions concerning the cyclic response of transitional soils.

Sites and Subsurface Conditions

Laboratory tests were undertaken on intact specimens prepared from thin-walled tube samples obtained from five different test sites (i.e., A, B, D, E, and F), as summarized in Table 1. Laboratory tests for Site C are presently ongoing. Test Site A consists of dynamic, in-situ testing panels UT and BL (i.e., A-UT and A-BL) investigated by Dadashiserej et al. (2022a) and Jana et al. (2022), respectively; the remainder of the test sites were investigated using boreholes for thin-walled tube sampling (e.g., B-13, B-14, and F-1). Intact samples were recovered in accordance with ASTM D1587 (ASTM 2015) using mud-rotary boreholes, Osterberg piston samplers, and specially fabricated thin-walled stainless steel Shelby tubes with machine-beveled cutting edges similar to that described by Wijewickreme et al. (2019). To prevent moisture loss during the transportation and storage, expandable packers, plastic caps, sealing tape, and plastic wrap were used to seal the tubes. The recovered Shelby tubes were padded and transported in an upright condition to the OSU Geotechnical Laboratory and stored upright in a climate-controlled moist room until extrusion and specimen preparation [ASTM D4220 (ASTM 2014)]. Prior to extrusion, Shelby tubes were cut into two to three sections using a four-wheel pipe cutter to minimize the travel distance of the soil within each tube and the corresponding disturbance. Laboratory tests generally begun within one week of drilling and completed within two to four weeks of retrieval.

Subsurface conditions for each of the sites, including the corrected cone tip resistance, q_t, soil behavior type index, I_c, Atterberg limits, natural moisture content, w_n, small strain shear wave velocity, V_s, OCR, and normalized undrained shear strength, $s_{u,\mathrm{DSS}}/\sigma'_{vc}$, are shown in Figs. S1–S6 of Appendix S1. The samples tested from these five sites are generally classified as nonplastic silt (ML), low-plasticity silt (ML) to clay (CL), and high plasticity silt (MH) per the Unified Soil Classification System, with PI ranging from 0 to 39 [Table 1; Fig. 1(a)]. The results of grain size distribution test indicate that the average fines, silt, and clay contents range from 35% to 97%, 54% to 83%, and 12% to 17%, respectively [Fig. 1(b)]. The lower limit of potentially liquefiable soils proposed by Tsuchida (1970) is also shown in Fig. 1(b) for reference; many specimens with particle sizes that exceed this limit are shown to exhibit sand-like behavior under sufficient cyclic loading (i.e., cyclic shear stress and number of loading cycles) in the results that follow. Fig. 1(b) reports the test site and borehole or test panel from which the samples have been retrieved (e.g., Site A-UT represents a sample retrieved from the UT Test Panel of Site A).

The intact soil samples retrieved from each test site were initially interpreted within the practice-oriented liquefaction susceptibility framework suggested by Armstrong and Malvick (2016). Fig. 1(c) indicates that the majority of intact specimens tested from Site F are deemed susceptible to liquefaction, whereas cyclic softening evaluation (i.e., laboratory testing) is suggested for the specimens tested from Sites A, B, D, and E. Details regarding the qualitative and quantitative assessment of hysteretic soil behavior (i.e., sand-like, clay-like, and intermediate responses) and susceptibility to liquefaction and cyclic softening failure are further explored in this paper.

Experimental Test Procedures and Program

The laboratory testing program consisted of the assessment of intact sample quality, evaluation of stress history and compressibility, constant-volume, monotonic DSS strength, and cyclic resistance. All laboratory tests were conducted on intact specimens at nearly saturated ($S > 99.5\%$) and fully saturated conditions, as inferred from compression wave velocities, $V_p > 700$ m/s (Stokoe and Santamarina 2000; Stokoe et al. 2016) and gravimetric water contents. The test designations in Tables S1–S6 (see Appendix S1) indicate the test site, borehole, or test panel from which each sample has been retrieved and the test type or test number conducted. For example, Test A-UT-CRS indicates that a constant-rate-of-strain (CRS) consolidation test has been conducted on a specimen prepared from a sample retrieved from the UT Test Panel of Site A.

Constant-Rate-of-Strain Consolidation Tests

Representative intact specimens were subjected to CRS tests with measurement of excess pore pressure, u_e, and without using

Table 1. Details of test sites and material characterization

Description	Site ID				
	A	B	D	E	F
Location	Columbia River Longview,WA	Willamette River Corvallis,OR	Columbia River Portland,OR	Columbia River Portland,OR	Willamette River Wilsonville,OR
Depth of groundwater table (m)	1.5	2.4	7.3	3.0	7.4
Range in sample depth (m)	2.4–3.2	2.4–9.3	9.1–11.2	7.3–12.0	6.2–10.1
Natural water content, w_n (%)	44–59	38–62	75	39–92	28–43
Liquid limit, LL (%)	39–51	39–48	70	38–81	28–50
Plasticity index, PI (%)	10–19	11–16	14–39	10–28	0–20
Vertical effective consolidation stress, σ'_{vc}	32–36	50–160	98–112	95–215	150–160
Overconsolidation ratio, OCR	3.0–4.2	1.4–2.0	1.6–2.2	1.0–2.2	1.0–2.7
Number of stress-controlled cyclic tests	8	11	16	31	22

J. Geotech. Geoenviron. Eng., 2023, 149(1): 04022125

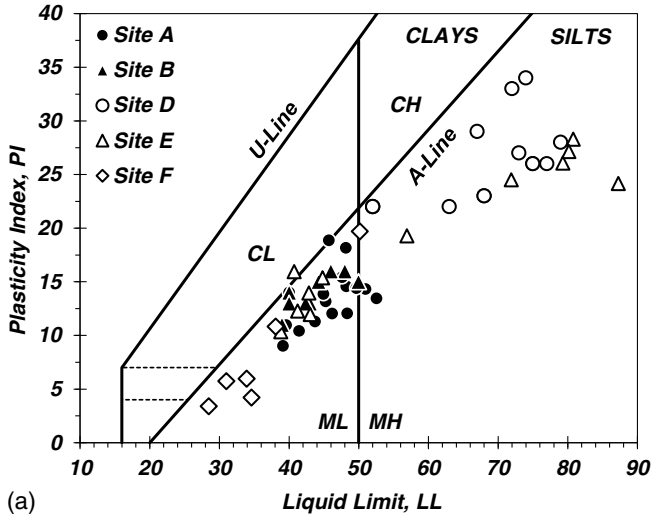

(a)

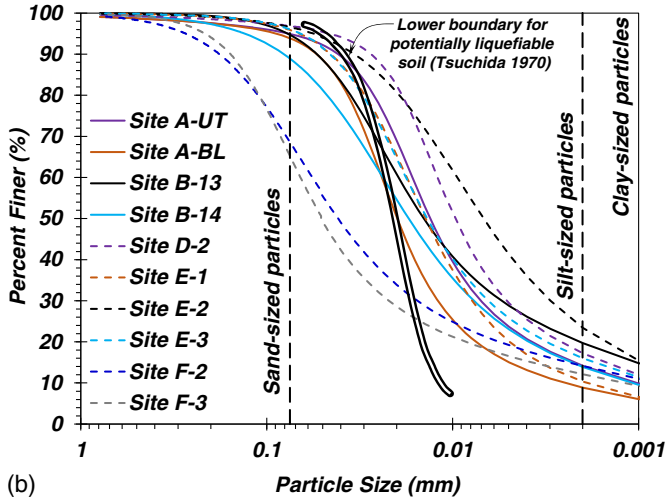

(b)

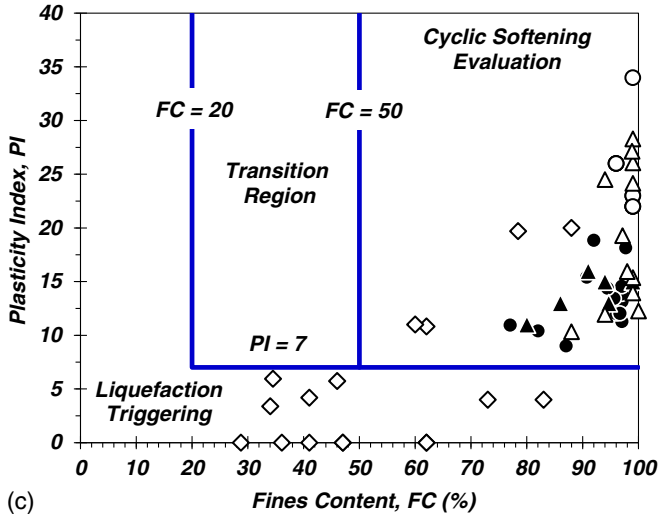

(c)

Fig. 1. Characterization of retrieved intact samples: (a) plasticity chart (nonplastic specimens omitted); (b) grain size distributions; and (c) set within the framework for assessing cyclic response [according to Armstrong and Malvick (2016)].

backpressure saturation, as described by Landon et al. (2018), to establish the preconsolidation stress, σ'_p, overconsolidation ratio, OCR, and the compression and recompression indices, C_c and C_r, respectively. Specimens were subjected to a strain rate of 0.45%–0.75%/h, selected based on soil characteristics (e.g., PI) such that the u_e measured at the base of specimens did not exceed 15% during or at the end of one-dimensional loading in accordance with ASTM D4186 (ASTM 2012).

Constant-Volume Monotonic Direct Simple Shear Tests

Constant-volume monotonic and cyclic DSS tests were performed using the SSH-100 cyclic DSS device manufactured by GCTS (Tempe, Arizona) with loading platens retrofitted to accommodate bender element (BE) and piezoelectric disc (PD) transducers, described in detail in by Dadashiserej et al. (2022b). Monotonic DSS specimens were consolidated using two approaches: (1) consolidation under vertical effective consolidation stresses, σ'_{vc}, equal to the in-situ vertical effective stress, σ'_{v0}, using the recompression technique (Bjerrum and Landva 1966) and which are intended to best represent in-situ conditions; and (2) the stress history and normalized soil engineering properties (SHANSEP) consolidation technique, where σ'_p is exceeded by a large margin followed by unloading to the desired σ'_{vc} (Ladd 1991). The recompression technique is preferred for high-quality specimens for which determination of σ'_p may be uncertain due to low plasticity and when the strength associated with in-situ conditions is desired (Ladd and DeGroot 2004; Grozic et al. 2003, 2005; Boone 2010; Dahl et al. 2018; Dadashiserej et al. 2022a, b). A second set of monotonic tests with different OCRs developed using the SHANSEP consolidation technique were conducted on representative intact specimens from selected sites to develop SHANSEP parameters (Ladd 1991). At the end of recompression or primary consolidation and unloading (i.e., SHANSEP), σ'_{vc} was maintained at least 10 times longer than that required for consolidation to complete one cycle of secondary compression, followed by constant-volume shearing with a strain rate of 5%/h.

Constant-Volume, Stress-Controlled Cyclic Direct Simple Shear Tests

Constant-volume, stress-controlled cyclic DSS tests were generally conducted on intact specimens consolidated under the estimated σ'_{v0} using the recompression technique. Additional cyclic DSS tests were performed on mechanically induced, normally consolidated (MC-NC; σ'_p exceeded) and quasi-SHANSEP, mechanically induced overconsolidated (MC-OC; σ'_{vc} approached or equaled σ'_p, followed by unloading) specimens to investigate the effect of stress history and consolidation technique on cyclic resistance. After completion of the consolidation and secondary compression phases, body wave velocities V_p and V_s were measured when possible, and the specimen was subjected to uniform sinusoidal horizontal cyclic shear stress cycles, τ_{cyc}, with a maximum amplitude specified in terms of the cyclic stress ratio, CSR $= \tau_{cyc}/\sigma'_{vc}$, and loading frequency of 0.1 Hz to generate a minimum single amplitude shear strain, γ, of 3.75%.

Experimental Test Results and Discussion

Constant-Rate-of-Strain Consolidation Tests

Fig. 2 presents the typical 1D compression responses of intact specimens from the sites investigated. Specimens with higher PI exhibit well-defined σ'_p and greater compressibility compared to the rounded compression responses of low PI specimens, consistent with observations by Boone (2010). For example, Specimen D-2-CRS with PI = 26 [Fig. 2(b)] exhibited a compression index of $C_c = 1.110$ compared to $C_c = 0.276$ for Specimen E-1-CRS with

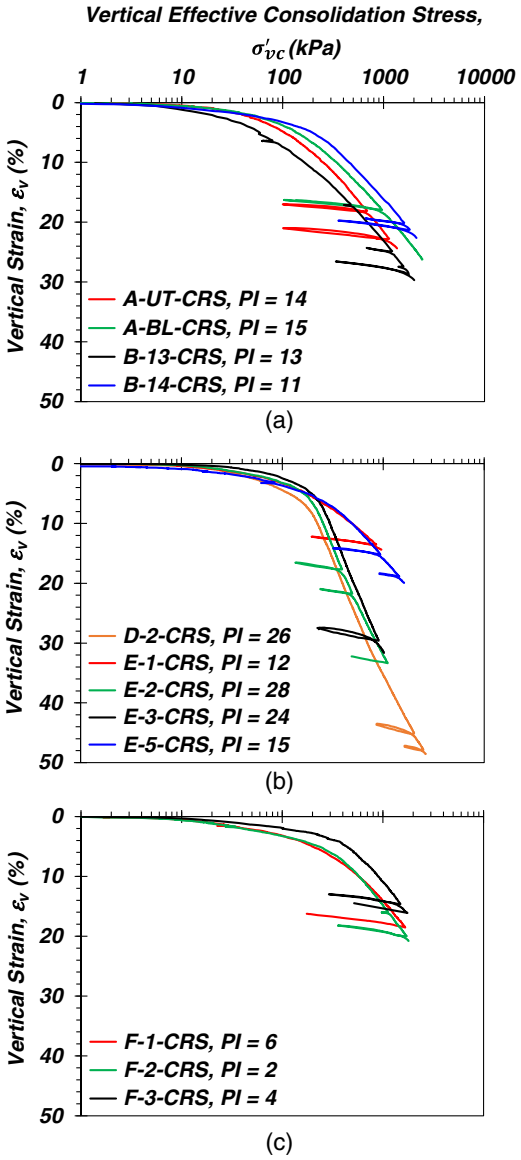

Fig. 2. One-dimensional compression response under constant-rate-of-strain (CRS) consolidation tests conducted on intact specimens from: (a) Sites A and B; (b) Sites D and E; and (c) Site F.

PI = 11. Multiple unloading–reloading cycles were conducted to quantify the recompression index, C_r. The σ'_p was determined using the average of the Casagrande construction (Casagrande 1936) and work-energy based methods (Becker et al. 1987; Wang and Frost 2004). The average σ'_p ranges from 95 kPa (i.e., Specimen B-13-CRS) to 427 kPa (i.e., F-3-CRS), and the CRS test results are summarized in Table S1. Given the range in sampling depths and corresponding σ'_{v0}, the intact soils comprising the experimental data set range from lightly overconsolidated (OCR < 2; Site B) to moderately overconsolidated (OCR < 4.2; Site A).

Specimen quality was assessed using the work- and strain-energy based criteria proposed by DeJong et al. (2018) for low plasticity soil. Based on this framework, the ratio of initial recompression index, C_{ri} ($= \Delta e/\Delta \log \sigma'_v$) to C_c, C_{ri}/C_c, and ratio of strain work-based recompression index, C_{rw} ($= \Delta W/\Delta \sigma'_v$), to work-based compression index, C_{rw}/C_{cw}, were calculated for each CRS specimen (Table S1). Specimens with compression ratios smaller than 0.15 are considered high-quality, whereas those falling between 0.15 and 0.40 are considered of moderate quality (DeJong et al. 2018). The C_{ri}/C_c and C_{rw}/C_{cw} ratios indicate specimens of high quality and moderate to high quality, respectively, with only two of 12 specimens exhibiting $C_{rw}/C_{cw} > 0.2$.

Constant-Volume, Monotonic Direct Simple Shear Tests

Fig. 3 presents the monotonic DSS response for selected intact, OC, and MC-NC and MC-OC silt specimens in terms of normalized shear stress-shear strain ($\tau_h/\sigma'_{vc} - \gamma$) curves and effective stress paths. Fig. 3 indicates that the specimens from Site B exhibit nearly perfectly plastic response, whereas specimens from Sites D-2, E-1, and E-3 exhibit strain hardening. Specimens with $1.5 \leq$ OCR ≤ 2.2 (except B-13-M1), exhibited similar responses up to $\gamma = 2\%$, after which they continued to show notable differences, depending on their PI. For example, Specimen E-1-M1 with PI = 12 exhibited dilative behavior at failure, compared to the contractive behavior of specimens from Sites D and E-3 with $21 \leq$ PI ≤ 33. Specimens with OCR ≤ 2.2 generally exhibit contractive behavior for the entirety of the prefailure stress path [Figs. 3(b, e, h, and k)], whereas specimens with larger OCR initially exhibit dilative tendencies followed by contraction in the pre-failure regime (except Specimen E-1-M4). The $s_{u,\mathrm{DSS}}$ was defined as the shear stress corresponding to $\gamma = 15\%$ (Table S2). Figs. 3(c, f, i, and l) present the variation of $s_{u,\mathrm{DSS}}/\sigma'_{vc}$ with OCR for Sites B, D, and E specimens; the corresponding SHANSEP parameters (i.e., S and m) indicate some variability from site to site and are consistent with Ladd (1991).

The $s_{u,\mathrm{DSS}}/\sigma'_{vc}$ appears to be insensitive to PI over the range of 0 to 28 (corresponding to the monotonic DSS test specimens), which exhibit an average $s_{u,\mathrm{DSS}}/\sigma'_{vc}$ of 0.42 and 0.64 for $1 \leq$ OCR ≤ 2, and $2 <$ OCR ≤ 4.2, respectively. The lack of trend of $s_{u,\mathrm{DSS}}/\sigma'_{vc}$ with PI occurs in part due to the strong positive correlation of e with PI, which stems from the larger aspect ratios of clay particles that increases with clay mineral activity. Low-PI silts will include a greater amount of nonplastic silts and sands (Fig. 1), which exhibit improved packing (Simpson and Evans 2016). Thus, for a given OCR, the increased $s_{u,\mathrm{DSS}}/\sigma'_{vc}$ expected for higher PI soils is offset by the decrease in $s_{u,\mathrm{DSS}}/\sigma'_{vc}$ associated with larger e. The variation of $s_{u,\mathrm{DSS}}/\sigma'_{vc}$ with PI and OCR exhibited by the specimens in this study appears to confirm observations by Dahl et al. (2018) corresponding to intact silty soils with $1 \leq$ PI ≤ 45, $27\% \leq$ FC $\leq 100\%$, and $1 \leq$ OCR ≤ 4.

Constant-Volume, Stress-Controlled Cyclic Direct Simple Shear Tests

Factors Affecting Cyclic Responses and Hysteretic Behavior

The cyclic testing program described herein serves to form the basis for establishing key trends among soil indices, stress history, and loading amplitude and duration to improve the understanding of cyclic resistance of transitional soils. Fig. 4 presents examples of the cyclic response of intact specimens from Sites B, D, E, and F in terms of the normalized shear stress-shear strain, CSR $- \gamma$, hysteresis, effective stress paths, and the accumulation of γ and u_e via the excess pore pressure ratio, r_u with number of loading cycles, N. Note that in these cyclic DSS tests the magnitude of r_u is related to the decrease in vertical effective stress, σ'_v (Dyvik et al. 1987): $r_u = 1 - \sigma'_v/\sigma'_{vc}$. The residual excess pore pressure, $r_{u,r}$ is defined herein as the r_u at the end of a given cycle, whereas $r_{u,\max}$ is the maximum r_u within any given cycle.

Specimen B-14-8 (PI = 13, OCR = 1.5, FC = 81%) was cyclically sheared under $\sigma'_{vc} = \sigma'_{v0} = 160$ kPa and CSR = 0.24, which

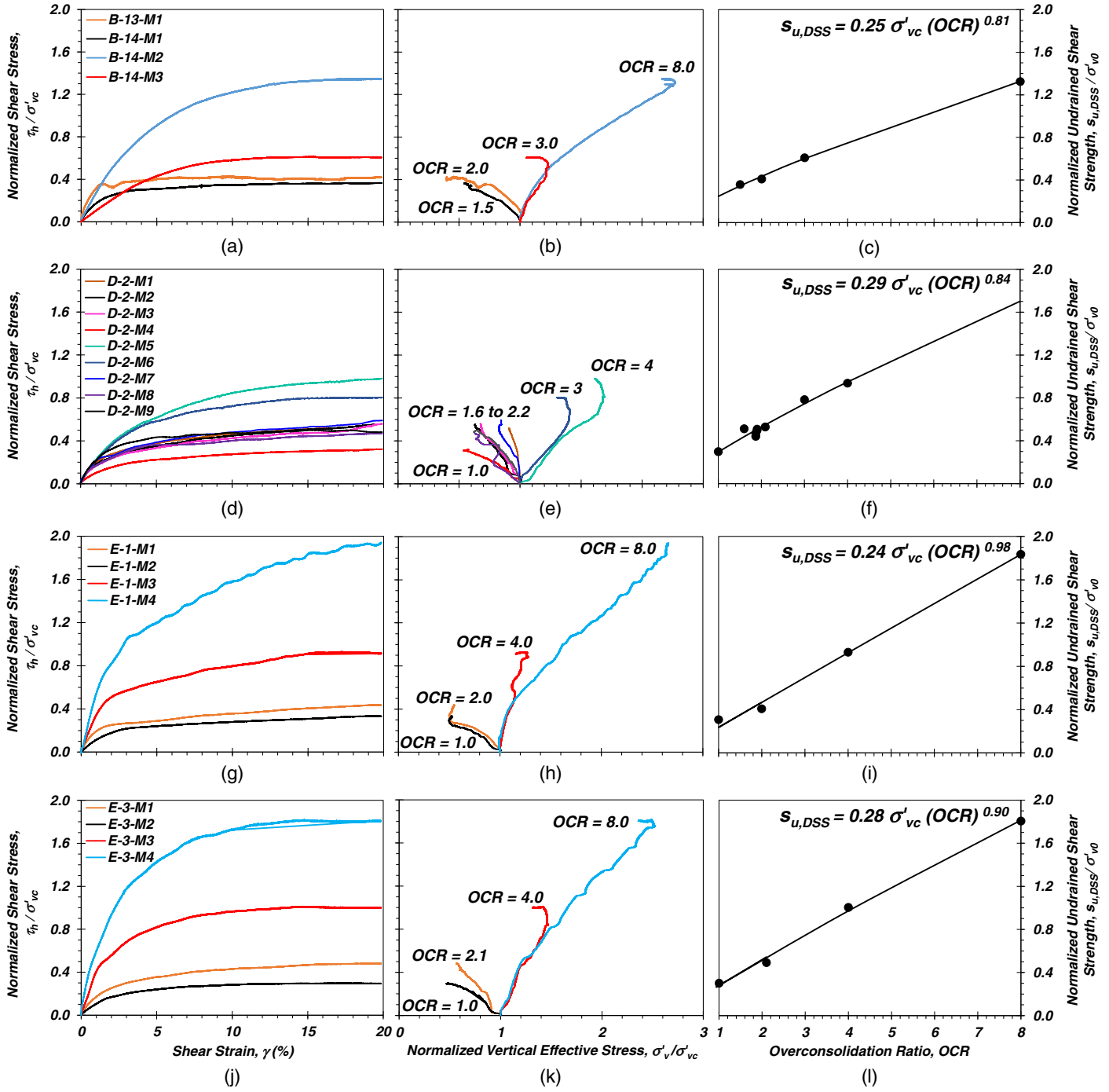

Fig. 3. Monotonic undrained DSS response of intact specimens of silt, indicating (a, d, g, and j) normalized shear stress-shear strain responses; (b, e, h, and k) effective stress paths; and (c, f, i, and l) SHANSEP representation of undrained shear strength: (a–c) Site B; (d–f) Site D; and (g–l) Site E.

resulted in $\gamma = 3\%$ and 3.75% at 22.2 and 26.2 cycles, respectively [i.e., $N_{\gamma=3\%} = 22.2$, Fig. 4(a), Table S3; $N_{\gamma=3.75\%} = 26.2$, Table S4]. The corresponding $r_{u,r}$ is about 15% for $N = 1$, 64% for $N = 22.2$ (i.e., $\gamma = 3\%$), with $r_{u,\max} \approx 96\%$ for the last cycle, $N_{\max} = 38$. The effective stress path [Fig. 4(b)] indicates cyclic mobility characterized by the incremental accumulation of γ [Fig. 4(c)], generation of u_e, and degradation of shear stiffness with transient, zero, or low shear stiffness [Fig. 4(a)] without an abrupt loss of strength (Castro and Poulos 1977; Boulanger et al. 1998; Sanin and Wijewickreme 2006; Price et al. 2017). Specimen F-2-5 (PI = 0, OCR = 2.4, FC = 36%) was subjected to CSR = 0.22 to result in $N_{\gamma=3\%} = 4.2$ [Fig. 4(e)] with corresponding $r_{u,r} = 65\%$ and $r_{u,\max} = 98\%$ [$N_{\max} = 11$; Fig. 4(h)], and exhibited a similar hysteretic response as B-14-8. It is notable that the hysteretic behavior of these two specimens display increasing sand-like behavior, characterized by inverted S-shaped loops (Wijewickreme et al. 2005; Boulanger and Idriss 2006), as N increases following exceedance of the commonly used cyclic strain failure criterion of $\gamma = 3\%$. Comparison of the cyclic response of Specimens B-14-8 and F-2-5 in terms of $N_{\gamma=3\%}$ [Figs. 4(a and e)] indicates that, although

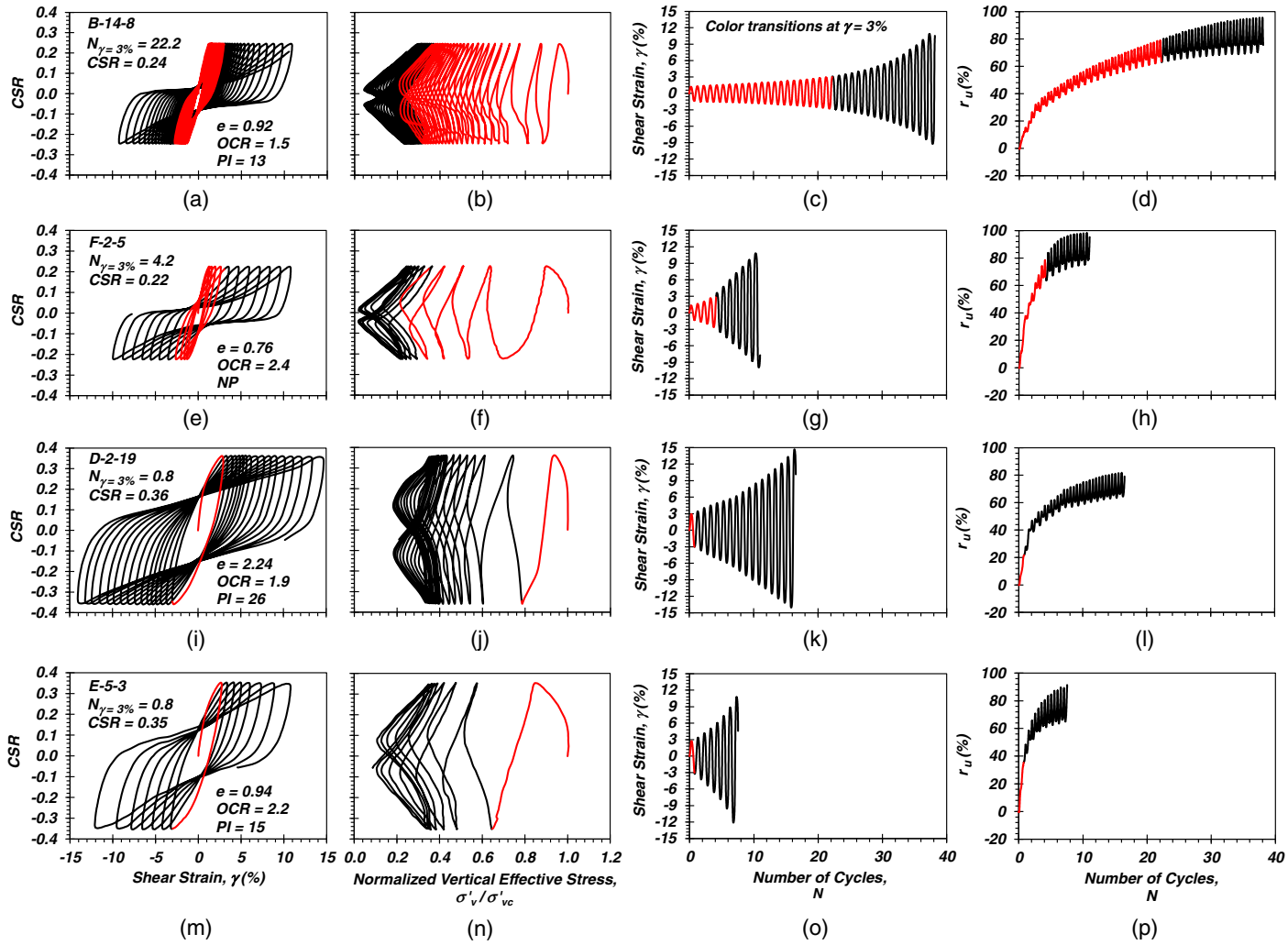

Fig. 4. Constant-volume, stress-controlled, cyclic response of intact specimens, indicating (a, e, i, and m) cyclic shear stress-shear strain, CSR–γ, hysteresis; (b, f, j, and n) effective stress path; (c, g, k, and o) accumulation of shear strain, γ, with number of loading cycles, N; and (d, h, l, and p) generation of excess pore pressure, r_u, with N: (a–d) Specimen B-14-8; (e–h) Specimen F-2-5; (i–l) Specimen D-2-19; and (m–p) Specimen E-5-3.

Specimen B-14-8 was subjected to higher CSR, it resulted in larger $N_{\gamma=3\%}$. The larger cyclic resistance can be attributed to its larger PI, which overshadowed the effects of lower OCR and density. Furthermore, depending on the liquefaction susceptibility criteria used, Specimen B-14-8 may not be considered susceptible to liquefaction (Boulanger and Idriss 2006: clay-like; Bray and Sancio 2006: moderately susceptible). Considering the Cascadia subduction zone (CSZ) capable of moment magnitude, $M_w \geq 8$ earthquakes (Goldfinger et al. 2012), $N \geq 38$ is reasonably expected for the soils at each of the study sites (described below), suggesting that the distinction between sand- and clay-like behavior may be subject to earthquake magnitude (i.e., duration of loading or N) and the corresponding magnitudes of γ and r_u.

Figs. 4(i–l) present the cyclic response of Specimen D-2-19 (PI = 26, OCR = 1.9, $e = 2.24$), consolidated under $\sigma'_{vc} =$ 119 kPa and loaded with $CSR = 0.36$ to result in $N_{\gamma=3\%} = 0.8$. Cyclic loading resulted in a progressive increase in u_e until reaching a limiting $r_{u,\max} = 83\%$ at large γ. The high PI Specimen D-2-19 developed broad hysteresis loops indicative of high dissipated strain energy (i.e., clay-like behavior) and without the transient, near-zero shear stiffness observed for the lower PI specimens. Specimens D-2-19 and E-5-3 (PI = 15, OCR = 2.2, $e = 0.94$) subjected to similar CSRs exhibit identical cyclic resistance interpreted in terms of $N_{\gamma=3\%}$ [Figs. 4(i and m)]. Given the similarity in stress history of these two specimens, the increase in cyclic resistance due to increased density appears to have been offset by decreased plasticity. Moreover, the effect of intensity of loading on the cyclic response of low- to medium-plasticity silt can be identified by the comparison of Specimens B-14-8 and E-5-3 [Figs. 4(a and m)], which have comparable PI, and e, with somewhat different OCR. For the same frequency of loading, Specimen B-14-8 subjected to the lower CSR = 0.24 exhibited a more sand-like cyclic mobility response compared to Specimen E-5-3 subjected to the larger CSR = 0.35. This observation can be attributed to the larger $r_{u,\max} = 96\%$ developed by Specimen B-14-8 compared to E-5-3 ($r_{u,\max} = 91\%$), suggesting that the intensity and duration of loading can be considered key factors, and that the maximum γ and corresponding $r_{u,\max}$ may play a role in whether the hysteretic response exhibits sand- or clay-like behavior. Tables S3 and S4 summarize the details of each intact specimen in the cyclic test program and results interpreted based on $N_{\gamma=3\%}$ and $N_{\gamma=3.75\%}$, respectively.

Hysteretic Soil Behavior: Sand-Like, Clay-Like, or Intermediate Behavior?

Identifying the hysteretic behavior of fine-grained soils in terms of sand-like, clay-like, and intermediate behavior is important for establishing the potential for transient loss of shear stiffness and strength during seismic loading. However, these assessments have often been made somewhat subjectively. Fig. 5(a) compares a single cycle of loading corresponding to a double-amplitude cyclic axial strain of approximately 5% (equivalent to a single-amplitude $\gamma = 3.75\%$) from cyclic triaxial tests conducted on reconstituted, normally consolidated mixtures of silts with varying PIs conducted by Romero (1995) and discussed by Boulanger and Idriss (2004). The nonplastic Silt #1 exhibited transient, near-zero shear stiffness and an $r_{u,\max} = 100\%$, with narrow, S-shaped hysteretic loops (Boulanger and Idriss 2004). Plastic Silts #2 and #3 exhibited increased shear stiffness with decreased pinching of the hysteresis, characteristics that increased with increases in PI. However, it is of interest to evaluate such behaviors in a quantitative manner so that subjectivity in the assessment of liquefaction susceptibility can be minimized.

Quantitative hysteretic metrics are evaluated for suitability in the consistent identification of soil behavior. Fig. 5(b) presents selected

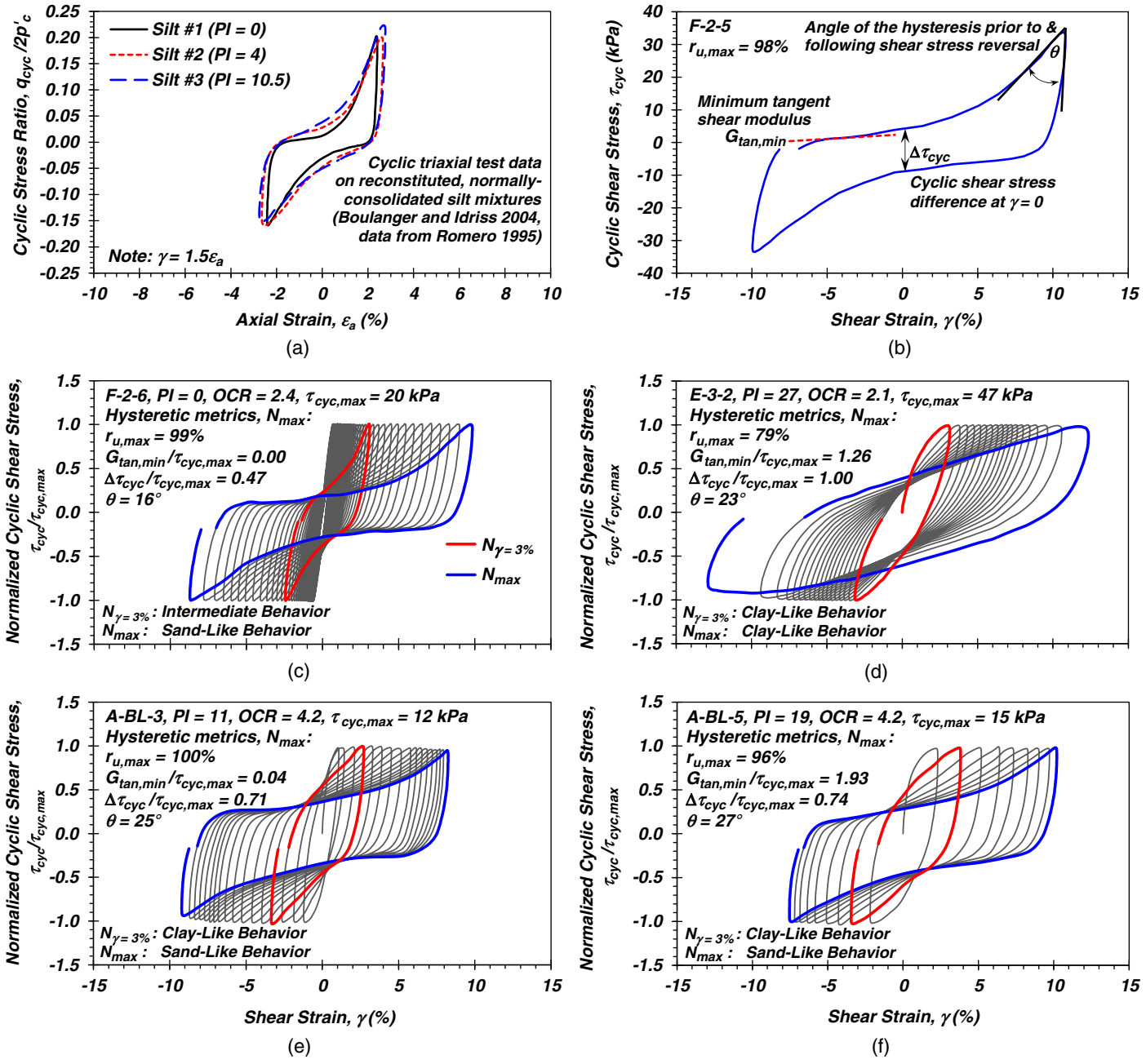

Fig. 5. Typical ranges in hysteretic behavior, including (a) trends in hysteretic response from cyclic triaxial tests conducted on reconstituted silt mixtures; and (b) selected metrics considered for the identification of hysteretic soil behavior at $N_{\gamma=3\%}$ and $N_{\max}$, and quantified examples of hysteretic behavior from cyclic DSS tests on intact specimens (this study) for $N_{\max}$: (c) initially intermediate behavior transitioning to sand-like; (d) clay-like; and (e and f) clay-like behavior transitioning to sand-like behavior. Compare hysteretic metrics tabulated in Table S5 at $N_{\max}$ to $N_{\gamma=3\%}$.

J. Geotech. Geoenviron. Eng., 2023, 149(1): 04022125

hysteretic metrics, including the difference in the cyclic shear stress at $\gamma = 0$, $\Delta\tau_{cyc}$, the minimum tangent shear modulus, $G_{tan,min}$, the angle of the hysteresis curves just prior to and following shear stress reversal, θ (computed in the $\tau_{cyc} - \gamma$ plane), and $r_{u,max}$, each calculated for $N_{\gamma=3\%}$ and the last cycle of each test, N_{max} for those specimens where γ exceeded 5% [Fig. 5(b) and Table S5]. Note that the initial portion of a following cycle was occasionally referenced when computing $\Delta\tau_{cyc}$, and that $G_{tan,min}$ considered the cyclic stresses and strains in the reloading portions of a given cycle on the approach to $\gamma = 0$ to avoid the low tangent shear modulus occasionally occurring at $|\tau_{cyc,max}|$ just prior to unloading. Large cyclic shear strain amplitudes (i.e., greater than 5%) are considered in addition to $\gamma = 3\%$ owing to the expected intensity and duration of loading associated with the subduction zone events anticipated in the Pacific Northwest, so that the ultimate hysteretic behavior could be observed.

To minimize the effect of scaling on the interpreted hysteretic behavior, $\Delta\tau_{cyc}$ and $G_{tan,min}$ were normalized by the corresponding maximum cyclic shear stress, $\tau_{cyc,max}$, (i.e., $\Delta\tau_{cyc}/\tau_{cyc,max}$ and $G_{tan,min}/\tau_{cyc,max}$, respectively). The $\tau_{cyc,max}$-normalized cyclic hysteretic loops presented in Figs. 5(c–f) are accompanied by the selected metrics for N_{max} and exhibit a range in behaviors that evolve with γ and N. Qualitatively, the hysteretic behavior of Specimen F-2-6 [Fig. 5(c); Tables S5 and S6] could be described as intermediate for $N_{\gamma=3\%}$ and sand-like for the last loading cycle (i.e., N_{max}) with its inverted S-shaped cyclic stress-strain hysteresis (indicative of low dissipated strain energy). Quantitively, $\theta = 7$ and 16°, and $\Delta\tau_{cyc}/\tau_{cyc,max} = 0.60$ and 0.47 for $N_{\gamma=3\%}$ and N_{max}, respectively. Importantly, this specimen exhibits nonzero and zero shear stiffness, with $G_{tan,min}/\tau_{cyc,max} = 10.1$ and 0, and $r_{u,max} = 93\%$ and 99%, for $N_{\gamma=3\%}$ and N_{max}, respectively. The evolution in the minimum transient shear stiffness and corresponding maximum excess pore pressure ratio throughout loading is objectively quantified using the hysteretic metrics, which indicate that the ultimate hysteretic behavior is sand-like. Note that zero shear stiffness occurs coincidentally with $r_{u,max}$ at phase transformation [Figs. S16(u and v)], but phase transformation does not occur during a state of zero shear stress as noted with some clean sands (e.g., Sriskandakumar 2004). The term "sand-like behavior" effectively captures this distinction.

In contrast, clay-like behavior is qualitatively characterized by wide stress-strain loops with nonzero shear stiffness and relatively low generated excess pore pressure. Specimen E-3-2 [Fig. 5(d); Tables S5 and S6] presents an example with clearly clay-like behavior, which did not evolve throughout cyclic loading, quantified with $\Delta\tau_{cyc}/\tau_{cyc,max} = 0.76$ and 1.00, $\theta = 8$ and 23°, $G_{tan,min}/\tau_{cyc,max} = 20.4$ and 1.26, and limited $r_{u,max} = 8$ and 79% for $N_{\gamma=3\%}$ and N_{max}, respectively. Specimens A-BL-3 and A-BL-5 exhibit frequently observed evolutionary hysteretic behavior, whereby the hysteresis at $\gamma = 3\%$ suggested a clay-like response, but upon continued loading the specimen transitioned to sand-like behavior at N_{max} with $G_{tan,min}/\tau_{cyc,max}$ less than 2 and $r_{u,max}$ greater than 95%, indicative of the substantial loss of stiffness and strength associated with transient liquefaction. Jana et al. (2022) describe a controlled blasting experiment of an instrumented low plasticity silt deposit at Site A (from which Specimens A-BL-3 and A-BL-5 originated), and showed that the relationship among maximum shear strain, γ_{max}, and excess pore pressure closely tracked that estimated for the Wildlife Site during the Superstition Hills earthquake by Zeghal and Elgamal (1994) to γ_{max} of 1.14%, lending strong evidence for the in-situ sand-like behavior of this material. Table S5 summarizes the hysteretic metrics calculated for each specimen where sufficient information to evaluate previous liquefaction susceptibility criteria was available (described below), whereas Table S6 reports the corresponding hysteretic behavior identified at $N_{\gamma=3\%}$ and N_{max}.

That the hysteretic behavior of these transitional soil specimens can evolve throughout loading highlights the role of earthquake duration (i.e., N) on the potential for exhibiting sand-like behavior. Thus, short duration crustal earthquakes may not produce sufficient loading cycles to trigger sand-like behavior, whereas longer duration (e.g., subduction zone) earthquakes, which can produce greater than 100 cycles of loading, depending on the power law exponent b describing the CRR-N relationship (Boulanger and Idriss 2015; Stuedlein et al. 2021), can lead to the transient loss of strength. Furthermore, it was observed that specimens that exceeded $\gamma = 3\%$ in the first cycle (i.e., subjected to large CSR) often required a number of additional cycles to satisfactorily establish the ultimate hysteretic behavior, indicating that significantly larger shear strains than those associated with common cyclic failure criteria are necessary to make determinations of sand-like or clay-like behavior. That large strains are necessary to observe the ultimate hysteretic behavior aligns with the view that liquefaction susceptibility should associated with the material itself, rather than representations of soil state.

The variation of $r_{u,max}$ with $\Delta\tau_{cyc}/\tau_{cyc,max}$ and $G_{tan,min}/\tau_{cyc,max}$ for $N_{\gamma=3\%}$ and N_{max} are presented in Fig. 6 and suggest that for the typical strain-based cyclic failure criterion of $\gamma = 3\%$, none of the specimens tested exhibited sand-like behavior, with each exhibiting $\Delta\tau_{cyc}/\tau_{cyc,max} \gtrapprox 0.55$, $G_{tan,min}/\tau_{cyc,max} > 5$, and $r_{u,max} < 95\%$ [Figs. 6(a and b)]. The hysteretic metrics for $N_{\gamma=3\%}$ further suggest that an approximate boundary of $90\% \lessapprox r_{u,max} < 95\%$ is consistent with precedent-based qualitative judgments of intermediate behavior, whereas those specimens with $r_{u,max} \lessapprox 90\%$ also tend to exhibit $\Delta\tau_{cyc}/\tau_{cyc,max} \gtrapprox 0.55$, $G_{tan,min}/\tau_{cyc,max} > 2$ for both $N_{\gamma=3\%}$ and N_{max}, providing a quantitative basis that is consistent with precedent-based judgments of clay-like behavior. When shear strain amplitudes exceed 3%, the hysteretic behavior of many specimens that previously exhibited intermediate and clay-like behavior transition to sand-like behavior, with $G_{tan,min}/\tau_{cyc,max} < 2$, and $r_{u,max}$ generally greater than or equal to 95%, which quantifies their significant transient loss of strength and stiffness [Figs. 6(d and e); compared to Fig. 5]. Based on the large-strain observations associated with N_{max}, approximate quantitative guidelines for identifying ultimate cyclic behavior of transitional soils may be summarized as

- clay-like behavior: $r_{u,max} \lessapprox 90\%$, $\Delta\tau_{cyc}/\tau_{cyc,max} \gtrapprox 0.55$ and $G_{tan,min}/\tau_{cyc,max} \gtrapprox 2$;
- sand-like behavior: $r_{u,max} \gtrapprox 95\%$ and $G_{tan,min}/\tau_{cyc,max} \lessapprox 2$; and
- intermediate behavior: $90\% \lessapprox r_{u,max} < 95\%$, $G_{tan,min}/\tau_{cyc,max} \gtrapprox 2$ and $\Delta\tau_{cyc}/\tau_{cyc,max} > 0.55$.

Since these boundaries are approximate, application of greater weight to $r_{u,max}$ and $G_{tan,min}/\tau_{cyc,max}$ is recommended when interpreting hysteretic behavior using the suggested criteria.

Some Observations on Liquefaction Susceptibility Criteria

The liquefaction susceptibility and the potential for cyclic softening failure of those test specimens taken to large shear strains (i.e., greater than 5%) was evaluated using criteria proposed by Boulanger and Idriss (2006; BI06), Bray and Sancio (2006; BS06), and the framework suggested by Armstrong and Malvick (2016; AM16). The full suite of assessments is reported in Table S6 and is accompanied by the cyclic test results in Figs. S7–S16 in Appendix S1. Comparison of liquefaction susceptibility using these three criteria indicates notable inconsistencies. For example, Specimens E-1-2 (PI = 10) and E-2-2 (PI = 28) have been identified as susceptible (S) and nonsusceptible (NS) to liquefaction (BS06), respectively. However, one possible interpretation of the

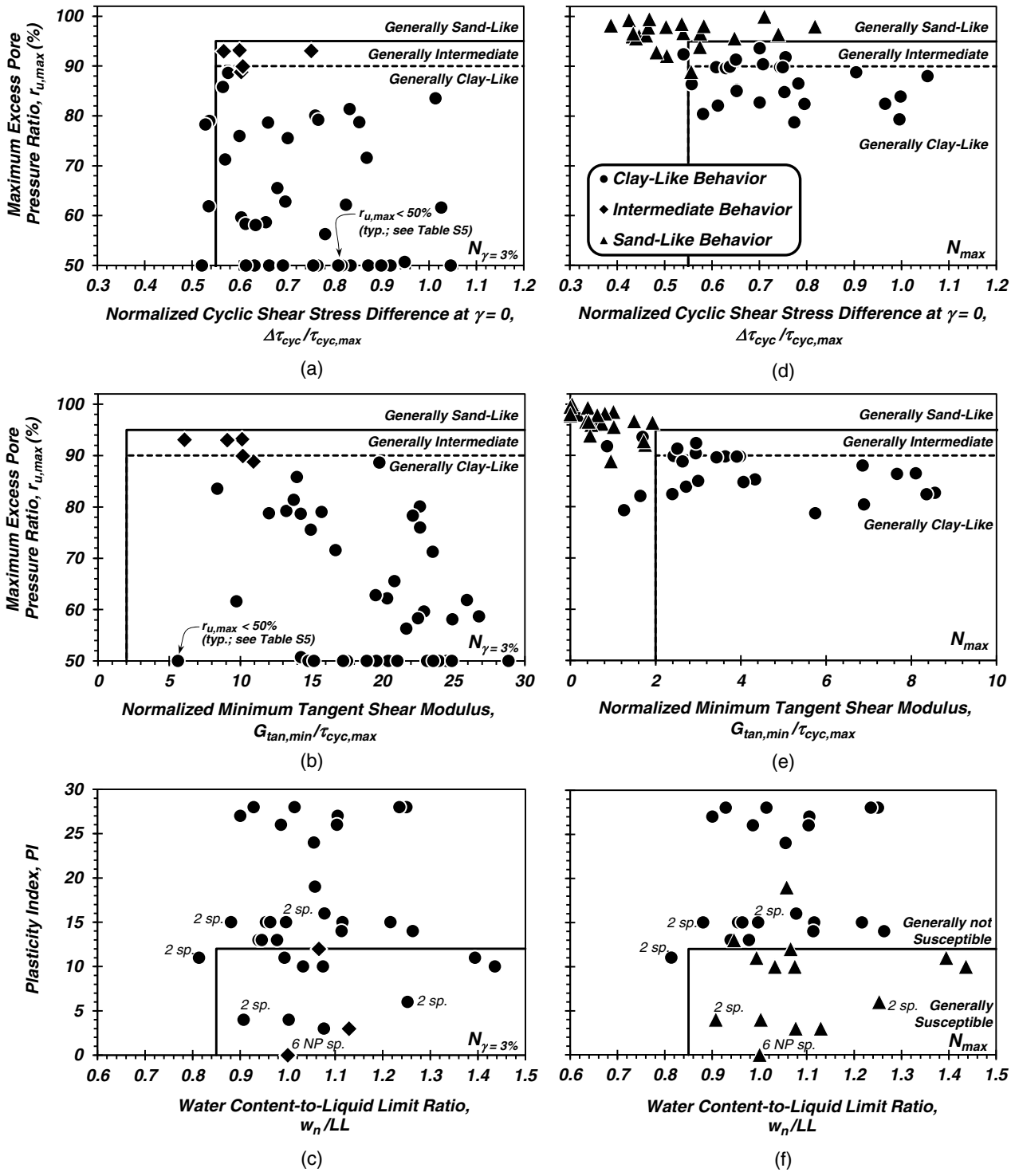

Fig. 6. Variation of selected hysteretic metrics with excess pore pressure ratio and liquefaction susceptibility assessment for: (a–c) $N_{\gamma=3\%}$; and (d–f) $N_{\max}$, indicating variation of maximum excess pore pressure ratio with: (a and d) normalized cyclic shear stress difference at $\gamma = 0$; (b and e) normalized minimum tangent shear modulus; and (c and f) the plasticity index-water content-to-liquid limit ratio of selected specimens. Note: (1) the number of specimens where markers coincide is indicated, and (2) nonplastic (NP) specimens assigned $w_n/\mathrm{LL} = 1.0$ for plotting purposes.

BI06 criterion would suggest that the fundamental behavior of both specimens should be clay-like; however, the purpose of the BI06 criterion is to differentiate between methods for estimating cyclic resistance and concentrates less on hysteretic behavior. Focusing on hysteretic behavior, the cyclic response of the lower PI Specimen E-1-2 [Figs. S11(e–h); Table S5] reveals a transient, near-zero shear stiffness at large strains with $G_{\mathrm{tan,min}}/\tau_{\mathrm{cyc,max}} = 0.46$ (i.e., sand-like behavior) relative to the clay-like behavior for the higher PI Specimen E-2-2 [Figs. S12(e–h) and Table S5; $G_{\mathrm{tan,min}}/\tau_{\mathrm{cyc,max}} = 3.0$, $r_{u,\max} = 85\%$], and is characterized by significantly higher

$r_{u,\max} = 94\%$ with narrower hysteresis loops ($\Delta\tau_{cyc}/\tau_{cyc,\max} = 0.57$). As noted above, the hysteretic behavior examined at $\gamma = 3\%$ can differ from that for γ corresponding to a greater number of loading cycles (e.g., $N_{\max}$; Table S6). The differences in the hysteretic responses at $\gamma = 3\%$ and γ corresponding to $N_{\max}$ for other specimens (Fig. 6; Table S6) indicate that the distinction between sand- and clay-like hysteretic behavior depends on the number of cycles of loading and the corresponding magnitude of γ and $r_{u,\max}$.

The observed disagreements between laboratory responses and those expected using the BI06 and AM16 criteria for the soils tested in this study indicate that the limits provided in Fig. 1(c) alone are insufficient to satisfactorily bound sand- and clay-like hysteretic behavior over the maximum γ and N, due to the existence of numerous contributing factors (e.g., soil mineralogy, OCR, state, and diagenesis) to soil response. We recognize, however, that one goal of these criteria was to judge if typical penetration test-based liquefaction triggering models would serve as adequate means to estimate cyclic resistance. Indeed, the cyclic resistance of sand-like specimens would be underestimated using CPT-based triggering models. However, the suitability of various liquefaction triggering models is not addressed in this study; the potential for transient loss of stiffness and strength forms are the sole focus of the assessments described herein. Evaluation of the BS06 criteria indicates that the 60% of the soils exhibiting clay-like behavior (15 of 25 specimens) would be incorrectly identified in this study as moderately susceptible (MS) to liquefaction over the maximum γ and N (Table S6). However, just one specimen exhibiting sand-like behavior of 22 was incorrectly identified as NS using the BS06 criteria. The CPT-based soil behavior type index, I_c, associated with these test specimens is larger than 2.6, with sand-like specimens characterized with I_c as large as 2.95 (Figs. S1–S6). This provides further evidence that CPT-based assessments of liquefaction susceptibility should not consider $I_c = 2.6$ as a deterministic threshold between sand- and clay-like behavior (e.g., Maurer et al. 2019).

The liquefaction susceptibility and cyclic resistance evaluation frameworks discussed above recognize that judgments of anticipated hysteretic behavior in the absence of site-specific cyclic data are necessary. Accordingly, the specimen behavior deduced using the quantitative criteria for $N_{\gamma=3\%}$ and $N_{\max}$ are assessed in terms of correlation to mineralogy and state through the PI and w_n/LL ratio, similar to the BS06 criteria. Comparison of Figs. 6(c and f) serves to reinforce the need to assess hysteretic behavior of transitional soils at large strain amplitudes (i.e., greater than 5%) given the lack of sand-like behaviors for $N_{\gamma=3\%}$. Fig. 6(f) shows that no specimen determined to exhibit clay-like behavior using hysteretic metrics is characterized with $w_n/LL > 0.85$ and PI < 12. In contrast, only one sand-like specimen with PI = 19 notably deviates from the PI = 12 boundary separating S and MS from NS using the BS06 criteria, whereas eight sand-like specimens are characterized with PI > 7 associated with the clay-like threshold proposed in the BI06 criteria. Based on the large-strain cyclic responses of specimens exhibiting sand- and clay-like hysteretic behavior (i.e., associated with $N_{\max}$), it appears that, in the absence of site-specific cyclic test data, transitional soils with PI>12 and/or $w_n/LL < 0.85$ may be reliably judged as clay-like, whereas soils with PI$\lessapprox$12 and $w_n/LL > 0.85$ may be reliably judged as sand-like provided that the associated soil deposit experiences sufficient loading cycles to trigger large-strain behavior.

Notably, earlier efforts to link stress history and soil state (through OCR and the liquidity index) appeared to support qualitative judgments of liquefaction susceptibility with varying degrees of success. However, when hysteretic behavior was assessed objectively in view of the selected metrics, these state-indicative variables were not found to reliably determine large-strain behavior. This may be due to the role of strain rate on the volume change tendencies exhibited by soils (Kutter and Sathialingam 1992; Yamamuro et al. 2011), which can serve to blur traditional lines separating state and stress history (e.g., OCR = 2; in the Modified Cam Clay model). Thus, we emphasize that the findings and liquefaction susceptibility criteria described above are approximate and have been developed based on observations of cyclic loading with a frequency of 0.1 Hz.

Furthermore, Fig. 6 includes just one specimen with $w_n/LL < 0.85$; thus, the reliability of this criterion cannot be robustly proven with the silts studied herein. A strong argument exists that liquefaction susceptibility assessments should not consider state or more generically environmental factors (including state, degree of saturation, and age) but rather be limited to material or inherent characteristics (e.g., plasticity, mineralogy). Thus, the PI $\approx$ 12 criterion would satisfactorily capture the material-based assessment of liquefaction susceptibility for these soils.

Factors Affecting the Cyclic Resistance of Intact Specimens

Figs. 7(a and b) present the variation CRR with $N_{\gamma=3\%}$ for the intact specimens presented herein with $1 \le OCR \le 4.2$ and $0 \le PI \le 39$. The cyclic resistance of these silt soils is sensitive to stress history and plasticity. Power-law expressions quantifying the cyclic resistance ratio, $CRR = a \cdot N^{-b}$ (Seed et al. 1975), defined as the CSR required to generate $\gamma = 3\%$ were obtained to facilitate comparison among the various soils (Table 2). Coefficient a equals the magnitude of CRR at $N = 1$, and exponent b represents the slope of the semilogarithmic CRR − N curve and controls the number of equivalent loading cycles, N_{eq}, associated with a given M_w (Boulanger and Idriss 2015). An exponent of $b = 0.135$ has been suggested to represent plastic, fine-grained soils for use within simplified method for cyclic softening evaluation based on a limited dataset (Idriss and Boulanger 2008). However, the results of this study indicate that, regardless of liquefaction susceptibility, exponent b ranges from 0.05 to 0.15 for the intact fine-grained soils (Table 2) for the ranges of OCR and PI tested and generally decreases with increases in PI. For example, $b = 0.07$ and $b = 0.15$ correspond to specimens with PI = 28 and PI = 3, respectively. As a result, N_{eq} and magnitude scaling factors, associated with fine-grained soils, would differ from those reported by Idriss and Boulanger (2008). For example, the number of loading cycles associated with $M_w = 7.5$ earthquakes may be characterized using $N_{eq} \cong 360$ and $N_{eq} \cong 23$ for $b = 0.07$ and $b = 0.15$, respectively (Boulanger and Idriss 2015); N_{eq} would be approximately 30% and 65% larger for subduction zone earthquakes with $M_w \cong 9.0$, respectively (Stuedlein et al. 2021).

Comparison of the cyclic resistance in Figs. 7(a and b) indicates that, for a given N, increases in OCR can result in increases in CRR. For example, for Site B specimens ($11 \le PI \le 16$) and $N = 10$ and 30, an increase in OCR from 1.5 (i.e., B-14; $\sigma'_{vc} = \sigma'_{v0} = 160$ kPa) to 1.9 (i.e., B-13; $\sigma'_{vc} = \sigma'_{v0} = 50$ kPa) resulted in an increase in CRR from 0.25 to 0.35 and 0.23 to 0.31, respectively; however, the smaller σ'_{vc} for the B-13 specimens also contributes to the larger CRR due to its greater potential for dilative tendencies. For comparable σ'_{v0} and OCRs, an increase in PI increases the cyclic resistance: consider specimens retrieved from Site E and $N = 18$: an increase from PI = 15 (i.e., E-5; $\sigma'_{v0} = 125$ kPa) to $PI = 28$ (i.e., E-2; $\sigma'_{v0} = 100$ kPa) results in an increase in CRR by 21%. Numerous factors in addition to PI and OCR contribute to the variation in CRR of intact soils (e.g., depositional environments, soil fabric, stress history, state, and diagenesis), and the contribution and identification of the dominant effect

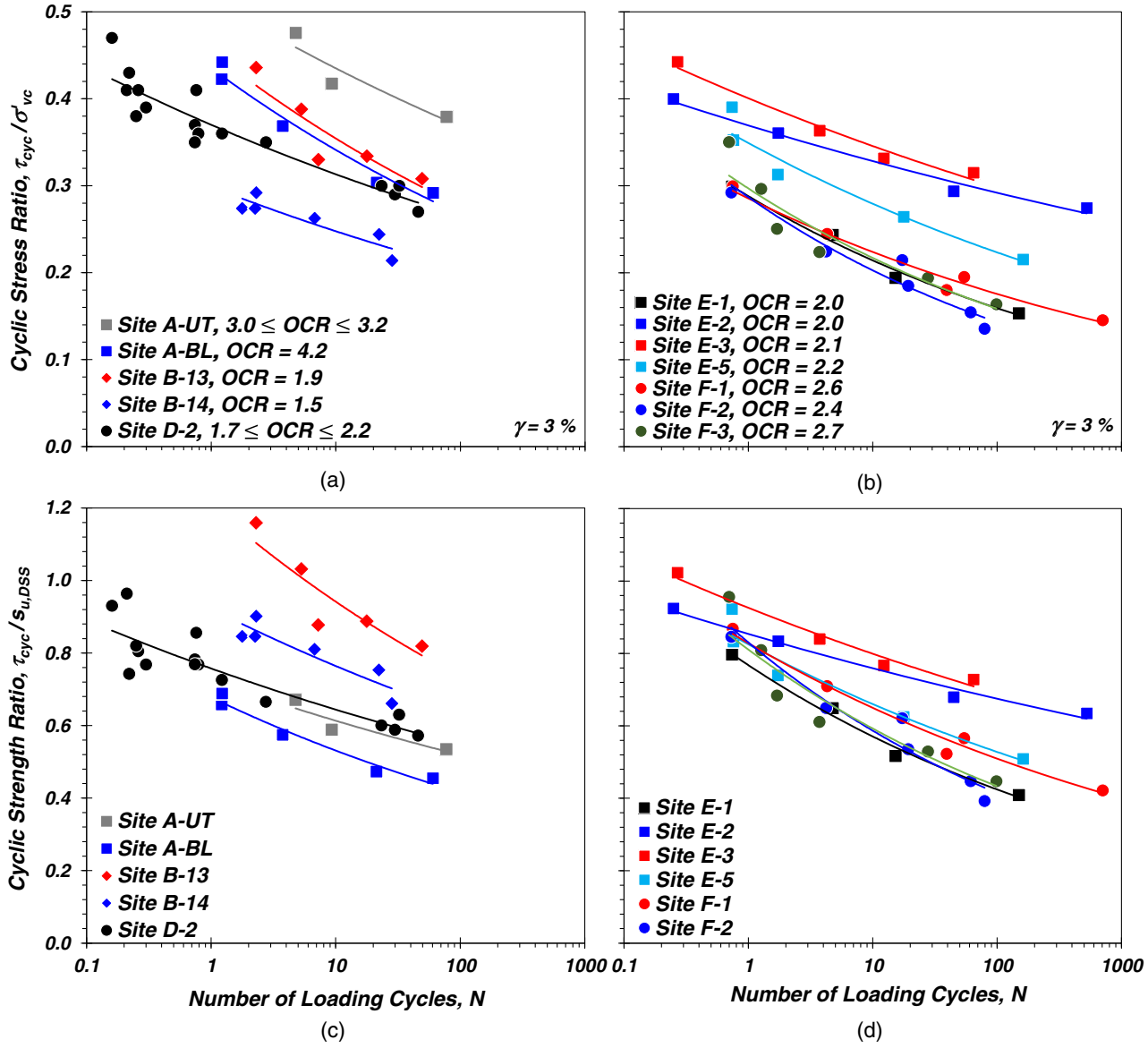

Fig. 7. Comparison of the cyclic resistance of intact specimens from (a and c) Sites A, B, D; and (b and d) Sites E and F, indicating variation of (a and b) cyclic stress ratio, CSR; and (c and d) cyclic strength ratio, $\tau_{cyc}/s_{u,DSS}$, with number of loading cycles, N to reach $\gamma = 3\%$.

of each are rather difficult to separate from the observed cyclic response.

Figs. 7(c and d) present the variation of cyclic strength ratios, $\tau_{cyc}/s_{u,DSS}$, required to reach $\gamma = 3\%$ with N, scaled to a frequency of 1 Hz representative of typical earthquake motion frequencies based on observations that the cyclic strength increases by ~9% for each logarithmic cycle increase in loading frequency (Lefebvre and LeBouef 1987; Zergoun and Vaid 1994; Lefebvre and Pfendler 1996; Boulanger et al. 1998; Idriss and Boulanger 2008). The variations of $\tau_{cyc}/s_{u,DSS}$ with PI essentially follow those noted above in terms of CRR, whereas the effect of OCR appears largely captured by the magnitude of $s_{u,DSS}$ (Ladd 1991). Fitted power-law parameters to represent the $\tau_{cyc}/s_{u,DSS}$ versus N data and the corresponding goodness-of-fit are summarized in Table 2. In addition, the variation of CRR and $\tau_{cyc}/s_{u,DSS}$ with $N_{\gamma=3.75\%}$ are presented in Fig. S17, and the corresponding fitted power-law parameters are summarized in Table S4. Although a limited number of specimens did not generate $\gamma = 3.75\%$ for the stated number of loading cycles, no appreciable difference in the trends of cyclic resistance have been identified between the cyclic shear strain failure criteria of 3% and 3.75%.

Figs. 8(a and b) illustrate the variation of CRR to trigger $\gamma = 3\%$ at $N = 10$ and $N = 30$ with PI, respectively, along with the results of cyclic DSS tests conducted on intact specimens compiled by Dahl et al. (2018). For specimens with PI ≥ 7 and OCR $= 1$ the CRR appears to be independent of PI and may be approximated by the constant CRR $= 0.203$ and CRR $= 0.184$ for $N = 10$ and $N = 30$, respectively. The latter is similar to CRR $= 0.183$ suggested by Boulanger and Idriss (2004) for clay-like NC fine grained soils [$N = 30$; Fig. 8(b)]. The beneficial role of stress history on CRR is somewhat obscured in Figs. 8(a and b) by the variability in the soil fabric, state, and PI of the specimens.

Figs. 8(c and d) present the variation of $\tau_{cyc}/s_{u,DSS}$ for $N = 10$ and $N = 30$ with PI, respectively, indicating that for PI $\lesssim 11$, $\tau_{cyc}/s_{u,DSS}$ does not appear sensitive to PI and can be approximated by 0.63 and 0.54, respectively. For the available data, $\tau_{cyc}/s_{u,DSS}$

J. Geotech. Geoenviron. Eng., 2023, 149(1): 04022125

Table 2. Summary of fitted parameters for cyclic resistance ratio (CRR $-$ N) and cyclic strength ratio expressions ($\tau_{cyc}/s_{u,DSS} - N$)

Test designation	Vertical effective consolidation stress, σ'_{v0} (kPa)	Over-consolidation ratio, OCR	Plasticity index, PI	CRR $-$ N relationship			$\tau_{cyc}/s_{u,DSS} - N$ relationship		
				Coefficient a	Exponent b	R^2	Coefficient a	Exponent b	R^2
A-UT-4	36	3.1	14	0.51	0.07	0.86	0.73	0.07	0.86
A-UT-6		3.2	12						
A-UT-7		3.0	15						
A-BL-2	32	4.2	10	0.44	0.11	0.97	0.68	0.11	0.97
A-BL-3			11						
A-BL-4			11						
A-BL-5			19						
A-BL-6			19						
B-13-15	50	1.9	16	0.45	0.11	0.81	1.21	0.11	0.81
B-13-18			15						
B-13-19			14						
B-13-20			15						
B-13-21			15						
B-14-7	160	1.5	13	0.30	0.08	0.82	0.92	0.08	0.82
B-14-8			13						
B-14-9			11						
B-14-14			15						
B-14-17			13						
B-14-22			13						
D-2-1	129	2.2	25	0.37	0.07	0.89	0.76	0.07	0.83
D-2-2	114	1.7	22						
D-2-3	108	2.0	29						
D-2-5	100	2.1	14						
D-2-6	100	2.1	31						
D-2-7	100	2.1	31						
D-2-9	100	2.0	34						
D-2-10	118	2.1	34						
D-2-11	118	2.1	39						
D-2-12	118	1.9	39						
D-2-13	118	1.9	28						
D-2-14	118	2.0	27						
D-2-15	105	1.9	28						
D-2-19	118	1.9	26						
D-2-27	122	2.0	21						
D-2-31	106	2.0	28						
E-1-1	95	2.0	12	0.29	0.13	0.99	0.77	0.13	0.99
E-1-2			10						
E-1-3			10						
E-1-4			12						
E-1-8		1.0	11	0.24	0.13	0.99	0.85	0.13	0.99
E-1-9			11						
E-1-10			11						
E-1-11			11						
E-2-1	100	2.0	26	0.37	0.05	0.98	0.85	0.05	0.98
E-2-2			28						
E-2-3			28						
E-2-4			28						
E-2-6	215	1.0	28	0.24	0.05	0.71	NA	NA	NA
E-2-7			28						
E-2-9			28						
E-2-10			28						
E-2-11			28						
E-2-12	100	2.0	28	0.42	0.04	0.98	NA	NA	NA
E-2-13			28						
E-2-14			28						
E-2-15			28						
E-3-1	107	2.1	24	0.40	0.06	0.97	0.93	0.06	0.97
E-3-2			27						
E-3-3			27						
E-3-4			24						

Table 2. (*Continued.*)

Test designation	Vertical effective consolidation stress, σ'_{v0} (kPa)	Over-consolidation ratio, *OCR*	Plasticity index, *PI*	CRR − *N* relationship			$\tau_{cyc}/s_{u,DSS}$ − *N* relationship		
				Coefficient *a*	Exponent *b*	R^2	Coefficient *a*	Exponent *b*	R^2
E-5-1	125	2.2	15	0.35	0.10	0.96	0.83	0.10	0.96
E-5-2			15						
E-5-3			15						
E-5-4			15						
E-5-5			15						
E-5-6			15						
F-1-1	120	2.6	NP	0.29	0.11	0.98	0.83	0.11	0.98
F-1-2			NP						
F-1-3			NP						
F-1-4			NP						
F-1-5			NP						
F-1-6	350	1.0	NP	0.22	0.07	0.90	0.68	0.07	0.90
F-1-7			NP						
F-1-8			NP						
F-1-9			NP						
F-1-10			NP						
F-2-1	150	2.4	6	0.29	0.15	0.92	0.83	0.15	0.92
F-2-2			6						
F-2-3			3						
F-2-4			3						
F-2-5			NP						
F-2-6			NP						
F-3-1	158	2.7	11	0.30	0.14	0.91	0.81	0.14	0.91
F-3-2			11						
F-3-3			4						
F-3-4			4						
F-3-5			4						
F-3-7			20						

Note: NP = nonplastic.

generally increases with increasing PI for $11 \le \text{PI} < 18$. For $\text{PI} \ge 18$, the specimens exhibited constant $\tau_{cyc}/s_{u,DSS} = 0.82$ and $\tau_{cyc}/s_{u,DSS} = 0.76$ for $N = 10$ and $N = 30$, respectively. These trends in the cyclic strength ratios deduced from intact specimens differ somewhat from the constant $\tau_{cyc}/s_{u,DSS} = 0.83$ suggested by Boulanger and Idriss (2007) for $N = 30$ and inferred from a limited number of cyclic tests conducted on intact and reconstituted silts and clays, particularly for $\text{PI} < 18$ [Fig. 8(d)]. The results of the current study correspond to the lower range in $\tau_{cyc}/s_{u,DSS}$ summarized by Boulanger and Idriss (2007) and imply that lower CRRs may be expected. For example, the CRR for $M_w = 7.5$, $\text{CRR}_{M_w=7.5}$, corresponding to $N = 30$ for uniaxial cyclic loading beneath level-ground sites may be estimated using

$$\text{CRR}_{M_w=7.5} = (\tau_{cyc}/s_{u,DSS})_{N=30} \cdot S \cdot \text{OCR}^m \quad (1)$$

where $(\tau_{cyc}/s_{u,DSS})_{N=30}$ is $(\tau_{cyc}/s_{u,DSS})$ corresponding to $N = 30$ (= 0.83 per Idriss and Boulanger 2008). The CRR calculated using Eq. (1) is 16% and 27% greater for Site B-13, and B-14, respectively, 49% greater for Site D-2, 111% greater for Site E-1 (OCR = 2), and 41% greater for Site E-3 (OCR = 2.1) than that obtained from the cyclic DSS tests. The observed differences between the measured and estimated $\text{CRR}_{M_w=7.5}$ for these fine-grained soils can be attributed, in part, to the multivariate effects of PI, state, soil fabric, and other possible contributors to cyclic resistance. Until further data are available, the CRR of fine-grained soils at $N = 30$ [Fig. 8(d)] may be estimated using Eq. (2)

$$(\tau_{cyc}/s_u)_{N=30} = 0.54 \quad 0 \le \text{PI} < 11 \quad (2a)$$

$$(\tau_{cyc}/s_u)_{N=30} = 0.030\text{PI} + 0.212 \quad 11 \le \text{PI} < 18 \quad (2b)$$

$$(\tau_{cyc}/s_u)_{N=30} = 0.76 \quad \text{PI} \ge 18 \quad (2c)$$

characterized with a standard deviation in the residuals (i.e., error), equal to 0.06.

Role of OCR and Consolidation Technique on the Cyclic Response of Intact Specimens

Select specimens from Sites E-1 (PI = 11, OCR = 2), E-2 (PI = 28, OCR = 2), and F-1 (PI = 0, OCR = 2.6) were mechanically normally consolidated (i.e., MC-NC) to study the cyclic response of these soils with particular emphasis on stress-dilatancy behavior, destruction of natural soil fabric, and excessive reduction in e by engaging the yield surface (i.e., exceeding σ'_p) prior to shearing. Figs. 9(a–d) compare the cyclic response of Specimen E-2-3 ($\sigma'_{vc} = 100$ kPa, $e = 1.98$) and MC-NC Specimen E-2-6 ($\sigma'_{vc} = 215$ kPa, $e = 1.87$) subjected to identical CSR = 0.29. Both specimens exhibit cyclic mobility-type behavior without transient zero shear stiffness during hysteresis [Figs. 9(a and b)]. For a given N, the MC-NC specimen exhibited larger γ, greater degradation in shear modulus and broader hysteresis loops [Figs. 9(a and c)], higher r_u [Fig. 9(d)], and lower $N_{\gamma=3\%}$ as compared to Specimen E-2-3 [Fig. 9(a)]. A similar response is observed for the nonplastic, intact silt Specimen F-1-2 ($\sigma'_{vc} = 120$ kPa, $e = 0.95$) and MC-NC specimen F-1-7 ($\sigma'_{vc} = 350$ kPa, $e = 0.91$; Figs. 9(e–h); Table S3).

Fig. 10 presents the variation of cyclic resistance of selected intact and MC-NC specimens with $N_{\gamma=3\%}$. For the range of $2 \le \text{OCR} \le 2.6$ and $0 \le \text{PI} \le 28$, the MC-NC specimens exhibit 17 to

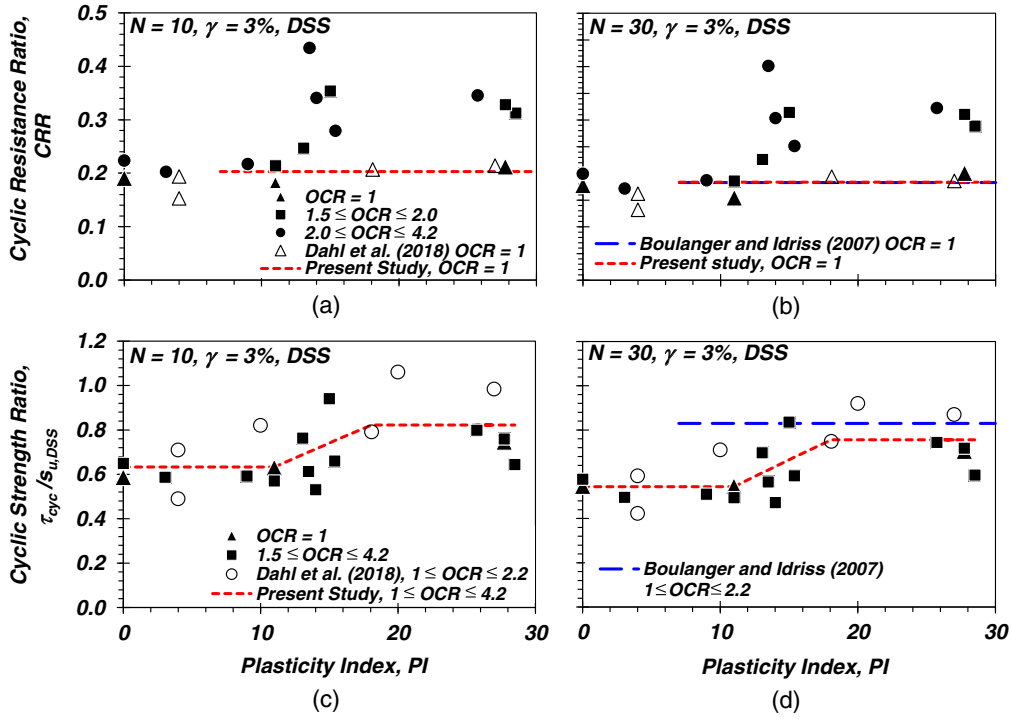

Fig. 8. Variation of cyclic resistance with PI and OCR at (a and c) $N = 10$; and (b and d) $N = 30$: (a and b) cyclic resistance ratio, CRR; and (c and d) cyclic strength ratio, $\tau_{cyc}/s_{u,DSS}$, $\gamma = 3\%$.

35% lower CRR for $N = 1$ and 6 to 35% lower CRR for $N = 100$, compared to the intact OC specimens, despite their smaller void ratios. A mechanically induced NC state results in a greater reduction in the CRR of soils with higher PI than those of low to medium plasticity. For example, MC-NC specimens of Site E-2 (PI = 28) is ~35% smaller than specimens from Sites E-1 (PI = 11) and Site F-1 (PI = 0), which exhibits ~17% and 6% to 22% smaller CRRs compared to their intact OC counterparts, respectively. Although the MC-NC specimens have lower e compared to their intact counterparts, it appears that the CRR is reduced due to the suppression of dilation under larger σ'_{vc} and destruction of the soil fabric through exceedance of σ'_p.

The effect of the consolidation technique on the cyclic resistance of intact specimens was also evaluated in this study through the comparison of recompression and quasi-SHANSEP specimens. The quasi-SHANSEP technique, whereby σ'_{vc} approaches or just equals σ'_p followed by unloading, was conducted to simulate the 1D principal stress hysteresis and the corresponding lateral stress state encountered in-situ. This consolidation technique relies on accurate estimates of σ'_p, which may be rather difficult for low to medium plasticity soils (Grozic et al. 2003, 2005; Boone 2010; Dahl et al. 2010; Umar and Sadrekarimi 2017), since in most cases even high-quality samples do not always exhibit a well-defined 1D yield stress. Use of inaccurate estimates of σ'_p during quasi-SHANSEP consolidation may lead to specimen states that are not representative of in-situ conditions. Fig. 11 compares the cyclic response of recompression Specimen E-2-2 ($\sigma'_{v0} = \sigma'_{vc} = 100$ kPa, OCR = 2, PI = 28) and MC-OC Specimen E-2-12 ($\sigma'_{vc} = 125$ kPa, OCR = 2, PI = 28) subjected to similar CSRs (refer to Fig. S18 for CRR $- N_\gamma = 3.75\%$). Following recompression and prior to cyclic shear, Specimen E-2-2 experienced a volumetric strain of $\varepsilon_v = 5.7\%$; thereafter, it exhibited lower cyclic resistance ($N_{\gamma=3\%} = 0.2$) and greater r_u for a given N compared to the MC-OC Specimen E-2-12 ($\varepsilon_v = 9.8\%$; $N_{\gamma=3\%} = 11.8$). Fig. 10 compares the cyclic resistance of tests conducted on the Site E-2 specimens using the recompression (OCR = 2, $\sigma'_{v0} = 100$ kPa, $e_{average} = 1.96$) and quasi-SHANSEP (OCR = 2, $\sigma'_{v0} = 125$ kPa, $e_{average} = 1.83$) methods; the latter exhibited CRRs 12% to 24% larger than those tested using the recompression method over the range in N evaluated. The observed differences in behavior can be attributed to the potentially larger lateral stresses and the smaller void ratios of the quasi-SHANSEP specimens. The specimens consolidated using the quasi-SHANSEP technique are not representative of in-situ conditions (e.g., e), and suggest a higher CRR than can be expected. The recompression technique is therefore preferred for establishing the cyclic response to capture in-situ conditions when testing high-quality samples.

Concluding Remarks

The cyclic response of nonplastic to plastic silt soils was investigated through a comprehensive laboratory testing program on intact lightly and moderately overconsolidated (OC) specimens. Metrics to quantify the cyclic shear stress-shear strain hysteresis were defined and found to provide reliable, though approximate, boundaries to aid the determination of liquefaction susceptibility, which appeared to track with similar minerology and state-based boundaries identified in previous efforts. The effects of OCR and PI on cyclic resistance was explored. The effects of vertical effective stress, destruction of the soil–fabric, and reconsolidation technique on cyclic resistance were identified through comparison of intact OC, mechanically consolidated normally consolidated (MC-NC), and mechanically consolidated overconsolidated (MC-OC) specimens. The following may be concluded as a result of this study:

- All of the specimens tested exhibited cyclic mobility, with narrow and wide hysteresis loops corresponding to low and high plasticity specimens, respectively. Hysteretic metrics were proposed to quantify cyclic behavior that can range from sand- to

J. Geotech. Geoenviron. Eng., 2023, 149(1): 04022125

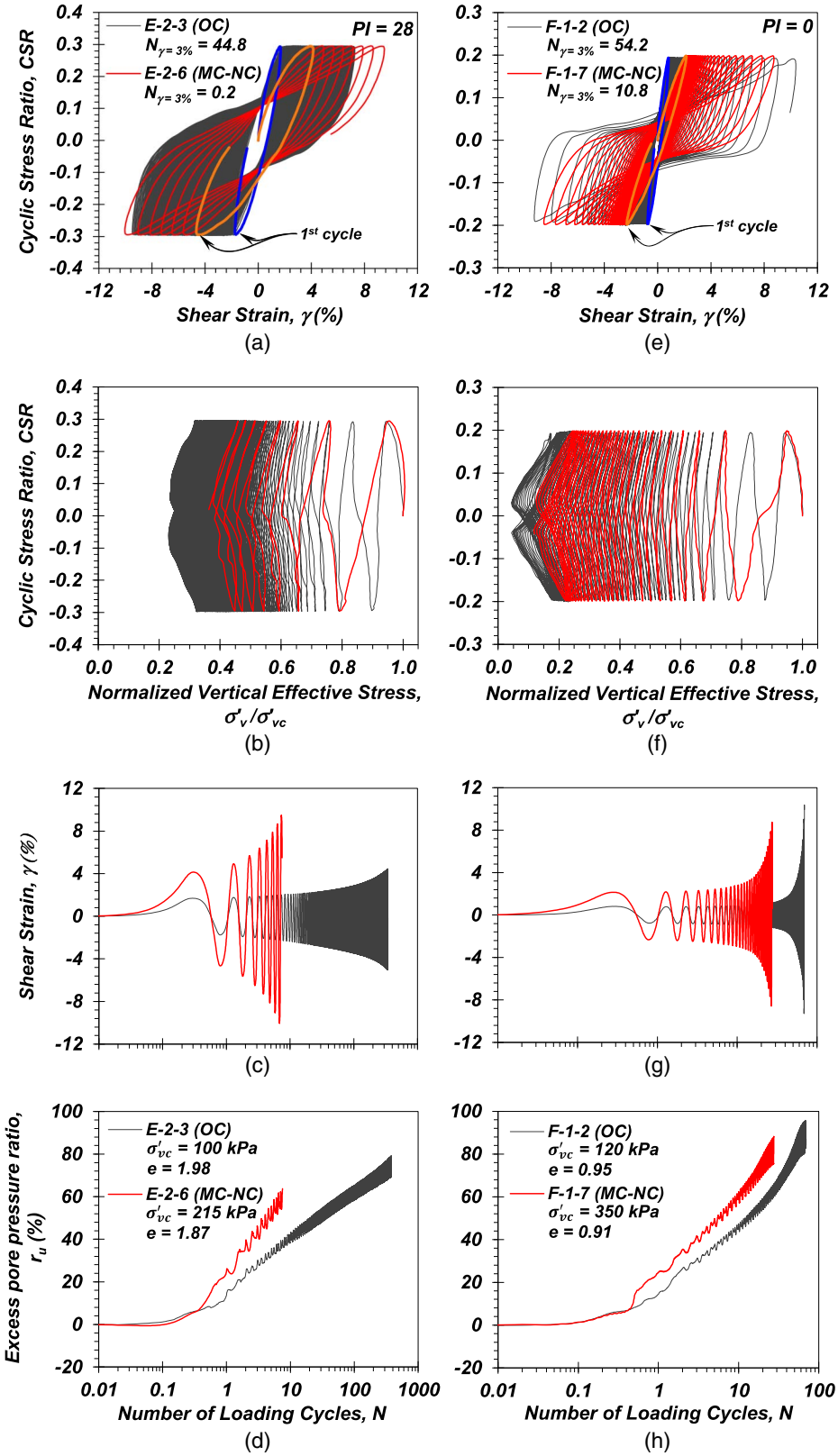

Fig. 9. Comparison of the cyclic responses of natural, intact (OC) specimens with mechanically, normally consolidated (MC-NC) specimens from (a–d) Site E; and (e–h) Site F in terms of (a and e) shear stress-shear strain, CSR–γ, hysteresis; (b and f) effective stress paths; (c and g) accumulation of γ; and (d and h) r_u with N.

clay-like, including the difference in the cyclic shear stress at $\gamma = 0$, $\Delta\tau_{cyc}$, and the minimum tangent shear modulus, $G_{tan,min}$, normalized by the corresponding maximum cyclic shear stress, $\tau_{cyc,max}$, $\Delta\tau_{cyc}/\tau_{cyc,max}$ and $G_{tan,min}/\tau_{cyc,max}$, respectively, along with the maximum excess pore pressure ratio, $r_{u,max}$. These metrics facilitated quantification in the evolution of hysteretic behavior with loading cycles, N and shear strain, γ.

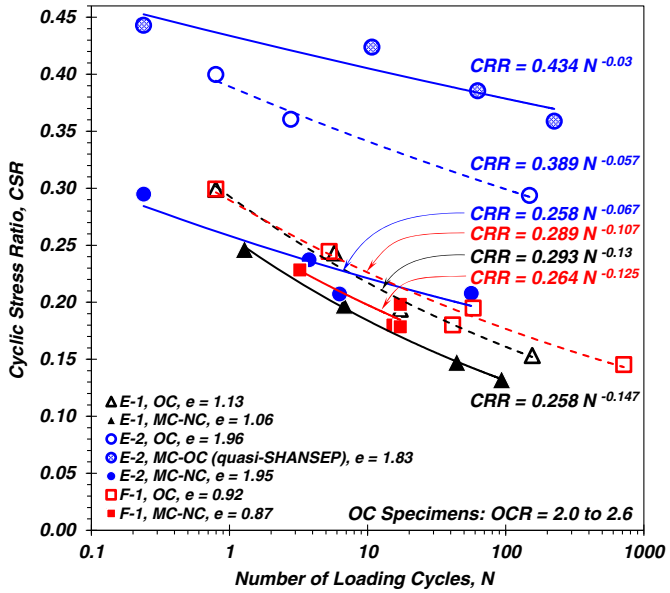

Fig. 10. Variation of the CSR with number of loading cycles, N, for $\gamma = 3\%$ derived from constant-volume, stress-controlled, cyclic DSS tests conducted on natural, intact OC, MC-NC, and MC-OC (quasi-SHANSEP) specimens from Sites E and F.

- Generally, nonplastic and low plasticity silt specimens exhibited sand-like behavior at large γ, with maximum excess pore pressures, $r_{u,\max} \gtrsim 95\%$, associated with a transient, near-zero or zero shear stiffness quantified with $G_{\tan,\min}/\tau_{\text{cyc},\max} \lesssim 2$ during the unloading portions of later loading cycles. These hysteretic quantities compared well with index test-based boundaries for sand-like behavior set approximately to $\text{PI} \lesssim 12$ and $w_n/\text{LL} > 0.85$. It is argued that $\text{PI} \lesssim 12$ provides a sufficient criterion for the evaluation of liquefaction susceptibility, which considers material characteristics alone.
- In contrast, clay-like behavior was quantified at large γ as those transitional soils with $r_{u,\max} \lesssim 90\%$, $\Delta\tau_{\text{cyc}}/\tau_{\text{cyc},\max} \gtrsim 0.55$, and $G_{\tan,\min}/\tau_{\text{cyc},\max} \gtrsim 2$, which compared well with index test-based boundaries for clay-like behavior set approximately to PI>12 and/or $w_n/\text{LL} < 0.85$. Intermediate behavior could be tentatively identified as corresponding to $90\% \lesssim r_{u,\max} < 95\%$, $G_{\tan,\min}/\tau_{\text{cyc},\max} \gtrsim 2$ and $\Delta\tau_{\text{cyc}}/\tau_{\text{cyc},\max} > 0.55$; however, no soil in this study exhibited such hysteretic behavior for the maximum loading cycle corresponding to $\gamma > 5\%$.
- The intensity and duration of loading were determined as key factors driving the cyclic behavior of these transitional soils, since the distinction between sand- and clay-like behavior and the accuracy of common liquefaction susceptibility criteria depend on the loading-induced maximum shear strain, γ, and corresponding $r_{u,\max}$. This suggests that magnitude and duration contribute to ultimate hysteretic behavior in addition to previously identified factors such as plasticity, which point to distinct implications for the liquefaction susceptibility of silt deposits in subduction zones. It is emphasized that conclusions regarding liquefaction susceptibility are based wholly on hysteretic response; the appropriate use of particular engineering models (e.g., estimates of cyclic resistance using penetration test results) is not considered in this study.
- For the available data, the CRR for specimens with OCR = 1 appears independent of PI and can be approximated as 0.203 and 0.184 for $N = 10$ and 30, respectively.

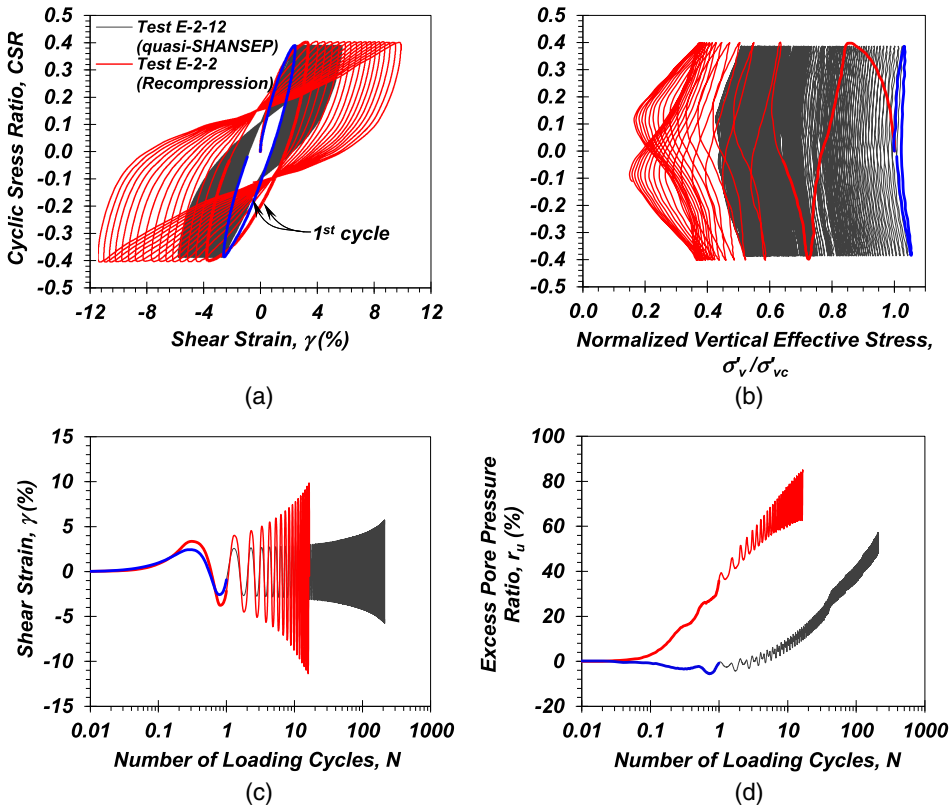

Fig. 11. Comparison of the cyclic response of specimens reconsolidated using the recompression and quasi-SHANSEP methods in terms of (a) CSR – γ hysteresis; (b) effective stress paths; (c) accumulation of γ; and (d) r_u with N.

J. Geotech. Geoenviron. Eng., 2023, 149(1): 04022125

- The variation of the cyclic strength ratios, $\tau_{cyc}/s_{u,DSS}$, with PI exhibited apparent trends for $N = 10$ and $N = 30$ as shown in Fig. 7. The observed scatter may be attributed to the differences in natural soil fabric and state of the specimens.
- For a given CSR and N, MC-NC silt specimens exhibited larger γ, greater degradation in shear modulus, higher r_u, lower CRR, and broader hysteresis loops compared to intact OC silt specimens. These results are due to the destruction of the natural soil fabric and change in state for the MC-NC specimens.
- Silt specimens consolidated using a quasi-SHANSEP procedure exhibited 12%–24% larger CRR than those reconsolidated using recompression, which can be attributed to the larger lateral consolidation stresses and lower void ratios. Use of the recompression method with high-quality samples of low to medium plasticity soils is preferred for establishing the cyclic resistance for in-situ conditions where significant uncertainty may exist in the quantification of preconsolidation stresses.

Data Availability Statement

Some or all data, models, or code generated or used during the study are available in a repository online in accordance with funder data retention policies. Specifically, the data described herein are available for public access in the Next Generation Liquefaction Database (https://nextgenerationliquefaction.org/about/index.html).

Acknowledgments

This material is based upon work supported by the National Science Foundation under Grant CMMI-1663654, the Oregon Department of Transportation (ODOT) under Grant SPR-304-911 and various ODOT projects, the Port of Portland, the Cascadia Lifelines Program (CLiP), and the Pacific Earthquake Engineering Research (PEER) Center under Grant 1175-NCTRSA. Any opinions, findings, and conclusions or recommendations expressed are those of the authors and do not necessarily reflect the views of the aforementioned sponsors. The writers wish to thank the anonymous reviewers for their helpful comments, which served to improve this paper.

Supplemental Materials

Appendix S1, Tables S1–S6, and Figs. S1–S18 are available online in the ASCE Library (www.ascelibrary.org).

References

Armstrong, R. J., and E. J. Malvick. 2016. "Practical considerations in the use of liquefaction susceptibility criteria." *Earthquake Spectra* 32 (3): 1941–1950. https://doi.org/10.1193/071114EQS100R.

ASTM. 2012. *Standard test method for one-dimensional consolidation properties of saturated cohesive soils using controlled-strain loading*. ASTM-D4186/4186M. West Conshohocken, PA: ASTM.

ASTM. 2014. *Standard practices for preserving and transporting soil samples*. ASTM-D4220. West Conshohocken, PA: ASTM.

ASTM. 2015. *Standard practice for thin-walled tube sampling of fine-grained soils for geotechnical purposes*. ASTM-D1587/1587M. West Conshohocken, PA: ASTM.

Becker, D., J. Crooks, K. Been, and M. Jefferies. 1987. "Work as a criterion for determining in situ and yield stresses in clays." *Can. Geotech. J.* 24 (4): 549–564. https://doi.org/10.1139/t87-070.

Beyzaei, C. Z., J. D. Bray, M. Cubrinovski, S. Bastin, M. Stringer, M. Jacka, S. van Ballegooy, M. Riemer, and R. Wentz. 2020. "Characterization of silty soil thin layering and groundwater conditions for liquefaction assessment." *Can. Geotech. J.* 57 (2): 263–276. https://doi.org/10.1139/cgj-2018-0287.

Beyzaei, C. Z., J. D. Bray, M. Cubrinovski, M. Riemer, and M. Stringer. 2018. "Laboratory-based characterization of shallow silty soils in southwest Christchurch." *Soil Dyn. Earthquake Eng.* 110 (Jun): 93–109. https://doi.org/10.1016/j.soildyn.2018.01.046.

Bjerrum, L., and A. Landva. 1966. "Direct simple shear tests on a Norwegian quick clay." *Géotechnique* 16 (1): 1–20. https://doi.org/10.1680/geot.1966.16.1.1.

Boone, S. J. 2010. "A critical reappraisal of preconsolidation pressure interpretations using the oedometer test." *Can. Geotech. J.* 47 (3): 281–296. https://doi.org/10.1139/T09-093.

Boulanger, R. W., and I. M. Idriss. 2004. *Evaluating the potential for liquefaction or cyclic failure of silts and clays*, 131. Davis, CA: Center for Geotechnical Modeling.

Boulanger, R. W., and I. M. Idriss. 2006. "Liquefaction susceptibility criteria for silts and clays." *J. Geotech. Geoenviron. Eng.* 132 (11): 1413–1426. https://doi.org/10.1061/(ASCE)1090-0241(2006)132:11(1413).

Boulanger, R. W., and I. M. Idriss. 2007. "Evaluation of cyclic softening in silts and clays." *J. Geotech. Geoenviron. Eng.* 133 (6): 641–652. https://doi.org/10.1061/(ASCE)1090-0241(2007)133:6(641).

Boulanger, R. W., and I. M. Idriss. 2015. "Magnitude scaling factors in liquefaction triggering procedures." *Soil Dyn. Earthquake Eng.* 79 (Jun): 296–303. https://doi.org/10.1016/j.soildyn.2015.01.004.

Boulanger, R. W., M. W. Meyers, L. H. Mejia, and I. M. Idriss. 1998. "Behavior of a fine-grained soil during the Loma Prieta earthquake." *Can. Geotech. J.* 35 (1): 146–158. https://doi.org/10.1139/t97-078.

Bray, J. D., et al. 2004. "Subsurface characterization at ground failure sites in Adapazari, Turkey." *J. Geotech. Geoenviron. Eng.* 130 (7): 673–685. https://doi.org/10.1061/(ASCE)1090-0241(2004)130:7(673).

Bray, J. D., and R. B. Sancio. 2006. "Assessment of the liquefaction susceptibility of fine-grained soils." *J. Geotech. Geoenviron. Eng.* 132 (9): 1165–1177. https://doi.org/10.1061/(ASCE)1090-0241(2006)132:9(1165).

Casagrande, A. 1936. "The determination of pre-consolidation load and its practical significance." In *Proc., Int. Conf. on Soil Mechanics and Foundation Engineering*, 60. Cambridge, MA: Harvard Univ.

Castro, G., and S. J. Poulos. 1977. "Factors affecting liquefaction and cyclic mobility." *J. Geotech. Geoenviron. Eng.* 103 (6): 501–516. https://doi.org/10.1061/AJGEB6.0000433.

Cubrinovski, M., D. Henderson, and B. A. Bradley. 2012. "Liquefaction impacts in residential areas in the 2010–2011 Christchurch earthquakes." In *Proc., Int. Symp. on Engineering Lessons Learned from the 2011 Great East Japan Earthquake*, 811–824. Tokyo: Japan Association for Earthquake Engineering.

Dadashiserej, A., A. Jana, A. W. Stuedlein, and T. M. Evans. 2022a. "Effect of strain history on the monotonic and cyclic response of natural and reconstituted silts." *Soil Dyn. Earthquake Eng.* 160 (Sep): 107329. https://doi.org/10.1016/j.soildyn.2022.107329.

Dadashiserej, A., A. Jana, A. W. Stuedlein, T. M. Evans, B. Zhang, Z. Xu, K. H. Stokoe, and B. R. Cox. 2022b. "*In-Situ* and laboratory cyclic response of an alluvial plastic silt deposit." In *Proc., 20th Int. Conf. on Soil Mechanics and Geotechnical Engineering*. Alexandria, VA: National Science Foundation.

Dahl, K., R. W. Boulanger, and J. T. DeJong. 2018. "Trends in experimental data of intermediate soils for evaluating dynamic strength." In *Proc., 11th US National Conf. on Earthquake Engineering*. Los Angeles: Earthquake Engineering Research Institute.

Dahl, K. R., R. W. Boulanger, J. T. DeJong, and M. W. Driller. 2010. "Effects of sample disturbance and consolidation procedures on cyclic strengths of intermediate soils." In *Proc., the 5th Int. Conf. on Recent Advances in Geotechnical Earthquake Engineering and Soil Dynamics and Symp. in Honor of Professor I.M. Idriss*, 1–20. Rolla, MO: Missouri Univ. of Science and Technology.

Dahl, K. R., J. T. DeJong, R. W. Boulanger, R. Pyke, and D. Wahl. 2014. "Characterization of an alluvial silt and clay deposit for monotonic, cyclic, and post-cyclic behavior." *Can. Geotech. J.* 51 (4): 432–440. https://doi.org/10.1139/cgj-2013-0057.

DeJong, J. T., C. P. Krage, B. M. Albin, and D. J. DeGroot. 2018. "Work-based framework for sample quality evaluation of low plasticity soils." *J. Geotech. Geoenviron. Eng.* 144 (10): 04018074. https://doi.org/10.1061/(ASCE)GT.1943-5606.0001941.

Dyvik, R., S. Lacasse, T. Berre, and B. Raadim. 1987. "Comparison of truly undrained and constant volume direct simple shear tests." *Géotechnique* 37 (1): 3–10. https://doi.org/10.1680/geot.1987.37.1.3.

Erken, A., and B. C. Ulker. 2007. "Effect of cyclic loading on monotonic shear strength of fine-grained soils." *Eng. Geol.* 89 (3–4): 243–257. https://doi.org/10.1016/j.enggeo.2006.10.008.

Goldfinger, C., et al. 2012. *Turbidite event history—Methods and implications for holocene paleoseismicity of the Cascadia subduction zone*, 184. Reston, VA: USGS.

Grozic, J. L. H., T. Lunne, and S. Pande. 2003. "An oedometer test study on the preconsolidation stress of glaciomarine clays." *Can. Geotech. J.* 40 (5): 857–872. https://doi.org/10.1139/t03-043.

Grozic, J. L. H., T. Lunne, and S. Pande. 2005. "Reply to the discussion by Clementino on an oedometer test study on the preconsolidation stress of glaciomarine clays." *Can. Geotech. J.* 42 (3): 975–976. https://doi.org/10.1139/t05-011.

Hazirbaba, K., and E. M. Rathje. 2009. "Pore pressure generation of silty sands due to induced cyclic shear strains." *J. Geotech. Geoenviron. Eng.* 135 (12): 1892–1905. https://doi.org/10.1061/(ASCE)GT.1943-5606.0000147.

Idriss, I. M., and R. W. Boulanger. 2008. *Soil liquefaction during earthquakes: Monograph MNO-12*. Oakland, CA: Earthquake Engineering Research Institute.

Jana, A., A. Dadashiserej, B. Zhang, A. W. Stuedlein, T. M. Evans, K. H. Stokoe II, and B. Cox. 2022. "Use and comparison of multi-directional vibroseis mobile shaking and controlled blasting to determine the in-situ dynamic nonlinear inelastic response of a low plasticity silt deposit." *J. Geotech. Geoenviron. Eng.* https://doi.org/10.1061/(ASCE)GT.1943-5606.0002924.

Jana, A., and A. W. Stuedlein. 2021. "Monotonic, cyclic and post-cyclic response of an alluvial plastic silt deposit." *J. Geotech. Geoenviron. Eng.* 147 (3): 04020174. https://doi.org/10.1061/(ASCE)GT.1943-5606.0002462.

Kaya, Z., and A. Erken. 2015. "Cyclic and post-cyclic monotonic behavior of Adapazari soils." *Soil Dyn. Earthquake Eng.* 77 (Oct): 83–96. https://doi.org/10.1016/j.soildyn.2015.05.003.

Kutter, B. L., and N. Sathialingam. 1992. "Elastic-viscoplastic modelling of the rate-dependent behaviour of clays." *Géotechnique* 42 (3): 427–441. https://doi.org/10.1680/geot.1992.42.3.427.

Ladd, C. C. 1991. "Stability evaluation during staged construction." *J. Geotech. Eng.* 117 (4): 540–615. https://doi.org/10.1061/(ASCE)0733-9410(1991)117:4(540).

Ladd, C. C., and D. J. DeGroot. 2004. *Recommended practice for soft ground site characterization: Arthur Casagrande lecture*, 60. Boston: Massachusetts Institute of Technology.

Landon, M. E., C. Marchetti, and D. J. DeGroot. 2018. "Constant rate of strain consolidation testing of saturated cohesive soils without back pressure saturation." *Geotech. Test. J.* 41 (2): 20170030. https://doi.org/10.1520/GTJ20170030.

Lefebvre, G., and D. LeBouef. 1987. "Rate effects and cyclic loading of sensitive clays." *J. Geotech. Geoenviron. Eng.* 113 (5): 476–489. https://doi.org/10.1061/(ASCE)0733-9410(1987)113:5(476).

Lefebvre, G., and P. Pfendler. 1996. "Strain rate and preshear effects in cyclic resistance of soft clay." *J. Geotech. Eng.* 122 (1): 21–26. https://doi.org/10.1061/(ASCE)0733-9410(1996)122:1(21).

Maurer, B. W., R. A. Green, S. van Ballegooy, and L. Wotherspoon. 2019. "Development of region-specific soil behavior type index correlations for evaluating liquefaction hazard in Christchurch, New Zealand." *Soil Dyn. Earthquake Eng.* 117 (Feb): 96–105. https://doi.org/10.1016/j.soildyn.2018.04.059.

Polito, C. P., and E. L. Sibley. 2020. "Threshold fines content and behavior of sands with nonplastic silts." *Can. Geotech. J.* 57 (3): 462–465. https://doi.org/10.1139/cgj-2018-0698.

Price, A., J. DeJong, and R. Boulanger. 2017. "Cyclic loading response of silt with multiple loading events." *J. Geotech. Geoenviron. Eng.* 143 (10): 04017080. https://doi.org/10.1061/(ASCE)GT.1943-5606.0001759.

Romero, S. 1995. "The behavior of silt as clay content is increased." M.S. thesis, Dept. of Civil and Environmental Engineering, Univ. of Calif.

Sanin, M., and D. Wijewickreme. 2006. "Cyclic shear response of channel-fill Fraser River Delta silt." *Soil Dyn. Earthquake Eng.* 26 (9): 854–869. https://doi.org/10.1016/j.soildyn.2005.12.006.

Seed, H. B., I. M. Idriss, F. Makdisi, and N. Banerjee. 1975. *Representation of irregular stress time histories by equivalent uniform stress series in liquefaction analyses*. Rep. No. EERC 75-29. Berkeley, CA: Univ. of California at Berkeley.

Simpson, D. C., and T. M. Evans. 2016. "Behavioral thresholds in mixtures of sand and kaolinite clay." *J. Geotech. Geoenviron. Eng.* 142 (2): 04015073. https://doi.org/10.1061/(ASCE)GT.1943-5606.0001391.

Sriskandakumar, S. 2004. "Cyclic loading response of Fraser River sand for validation of numerical models simulating centrifuge tests." M.S. thesis, Dept. of Civil Engineering, Univ. of British Columbia.

Stokoe, K. H., J. N. Roberts, S. Hwang, B. R. Cox, and F. Menq. 2016. "Effectiveness of inhibiting liquefaction triggering by shallow ground improvement methods: Field shaking trials with T-Rex at one area in Christchurch, New Zealand." In *Proc., 24th Geotechnical Conf. of Torino*. Oxfordshire, UK: Taylor & Francis.

Stokoe, K. H., and J. C. Santamarina. 2000. "Seismic-wave-based testing in geotechnical engineering." In *Proc., Int. Conf. on Geotechnical and Geological Engineering*, 1490–1536. Lanchester, PA: Technomic.

Stuedlein, A., T. Evans, A. Dadashiserej, and A. Jana. 2021. "Cyclic response and softening of Western Oregon silts and assessment within the simplified method framework with updates relevant for application to the Cascadia subduction zone." In *Final report, version 2, Cascadia lifelines program*. Corvallis, OR: Oregon State Univ.

Tsuchida, H. 1970. "Prediction and countermeasure against the liquefaction in sand deposits." In *Proc., Abstract of the seminar in the Port and Harbor Research Institute*, 31–333. Yokosuka City, Japan: Port and Airport Research Institute.

Umar, M., and A. Sadrekarimi. 2017. "Accuracy of determining preconsolidation pressure from laboratory tests." *Can. Geotech. J.* 54 (3): 441–450. https://doi.org/10.1139/cgj-2016-0203.

Wang, L., and J. Frost. 2004. "Dissipated strain energy method for determining preconsolidation pressure." *Can. Geotech. J.* 41 (4): 760–768. https://doi.org/10.1139/t04-013.

Wijewickreme, D., A. Soysa, and P. Verma. 2019. "Response of natural fine-grained soils for seismic design practice: A collection of research findings from British Columbia, Canada." *Soil Dyn. Earthquake Eng.* 124 (Sep): 280–296. https://doi.org/10.1016/j.soildyn.2018.04.053.

Wijewickreme, D., S. Sriskandakumar, and P. Byrne. 2005. "Cyclic loading response of loose air-pluviated Fraser River sand for validation of numerical models simulating centrifuge tests." *Can. Geotech. J.* 42 (2): 550–561. https://doi.org/10.1139/t04-119.

Yamamuro, J. A., A. E. Abrantes, and P. V. Lade. 2011. "Effect of strain rate on the stress-strain behavior of sand." *J. Geotech. Geoenviron. Eng.* 137 (12): 1169–1178. https://doi.org/10.1061/(ASCE)GT.1943-5606.0000542.

Zeghal, M., and A. W. Elgamal. 1994. "Analysis of site liquefaction using earthquake records." *J. Geotech. Eng.* 120 (6): 996–1017. https://doi.org/10.1061/(ASCE)0733-9410(1994)120:6(996).

Zergoun, M., and Y. Vaid. 1994. "Effective stress response of clay to undrained cyclic loading." *Can. Geotech. J.* 31 (5): 714–727. https://doi.org/10.1139/t94-083.

SUPPLEMENTAL MATERIALS

ASCE *Journal of Geotechnical and Geoenvironmental Engineering*

Liquefaction Susceptibility and Cyclic Response of Intact Nonplastic and Plastic Silts

Armin W. Stuedlein, Ali Dadashiserej, Amalesh Jana,
and T. Matthew Evans

DOI: 10.1061/(ASCE)GT.1943-5606.0002935

APPENDIX S1

Table S1. Summary of consolidation parameters and compression ratios to evaluate sample quality.

Test Designation	*In-Situ* Vertical Effective Stress, σ'_{v0} (kPa)	*In-Situ* Pre-consolidation Stress, σ'_{p} [1] (kPa)	Over-consolidation Ratio OCR	C_{ri}	C_c	C_{ri}/C_c	C_{rw}	C_{cw}	C_{rw}/C_{cw}
A-UT-CRS	36	112	3.1	0.055	0.646	0.085	0.011	0.096	0.115
A-BL-CRS	32	134	4.2	0.031	0.379	0.083	0.007	0.069	0.105
B-13-CRS	50	95	1.9	0.080	0.412	0.194	0.021	0.076	0.276
B-14-CRS	160	250	1.5	0.050	0.410	0.122	0.015	0.084	0.179
D-2-CRS	112	224	2.0	0.130	1.110	0.120	0.020	0.194	0.100
E-1-CRS	95	190	2.0	0.041	0.276	0.147	0.015	0.055	0.269
E-2-CRS	100	200	2.0	0.073	1.046	0.069	0.015	0.139	0.111
E-3-CRS	107	225	2.1	0.111	1.662	0.067	0.016	0.169	0.092
E-5-CRS	125	275	2.2	0.052	0.403	0.130	0.016	0.084	0.194
F-1-CRS	120	314	2.6	0.058	0.404	0.144	0.015	0.084	0.181
F-2-CRS	150	360	2.4	0.055	0.432	0.128	0.014	0.093	0.153
F-3-CRS	158	427	2.7	0.036	0.419	0.087	0.010	0.091	0.105

[1] Average of Casagrande construction and Becker et al. (1987) strain-energy based methods.

Table S2. Summary of constant-volume, monotonic DSS test results.

Test Designation	Vertical Effective Consolidation Stress, σ'_{vc} (kPa)	Over-consolidation Ratio, OCR	Undrained Shear Strength, $s_{u,DSS}$ (kPa)	Natural Moisture Content, w_n (%)	Degree of Saturation, S (%)	Plasticity Index, PI	Void Ratio, e	Fines Content, FC (%)
A-UT-M1	36	3.1	29	71	100.0	14	1.83	98
A-BL-M1	32	4.2	22	50	100.0	15	1.26	91
B-13-M1	48	2.0	21	47	93.7	13	1.33	95
B-14-M1	160	1.5	57	40	100.0	11	0.95	80
B-14-M2	100	8.0	133	42	100.0	NA[1]	0.77	NA
B-14-M3	267	3.0	163	42	100.0	11	0.81	99
D-2-M1	138	1.6	71	53	99.0	22	1.41	99
D-2-M2	106	1.9	54	86	96.0	27	2.37	91
D-2-M3	106	1.9	50	87	NA	28	NA	99
D-2-M4	262	1.0	79	74	98.5	27	1.98	95
D-2-M5	106	4.0	100	65	99.0	33	1.73	99
D-2-M6	106	3.0	83	NA	99.0	27	NA	94
D-2-M7	118	2.1	63	85	98.0	26	2.29	96
D-2-M8	102	1.9	45	70	100.0	23	1.85	99
D-2-M9	100	1.9	50	69	99.6	23	1.83	99
E-1-M1	95	2.0	39	46	100.0	12	NA	98
E-1-M2	300	1.0	93	43	100.0	NA	0.98	NA
E-1-M3	75	4.0	70	43	100.0	NA	0.95	NA
E-1-M4	38	8.0	70	36	100.0	NA	0.93	NA
E-2-M1	100	2.0	46	73	100.0	28	NA	99
E-3-M1	107	2.1	50	92	100.0	24	NA	99
E-3-M2	300	1.0	91	74	100.0	25	1.62	99
E-3-M3	75	4.0	75	72	100.0	19	1.57	97
E-3-M4	38	8.0	68	58	100.0	19	1.26	96
E-5-M1	125	2.2	58	39	100.0	15	NA	98
F-1-M1	120	2.6	45	NA	NA	NP[2]	NA	34
F-2-M1	150	2.4	57	39	100.0	3	0.95	38
F-3-M1	158	2.7	63	37	100.0	20	NA	71

[1]Not available.
[2]Non-plastic.

Table S3. Summary of constant-volume, stress-controlled, cyclic DSS test results interpreted based on $N_{\gamma=3\%}$.

Test Designation	Sample Depth Interval (m)	Vertical Effective Consolidation Stress, σ'_{vc} (kPa)	Overconsolidation Ratio, OCR	Void Ratio, e	Fines Content, FC (%)	Plasticity Index, PI	Undrained Shear Strength Ratio, $s_{u,DSS}/\sigma'_{vc}$	Cyclic Stress Ratio, CSR	Cyclic Strength Ratio, $\tau_{cyc}/s_{u,DSS}$	$N_{\gamma=3\%}$[1]
A-UT-4	2.6 - 3.2	36	3.1	1.44	97	14	0.77	0.38	0.53	77.3
A-UT-6			3.2	1.39	96	12		0.42	0.59	9.3
A-UT-7			3.0	1.39	97	15		0.48	0.67	4.8
A-BL-2	2.4 - 3.0	32	4.2	1.49	82	10	0.70	0.30	0.47	21.3
A-BL-3				1.41	77	11		0.37	0.57	3.7
A-BL-4				1.30	NA[2]	11		0.42	0.66	1.2
A-BL-5				1.35	92	19		0.44	0.69	1.2
A-BL-6				1.51	90	19		0.29	0.45	60.3
B-13-15	2.4 - 3.2	50	1.9	1.35	91	16	0.41	0.44	1.16	2.3
B-13-18				1.38	NA	15		0.39	1.03	5.3
B-13-19				1.35	95	14		0.33	0.88	7.2
B-13-20				1.47	NA	15		0.31	0.82	49.3
B-13-21				1.50	NA	15		0.33	0.89	17.8
B-14-7	8.5 - 9.3	160	1.5	0.95	86	13	0.35	0.29	0.90	2.3
B-14-8				0.92	81	13		0.24	0.75	22.2
B-14-9				0.90	80	11		0.21	0.66	28.2
B-14-14				0.98	99	15		0.27	0.85	1.8
B-14-17				1.00	NA[2]	13		0.27	0.85	2.3
B-14-22				0.89	98	13		0.26	0.81	6.8
D-2-1	9.1 - 11.2	129	2.2	2.06	98	25	0.60	0.35	0.67	2.8
D-2-2		114	1.7	1.24	NA	22	0.46	0.41	0.96	0.2
D-2-3		108	2.0	2.19	99	29	0.73	0.41	0.86	0.8
D-2-5		100	2.1	1.28	76	14	0.38	0.47	0.93	0.2
D-2-6		100	2.1	1.79	96	31	0.67	0.39	0.77	0.3
D-2-7		100	2.1	2.01	98	31	0.67	0.36	0.73	1.2
D-2-9		100	2.0	2.22	99	34	0.74	0.43	0.74	0.2
D-2-10		118	2.1	2.16	93	34	0.63	0.41	0.80	0.3
D-2-11		118	2.1	2.24	95	39	0.63	0.30	0.60	23.3
D-2-12		118	1.9	2.10	93	39	0.63	0.38	0.82	0.3
D-2-13		118	1.9	2.05	NA	28	0.58	0.37	0.78	0.7
D-2-14		118	2.0	2.19	99	27	0.63	0.29	0.59	29.8

D-2-15		105	1.9	2.24	99	28	0.65	0.27	0.57	45.8
D-2-19		118	1.9	2.24	99	26	0.65	0.36	0.77	0.8
D-2-27		122	2.0	2.24	99	21	0.43	0.35	0.77	0.7
D-2-31		106	2.0	2.24	99	28	0.64	0.30	0.63	32.3
E-1-1	7.3 - 7.9	95	2.0	1.10	94	12	0.41	0.30	0.80	0.7
E-1-2				1.17	87	10		0.24	0.65	4.7
E-1-3				1.13	89	10		0.19	0.52	15.2
E-1-4				1.13	100	12		0.15	0.41	149.8
E-1-8				1.10	NA	11		0.20	0.70	5.7
E-1-9		250	1.0	1.05	NA	11	0.31	0.15	0.52	42.3
E-1-10				1.05	NA	11		0.25	0.87	0.7
E-1-11				1.03	NA	11		0.13	0.47	91.2
E-2-1	8.2 - 8.8	100	2.0	1.92	99	26	0.47	0.36	0.83	1.7
E-2-2				2.01	99	28		0.40	0.92	0.2
E-2-3				1.98	99	28		0.29	0.68	44.8
E-2-4				1.94	99	28		0.27	0.63	525.8
E-2-6		215	1.0	1.87	NA	28	NA	0.29	NA	0.2
E-2-7				1.95	NA	28		0.24	NA	0.7
E-2-9				1.96	NA	28		0.21	NA	1.2
E-2-10				1.98	NA	28		0.19	NA	251.8
E-2-11				1.99	NA	28		0.21	NA	10.3
E-2-12		125	2.0	1.93	NA	28	NA	0.39	NA	11.8
E-2-13				1.92	NA	28		0.42	NA	1.3
E-2-14				1.83	NA	28		0.36	NA	58.8
E-2-15				1.64	NA	28		0.44	NA	0.2
E-3-1	9.4 - 10.0	107	2.1	2.33	99	24	0.47	0.31	0.73	64.8
E-3-2				2.30	99	27		0.44	1.02	0.3
E-3-3				2.19	99	27		0.36	0.84	3.7
E-3-4				2.22	94	24		0.33	0.77	12.3
E-5-1	11.4 - 12.0	125	2.2	0.99	100	15	0.46	0.39	0.92	0.7
E-5-2				0.94	99	15		0.35	0.83	0.8
E-5-3				0.94	100	15		0.35	0.83	0.8
E-5-4				0.96	99	15		0.31	0.74	1.7
E-5-5				0.68	99	15		0.22	0.51	161.8
E-5-6				1.00	98	15		0.26	0.62	17.8
F-1-1	6.2 – 6.9	120	2.6	0.84	62	NP[3]	0.38	0.30	0.87	0.7
F-1-2				0.95	62			0.20	0.57	54.2
F-1-3				0.89	47			0.24	0.71	4.3
F-1-4				0.99	47			0.18	0.52	39.2
F-1-5				0.91	41			0.15	0.42	705.8

F-1-6				0.85	NA			0.15	0.46	675.8
F-1-7				0.91	NA			0.20	0.61	10.8
F-1-8		350	1.0	0.92	NA		0.35	0.23	0.70	1.2
F-1-9				0.81	NA			0.18	0.55	10.2
F-1-10				0.85	NA			0.18	0.55	12.2
F-2-1				0.84	44	6		0.29	0.85	0.7
F-2-2				0.86	48	6		0.21	0.62	17.2
F-2-3	8.5 - 9.1	150	2.4	0.81	38	3	0.38	0.19	0.54	19.2
F-2-4				0.81	30	3		0.15	0.45	61.2
F-2-5				0.76	36	NP		0.22	0.65	4.2
F-2-6				0.68	29	NP		0.14	0.39	79.2
F-3-1				0.64	62	11		0.25	0.68	1.7
F-3-2				0.67	60	11		0.22	0.61	3.7
F-3-3	9.5 - 10.1	158	2.7	0.76	41	4	0.40	0.16	0.45	98.8
F-3-4				0.80	73	4		0.30	0.81	1.3
F-3-5				0.81	83	4		0.19	0.53	27.7
F-3-7				0.88	88	20		0.35	0.96	0.7

[1] Number of loading cycles to generate γ_{SA} = 3%.
[2] Not available.
[3] Non-plastic.

Table S4. Summary of constant-volume, stress-controlled, cyclic DSS test results interpreted based on $N_{\gamma=3.75\%}$.

Test Designation	Vertical Effective Consolidation Stress, σ'_{vc} (kPa)	Overconsolidation Ratio, OCR	Cyclic Stress Ratio, CSR	Cyclic Strength Ratio, $\tau_{cyc}/s_{u,DSS}$	$N_{\gamma=3.75\%}$[1]	$CRR - N$ Relationship			$\tau_{cyc}/s_{u,DSS} - N$ Relationship		
						Coefficient a	Exponent b	R^2	Coefficient a	Exponent b	R^2
A-UT-4	36	3.1	0.38	0.53	104.3[2]	0.62	0.13	1.00	0.88	0.13	1.00
A-UT-6		3.2	0.42	0.59	20.8						
A-UT-7		3.0	0.48	0.67	7.8						
A-BL-2	32	4.2	0.30	0.47	25.3	0.44	0.10	0.97	0.68	0.10	0.97
A-BL-3			0.37	0.57	4.8						
A-BL-4			0.42	0.66	1.3						
A-BL-5			0.44	0.69	1.3						
A-BL-6			0.29	0.45	75.3						
B-13-15	50	1.9	0.44	1.16	4.2	0.49	0.12	0.81	1.30	0.12	0.81
B-13-18			0.39	1.03	8.2						
B-13-19			0.33	0.88	11.3						
B-13-20			0.31	0.82	65.3						
B-13-21			0.33	0.89	24.8						
B-14-7	160	1.5	0.29	0.90	4.2	0.31	0.10	0.82	0.99	0.10	0.82
B-14-8			0.24	0.75	26.2						
B-14-9			0.21	0.66	34.2						
B-14-14			0.27	0.85	3.2						
B-14-17			0.27	0.85	4.2						
B-14-22			0.26	0.81	10.7						
D-2-1	129	2.2	0.35	0.67	14.8	0.39	0.07	0.91	0.81	0.07	0.79
D-2-2	114	1.7	0.41	0.96	0.2						
D-2-3	108	2.0	0.41	0.86	1.7						
D-2-5	100	2.1	0.47	0.93	0.2						
D-2-6	100	2.1	0.39	0.77	0.8						
D-2-7	100	2.1	0.36	0.73	2.3						
D-2-9	100	2.0	0.43	0.74	0.3						
D-2-10	118	2.1	0.41	0.80	0.7						
D-2-11	118	2.1	0.30	0.60	71.3						
D-2-12	118	1.9	0.38	0.82	2.3						
D-2-13	118	1.9	0.37	0.78	2.8						
D-2-14	118	2.0	0.29	0.59	77.8						

D-2-15	105	1.9	0.27	0.57	88.8						
D-2-19	118	1.9	0.36	0.77	2.2						
D-2-27	122	2.0	0.35	0.77	2.8						
D-2-31	106	2.0	0.30	0.63	99.3						
E-1-1	95	2.0	0.30	0.80	0.8	0.29	0.13	0.98	0.78	0.13	0.98
E-1-2			0.24	0.65	5.8						
E-1-3			0.19	0.52	17.2						
E-1-4			0.15	0.41	155.8						
E-1-8	250	1.0	0.20	0.70	6.8	0.26	0.15	1.00	0.91	0.15	1.00
E-1-9			0.15	0.52	44.3						
E-1-10			0.25	0.87	1.3						
E-1-11			0.13	0.47	93.3						
E-2-1	100	2.0	0.36	0.83	2.8	0.39	0.06	0.99	0.90	0.06	0.99
E-2-2			0.40	0.92	0.8						
E-2-3			0.29	0.68	148.8						
E-2-4			0.27	0.63	720.0[2]						
E-2-6	215	1.0	0.29	NA[3]	0.2	0.26	0.07	0.87	NA	NA	NA
E-2-7			0.24	NA	3.8						
E-2-9			0.21	NA	6.3						
E-2-10			0.19	NA	301.2[2]						
E-2-11			0.21	NA	56.3						
E-2-12	125	2.0	0.39	NA	62.8	0.43	0.03	0.86	NA	NA	NA
E-2-13			0.42	NA	10.8						
E-2-14			0.36	NA	224.8						
E-2-15			0.44	NA	0.2						
E-3-1	107	2.1	0.31	0.73	216.8	0.44	0.07	0.96	1.02	0.07	0.96
E-3-2			0.44	1.02	1.3						
E-3-3			0.36	0.84	11.8						
E-3-4			0.33	0.77	37.3						
E-5-1	125	2.2	0.39	0.92	0.8	0.37	0.10	0.97	0.87	0.10	0.97
E-5-2			0.35	0.83	1.7						
E-5-3			0.35	0.83	1.7						
E-5-4			0.31	0.74	2.8						
E-5-5			0.22	0.51	208.8						
E-5-6			0.26	0.62	25.7						
F-1-1	120	2.6	0.30	0.87	0.8	0.29	0.11	0.98	0.84	0.11	0.98
F-1-2			0.20	0.57	58.2						
F-1-3			0.24	0.71	5.3						
F-1-4			0.18	0.52	41.3						
F-1-5			0.15	0.42	716.8						

F-1-6			0.15	0.46	715.5[2]						
F-1-7			0.20	0.61	17.3						
F-1-8	350	1.0	0.23	0.70	3.2	0.26	0.13	0.83	0.81	0.13	0.83
F-1-9			0.18	0.55	15.2						
F-1-10			0.18	0.55	17.2						
F-2-1			0.29	0.85	0.8						
F-2-2			0.21	0.62	19.2						
F-2-3	150	2.4	0.19	0.54	22.2	0.29	0.15	0.93	0.85	0.15	0.93
F-2-4			0.15	0.45	63.3						
F-2-5			0.22	0.65	5.2						
F-2-6			0.14	0.39	82.2						
F-3-1			0.25	0.68	1.7						
F-3-2			0.22	0.61	4.8						
F-3-3	158	2.7	0.16	0.45	104.7	0.30	0.14	0.89	0.83	0.14	0.89
F-3-4			0.30	0.81	1.8						
F-3-5			0.19	0.53	32.7						
F-3-7			0.35	0.96	0.7						

[1]Number of loading cycles to generate γ_{SA} = 3.75%.

[2]These specimens did not reach the target shear strain amplitude (γ_{SA} = 3.75%) for the stated number of loading cycles.

[3]Not available.

Table S5. Calculated metrics describing the hysteretic behavior of test specimens, computed for the cycle corresponding γ= 3% and last cycle of loading.

Test Designation	$\Delta\tau_{cyc}$[1]/$\tau_{cyc,max}$[2]		$G_{tan,min}$[3]/$\tau_{cyc,max}$		θ[4] (deg.)		$r_{u,max}$[5] (%)	
	N_{max}	$N_{\gamma=3\%}$	N_{max}	$N_{\gamma=3\%}$	N_{max}	$N_{\gamma=3\%}$	N_{max}	$N_{\gamma=3\%}$
A-BL-2	0.82	1.01	0.18	8.38	32	5	98	84
A-BL-3	0.71	0.85	0.04	12.01	25	5	100	79
A-BL-5	0.74	1.03	1.93	9.74	27	6	96	62
B-13-15	0.76	0.81	0.86	17.51	25	4	92	49
B-13-18	0.80	0.82	8.36	20.33	12	4	82	62
B-13-19	0.78	0.68	8.11	20.83	11	5	87	66
B-13-20	1.05	0.77	6.86	13.24	11	5	88	79
B-14-8	0.44	0.54	1.02	15.71	12	5	96	79
B-14-9	0.43	0.53	0.37	22.13	13	5	97	78
B-14-14	0.90	0.61	2.63	21.04	50	5	89	47
B-14-17	0.58	0.52	6.89	17.22	8	5	80	46
B-14-22	0.54	0.54	2.95	25.93	7	5	92	62
D-2-5	0.61	0.82	1.64	2.83	38	34	82	11
D-2-15	0.75	0.70	3.91	19.52	19	7	90	63
D-2-19	0.97	0.90	2.39	23.57	37	5	82	20
D-2-31	0.70	0.61	8.56	22.50	8	5	83	58
E-1-1	0.56	1.05	0.95	15.17	21	8	89	34
E-1-2	0.57	0.87	0.46	16.69	24	15	94	72
E-1-3	0.58	0.83	0.43	13.76	18	10	97	81
E-1-4	0.58	0.75	0.00	6.08	16	9	98	93
E-2-1	0.65	0.76	4.33	24.88	14	6	85	32
E-2-2	0.65	0.92	3.00	18.89	17	12	85	13
E-2-3	0.75	0.63	4.06	24.91	14	4	85	58
E-3-1	0.56	0.60	7.67	22.92	6	4	86	60
E-3-2	1.00	0.76	1.26	20.41	23	8	79	8
E-3-3	1.00	0.63	2.71	24.51	33	4	84	41
E-3-4	0.77	0.69	5.75	23.95	11	5	79	50
E-5-1	0.63	0.91	3.43	19.59	12	6	90	34
E-5-2	0.64	0.87	2.42	23.14	15	9	90	32
E-5-3	0.65	0.83	2.51	24.09	16	7	91	35
E-5-4	0.71	0.66	2.94	28.85	18	6	90	46
E-5-6	0.70	0.57	1.70	23.53	17	3	94	71
F-1-1	0.45	0.95	0.58	14.26	17	14	96	51
F-1-2	0.65	0.60	1.01	10.93	13	8	96	89
F-1-3	0.46	0.70	0.74	14.95	18	11	96	76
F-1-4	0.47	0.61	0.00	10.18	14	8	98	90
F-2-1	0.43	0.91	0.49	14.80	14	12	96	49
F-2-2	0.54	0.57	1.50	13.98	15	5	97	86
F-2-3	0.54	0.76	1.01	22.62	10	5	99	80
F-2-4	0.42	0.57	0.41	9.07	12	6	99	93
F-2-5	0.39	0.66	0.81	14.25	11	9	98	79
F-2-6	0.47	0.60	0.00	10.12	16	7	99	93
F-3-1	0.61	0.78	3.63	21.67	17	8	90	56
F-3-2	0.74	0.66	3.98	26.79	17	5	90	59
F-3-3	0.50	0.58	0.63	19.78	15	5	98	89
F-3-4	0.50	0.69	1.75	19.57	14	5	92	48
F-3-5	0.48	0.60	1.72	22.64	9	5	93	76

[1] $\Delta\tau_{cyc}$: Difference in cyclic shear stress at γ= 0.
[2] $\tau_{cyc,max}$: Maximum cyclic shear stress.
[3] $G_{tan,min}$: Minimum tangent shear modulus.
[4] Angle prior to shear stress reversal.
[5] Maximum excess pore pressure ratio.

Table S6. Examination of liquefaction and cyclic softening susceptibility of intact specimens subjected to constant-volume, stress-controlled cyclic tests.

Test Designation	OCR	PI	FC (%)	w_n/LL	LI	CSR	N_{max}[1]	γ_{max}[2] (%)	$r_{u,max}$[3] (%) at:		BI06[4]	BS06[5]	AM16[6]	Hysteretic Behavior Observed for:	
									$\gamma =$ 3%, 3.75%	N_{max}				$\gamma =$ 3%, 3.75%	N_{max}
A-BL-2	4.2	10	82	1.44	2.81	0.30	56	8.3	84 - 88	98	Clay-Like	S[9]	CS	Clay-Like	Sand-Like
A-BL-3		11	77	1.39	2.42	0.37	18	9.2	79 - 85	100	Clay-Like	S	CS	Clay-Like	Sand-Like
A-BL-5		19	92	1.06	1.14	0.44	9	10.2	62 - 62	96	Clay-Like	NS[10]	CS	Clay-Like	Sand-Like
B-13-15	1.9	16	91	1.08	1.23	0.44	17	11.5	49 - 65	92	Clay-Like	MS	CS	Clay-Like	Clay-Like
B-13-18		15	94	1.12	1.38	0.39	13	5.1	62 - 73	82	Clay-Like	MS	CS	Clay-Like	Clay-Like
B-13-19		14	95	1.11	1.40	0.33	19	5.4	66 - 75	87	Clay-Like	MS	CS	Clay-Like	Clay-Like
B-13-20		15	94	1.22	1.71	0.31	87	5.2	79 - 84	88	Clay-Like	MS	CS	Clay-Like	Clay-Like
B-14-8	1.5	13	81	0.95	0.83	0.24	38	10.9	79 - 85	96	Clay-Like	MS	CS	Clay-Like	Sand-Like
B-14-9		11	80	0.99	0.98	0.21	53	12.7	78 - 85	97	Clay-Like	S	CS	Clay-Like	Sand-Like
B-14-14		15	99	0.96	0.89	0.27	10	17.5	47 - 63	88	Clay-Like	MS	CS	Clay-Like	Clay-Like
B-14-17		13	NA[11]	0.98	0.93	0.27	8	5.9	46 - 63	80	Clay-Like	MS	CS	Clay-Like	Clay-Like
B-14-22		13	98	0.94	0.81	0.26	26	8.5	62 - 74	92	Clay-Like	MS	CS	Clay-Like	Clay-Like
D-2-5	2.1	14	76	1.26	1.71	0.47	2	18.7	11 - 14	82	Clay-Like	MS	CS	Clay-Like	Clay-Like
D-2-15	1.9	28	99	1.24	1.57	0.27	223	7.3	63 - 70	90	Clay-Like	NS	CS	Clay-Like	Clay-Like
D-2-19		26	99	1.10	1.31	0.36	19	18.4	20 - 44	78	Clay-Like	NS	CS	Clay-Like	Clay-Like
D-2-31	2.0	28	99	1.25	1.61	0.30	297	5.6	36 - 42	83	Clay-Like	NS	CS	Clay-Like	Clay-Like
E-1-1	2.0	12	94	1.06	1.23	0.30	6	12.6	34 - 36	89	Clay-Like	MS	CS	Clay-Like	Sand-Like
E-1-2		10	87	1.03	1.13	0.24	16	12.4	72 - 77	94	Clay-Like	S	CS	Clay-Like	Sand-Like
E-1-3		10	89	1.07	1.29	0.19	29	9.3	81 - 86	97	Clay-Like	S	CS	Clay-Like	Sand-Like
E-1-4		12	100	1.07	1.23	0.15	182	8.2	93 - 95	98	Clay-Like	MS	CS	Intermediate	Sand-Like
E-2-1		26	99	0.99	0.96	0.36	40	10.6	32 - 40	85	Clay-Like	NS	CS	Clay-Like	Clay-Like
E-2-2		28	99	0.93	0.79	0.40	17	11.4	13 – 28	85	Clay-Like	NS	CS	Clay-Like	Clay-Like
E-2-3		28	99	1.01	1.04	0.29	587	9.5	58 - 69	85	Clay-Like	NS	CS	Clay-Like	Clay-Like
E-3-1	2.1	24	99	1.05	1.19	0.31	677	5.6	60 - 70	86	Clay-Like	NS	CS	Clay-Like	Clay-Like
E-3-2		27	99	1.11	1.31	0.44	18	12.9	8 - 34	79	Clay-Like	NS	CS	Clay-Like	Clay-Like
E-3-3		27	99	0.90	0.70	0.36	161	12.2	41 - 56	84	Clay-Like	NS	CS	Clay-Like	Clay-Like
E-3-4		24	94	1.06	1.17	0.33	191	7.5	50 - 61	79	Clay-Like	NS	CS	Clay-Like	Clay-Like
E-5-1	2.2	15	100	0.88	0.64	0.39	7	10.8	34 - 35	90	Clay-Like	MS	CS	Clay-Like	Clay-Like
E-5-2		15	99	0.88	0.64	0.35	9	13.0	32 - 55	90	Clay-Like	MS	CS	Clay-Like	Clay-Like
E-5-3		15	100	1.00	0.99	0.35	8	12.1	35 - 58	91	Clay-Like	MS	CS	Clay-Like	Clay-Like
E-5-4		15	99	1.00	0.99	0.31	13	12.7	46 - 57	90	Clay-Like	MS	CS	Clay-Like	Clay-Like

E-5-6		15	98	0.95	0.88	0.26	58	11.3	71 - 78	94	Clay-Like	MS	CS	Clay-Like	Clay-Like
F-1-1	2.6	0	63	NP[12]	NP	0.30	3	12.8	51 - 51	96	Sand-Like	S	LT[13]	Clay-Like	Sand-Like
F-1-2		0	62	NP	NP	0.20	69	10.4	89 - 92	96	Sand-Like	S	LT	Intermediate	Sand-Like
F-1-3		0	47	NP	NP	0.24	12	11.2	76 - 83	96	Sand-Like	S	LT	Clay-Like	Sand-Like
F-1-4		0	47	NP	NP	0.18	54	9.9	90 - 92	98	Sand-Like	S	LT	Intermediate	Sand-Like
F-2-1	2.4	6	44	1.25	2.30	0.29	4	12.2	49 - 49	96	Sand-Like	S	LT	Clay-Like	Sand-Like
F-2-2		6	48	1.25	2.30	0.21	30	11.4	86 - 89	97	Sand-Like	S	LT	Clay-Like	Sand-Like
F-2-3		3	38	1.08	1.72	0.19	35	11.5	80 - 87	99	Sand-Like	S	LT	Clay-Like	Sand-Like
F-2-4		3	30	1.13	2.22	0.15	77	10.6	93 - 95	99	Sand-Like	S	LT	Intermediate	Sand-Like
F-2-5		0	36	NP	NP	0.22	11	10.8	79 - 87	98	Sand-Like	S	LT	Clay-Like	Sand-Like
F-2-6		0	29	NP	NP	0.14	93	9.8	93 - 96	99	Sand-Like	S	LT	Intermediate	Sand-Like
F-3-1	2.7	11	62	0.81	0.35	0.25	6	10.0	56 - 56	90	Clay-Like	MS	CS	Clay-Like	Clay-Like
F-3-2		11	60	0.81	0.35	0.22	16	10.2	59 - 65	90	Clay-Like	MS	LT	Clay-Like	Clay-Like
F-3-3		4	51	0.91	0.20	0.16	125	11	89 - 92	98	Sand-Like	S	LT	Clay-Like	Sand-Like
F-3-4		4	73	0.91	0.20	0.30	7	11.4	48 - 61	92	Sand-Like	S	LT	Clay-Like	Sand-Like
F-3-5		4	83	1.00	1.02	0.19	53	9.1	76 - 81	93	Sand-Like	S	LT	Clay-Like	Sand-Like

[1] Maximum number of loading cycles.
[2] Maximum single amplitude shear strain.
[3] Maximum excess pore pressure ratio.
[4] Liquefaction and cyclic softening susceptibility criterion proposed by Boulanger and Idriss (2006).
[5] Liquefaction and cyclic softening susceptibility criterion proposed by Bray and Sancio (2006).
[6] Framework suggested by Armstrong and Malvick (2016) for assessing cyclic response of soil.
[7] Moderately susceptible to liquefaction.
[8] Cyclic softening.
[9] Susceptible to liquefaction.
[10] Non-susceptible to liquefaction.
[11] Not available.
[12] Nonplastic.
[13] Liquefaction triggering

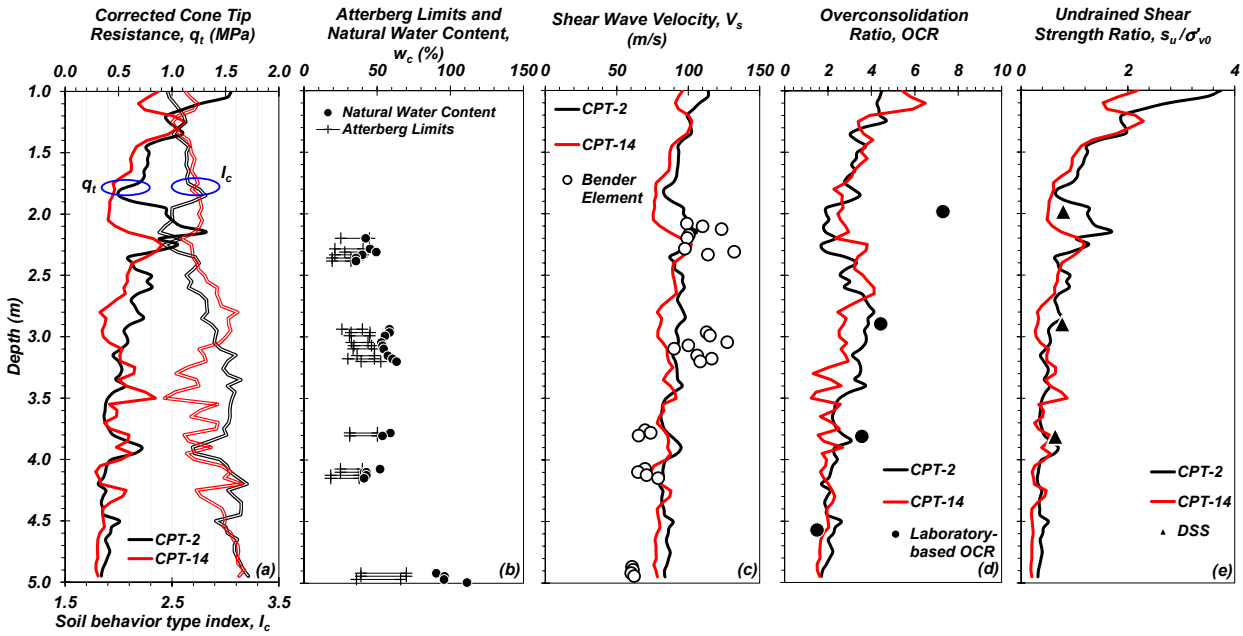

Fig. S1. Subsurface characterization of the natural silt deposit at Site A-UT indicating: (a) corrected cone tip resistance, q_t, and soil behavioral type index, I_c, (b) Atterberg limits and water content (including nearby split-spoon samples), and comparison of laboratory-based and *in-situ* tests: (c) shear wave velocity (correlation according to Andrus et al. 2007), (d) overconsolidation ratio (correlation according to Mayne et al. 2009), and (e) undrained shear strength ratio (correlation according to Mayne and Peuchen 2018).

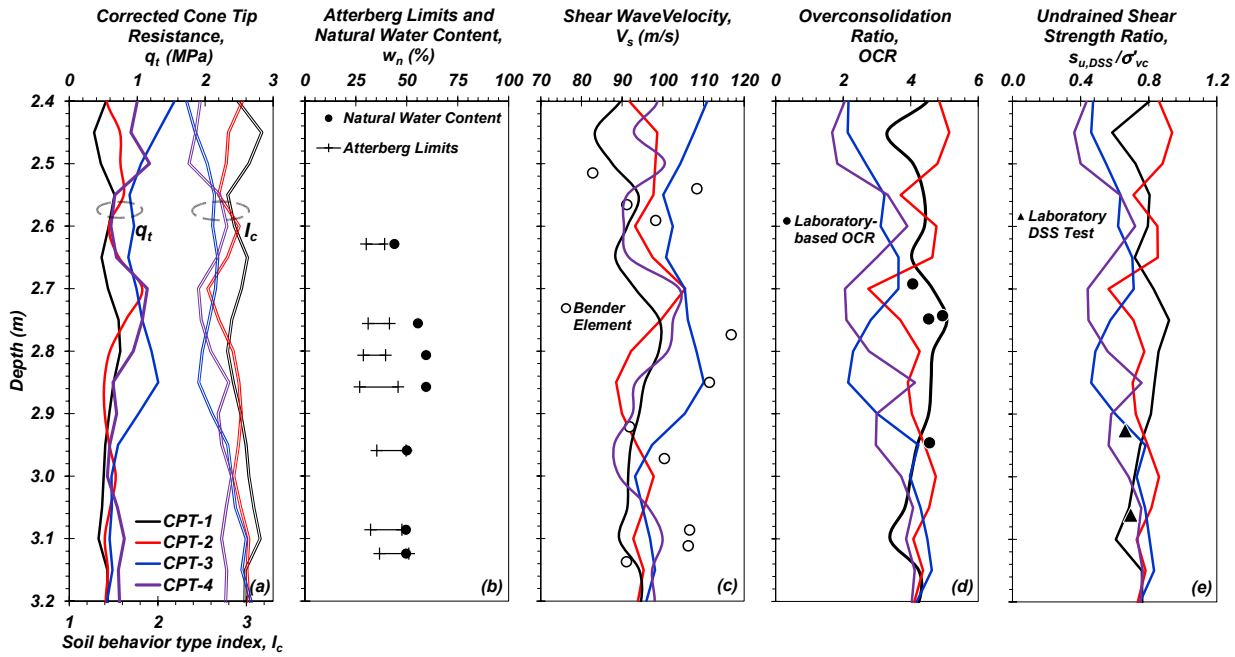

Fig. S2. Subsurface characterization of the natural silt deposit at Site A-BL indicating: (a) corrected cone tip resistance, q_t, and soil behavioral type index, I_c, (b) Atterberg limits and water content, and comparison of laboratory-based and *in-situ* tests: (c) shear wave velocity (correlation according to Andrus et al. 2007), (d) overconsolidation ratio (correlation according to Mayne et al. 2009), and (e) undrained shear strength ratio (correlation according to Rix et al. 2019).

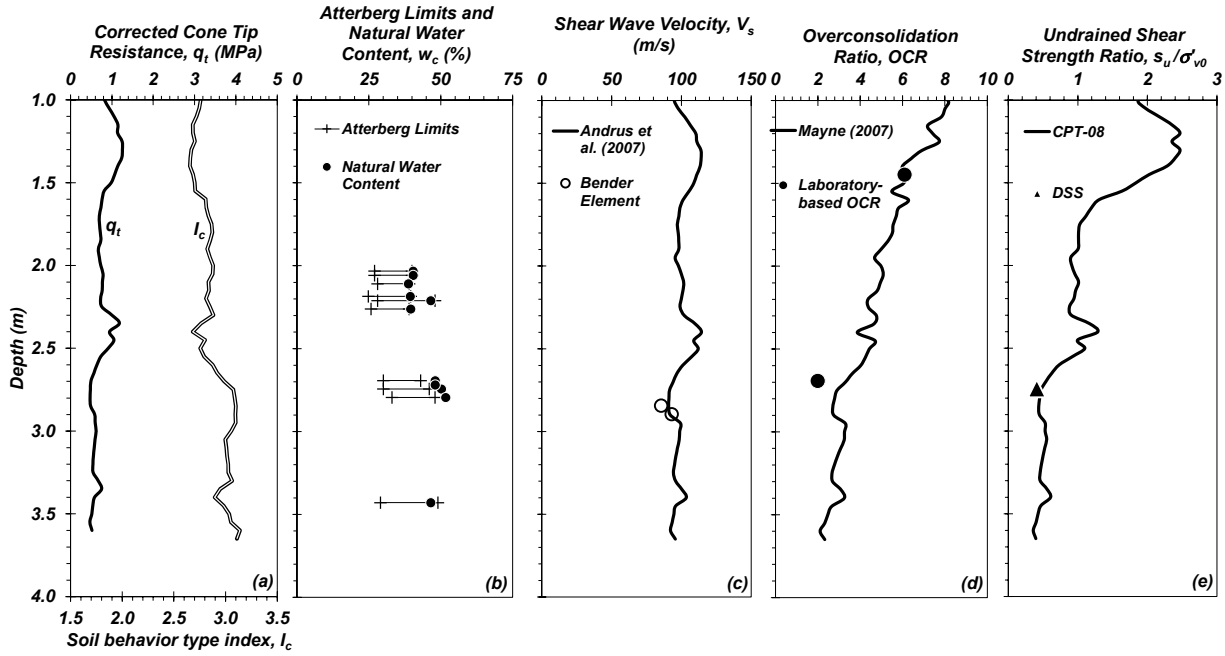

Fig. S3. Subsurface characterization of the natural silt deposit at Site B indicating: (a) corrected cone tip resistance, q_t, and soil behavioral type index, I_c, (b) Atterberg limits and water content, and comparison of laboratory-based and *in-situ* tests: (c) shear wave velocity (correlation according to Andrus et al. 2007), (d) overconsolidation ratio (correlation according to Mayne et al. 2009), and (e) undrained shear strength ratio (correlation according to Mayne and Peuchen 2018).

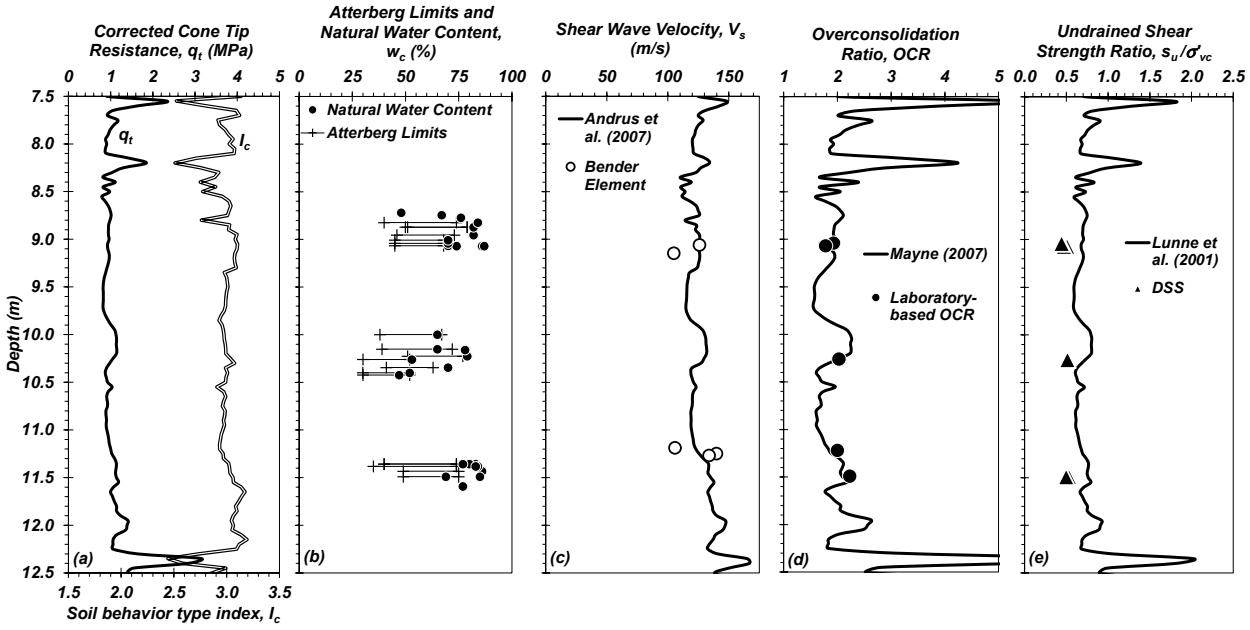

Fig. S4. Subsurface characterization of the natural silt deposit at Site D indicating: (a) corrected cone tip resistance, q_t, and soil behavioral type index, I_c, (b) Atterberg limits and water content, and comparison of laboratory-based and *in-situ* tests: (c) shear wave velocity (correlation according to Andrus et al. 2007), (d) overconsolidation ratio (correlation according to Mayne et al. 2009), and (e) undrained shear strength ratio (site-specific N_k = 10; Jana and Stuedlein 2021).

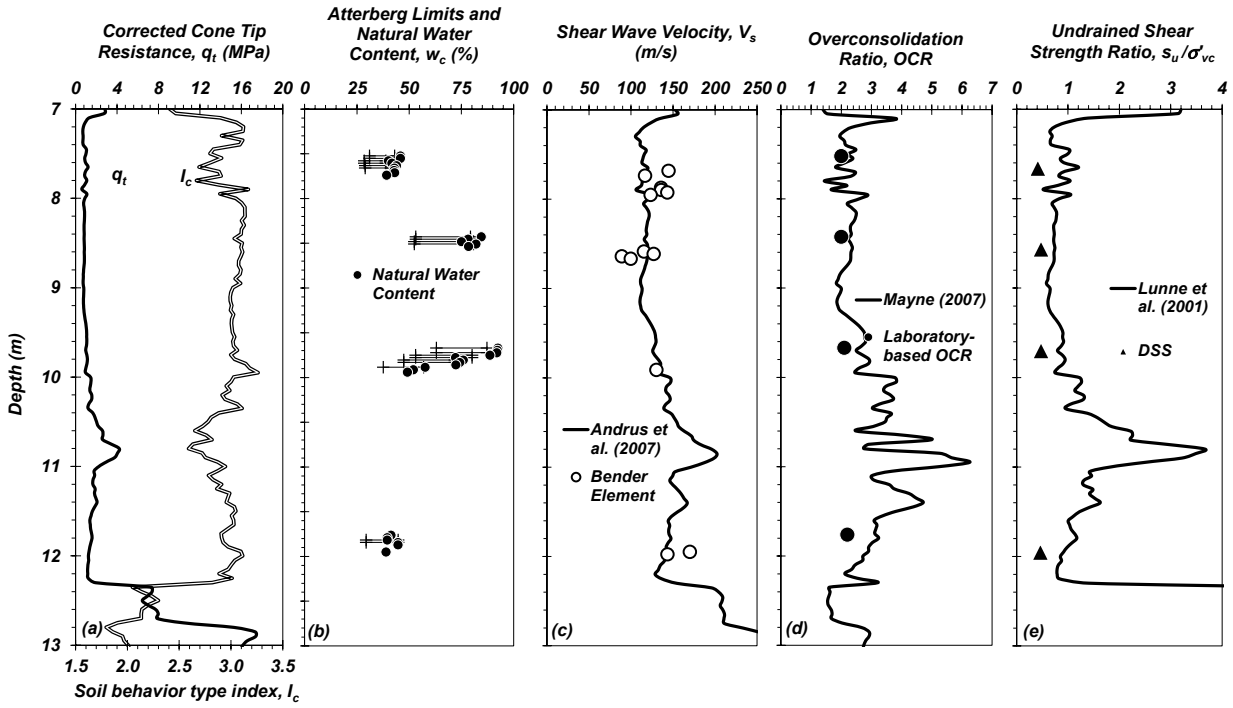

Fig. S5. Subsurface characterization of the natural silt deposit at Site E indicating: (a) corrected cone tip resistance, q_t, and soil behavioral type index, I_c, (b) Atterberg limits and water content, and comparison of laboratory-based and *in-situ* tests: (c) shear wave velocity (correlation according to Andrus et al. 2007), (d) overconsolidation ratio (correlation according to Mayne et al. 2009), and (e) undrained shear strength ratio (site-specific N_k = 10; Jana and Stuedlein 2021).

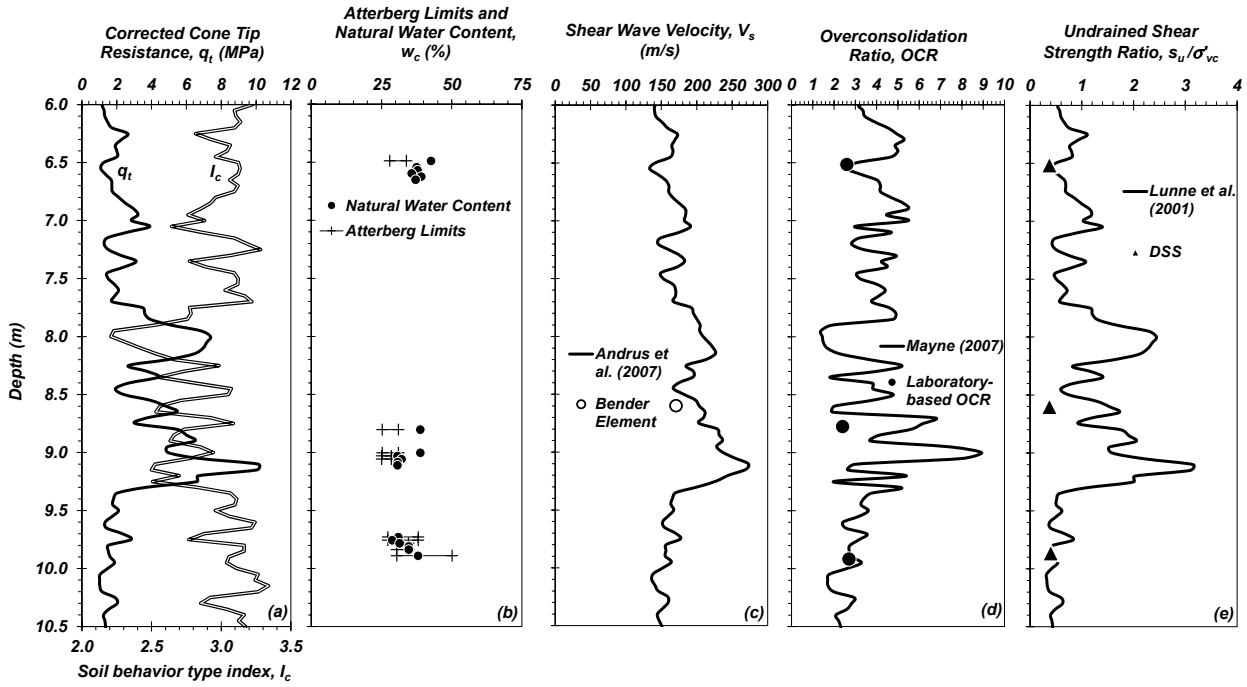

Fig. S6. Subsurface characterization of the natural silt deposit at Site F indicating: (a) corrected cone tip resistance, q_t, and soil behavioral type index, I_c, (b) Atterberg limits and water content, and comparison of laboratory-based and *in-situ* tests: (c) shear wave velocity (correlation according to Andrus et al. 2007), (d) overconsolidation ratio (correlation according to Mayne et al. 2009), and (e) undrained shear strength ratio (correlation according to Mayne and Peuchen 2018).

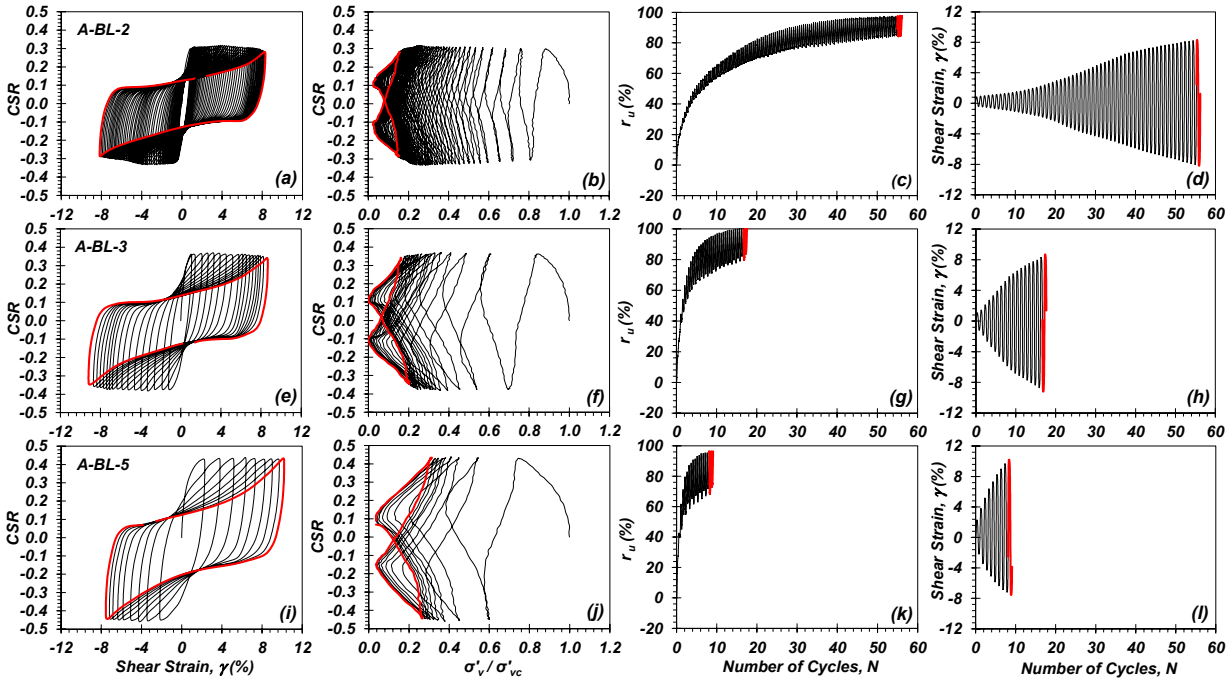

Figure S7. Constant-volume, stress-controlled, cyclic response of intact specimens indicating cyclic shear stress-shear strain, *CSR* - γ, hysteresis (a, e, and i), effective stress path (b, f, and, j), generation of excess pore pressure, r_u, (c, g, and k), and accumulation of shear strain, γ, with number of loading cycles, *N* (d, h, and l): (a - d) Specimen A-BL-2, (e - h) Specimen A-BL-3, and (i - l) Specimen A-BL-5.

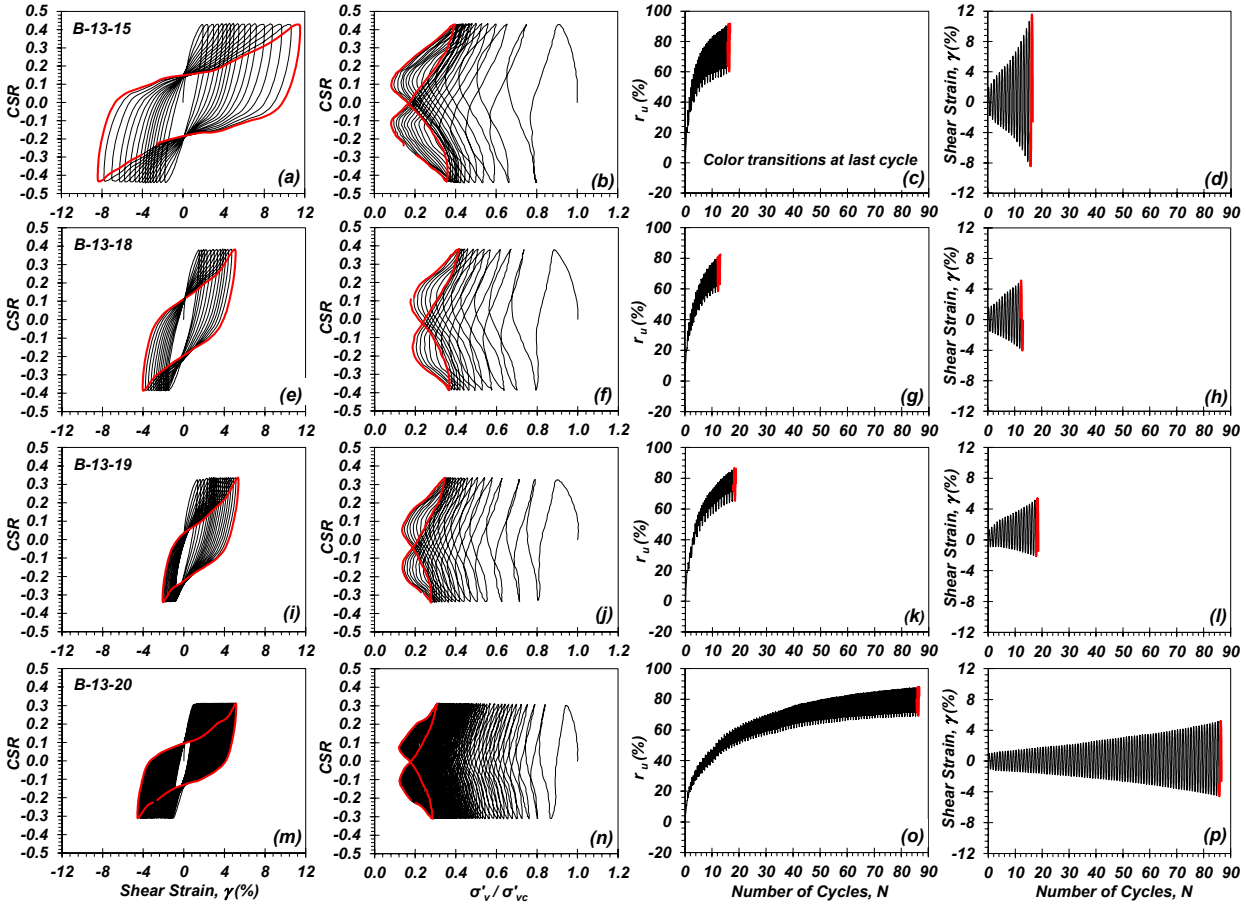

Figure S8. Constant-volume, stress-controlled, cyclic response of intact specimens indicating cyclic shear stress-shear strain, *CSR* - γ, hysteresis (a, e, i, and m), effective stress path (b, f, j, and n), generation of excess pore pressure, r_u, (c, g, k, and o), and accumulation of shear strain, γ, with number of loading cycles, *N* (d, h, l, and p): (a - d) Specimen B-13-15, (e - h) Specimen B-13-18, (i - l) Specimen B-13-19, and (m - p) Specimen B-13-20.

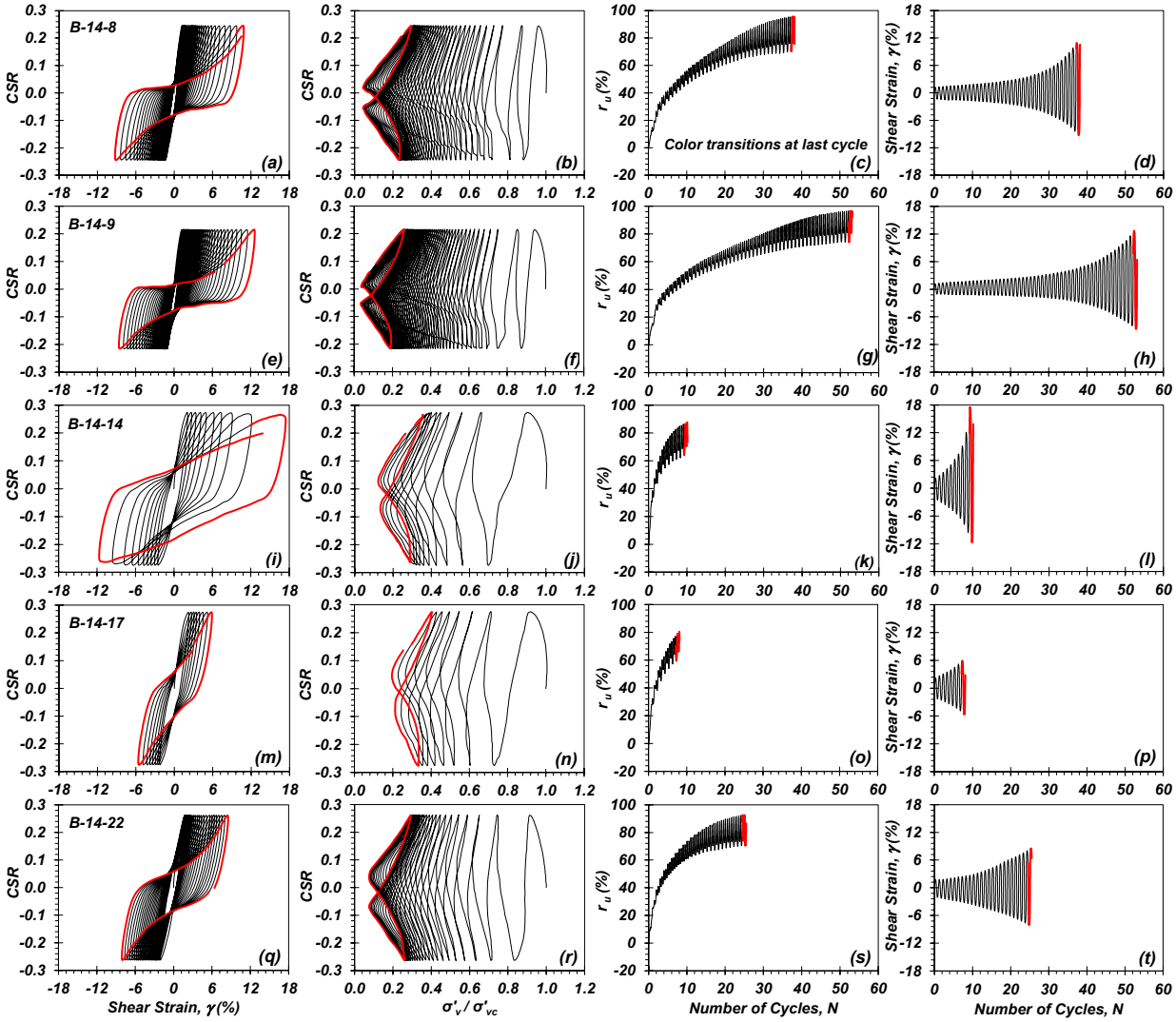

Figure S9. Constant-volume, stress-controlled, cyclic response of intact specimens indicating cyclic shear stress-shear strain, *CSR* - γ, hysteresis (a, e, i, m, and q), effective stress path (b, f, j, n, and r), generation of excess pore pressure, r_u, (c, g, k, o, and s), and accumulation of shear strain, γ, with number of loading cycles, N (d, h, l, p, and t): (a - d) Specimen B-14-8, (e - h) Specimen B-14-9, (i - l) Specimen B-14-14, (m - p) Specimen B-14-17, and (q - t) Specimen B-14-22.

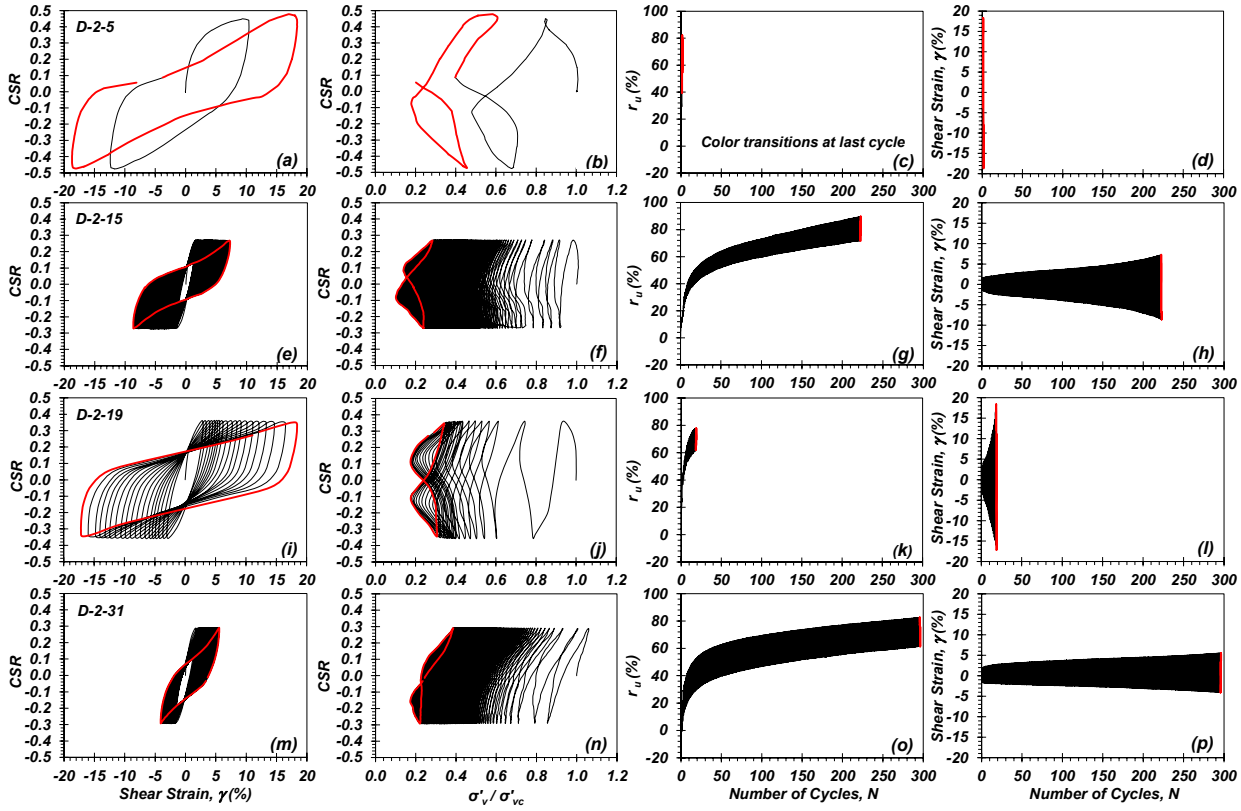

Figure S10. Constant-volume, stress-controlled, cyclic response of intact specimens indicating cyclic shear stress-shear strain, *CSR* - γ, hysteresis (a, e, i, and m), effective stress path (b, f, j, and n), generation of excess pore pressure, r_u, (c, g, k, and o), and accumulation of shear strain, γ, with number of loading cycles, *N* (d, h, l, and p): (a - d) Specimen D-2-5, (e - h) Specimen D-2-15, (i - l) Specimen D-2-19, and (m - p) Specimen D-2-31.

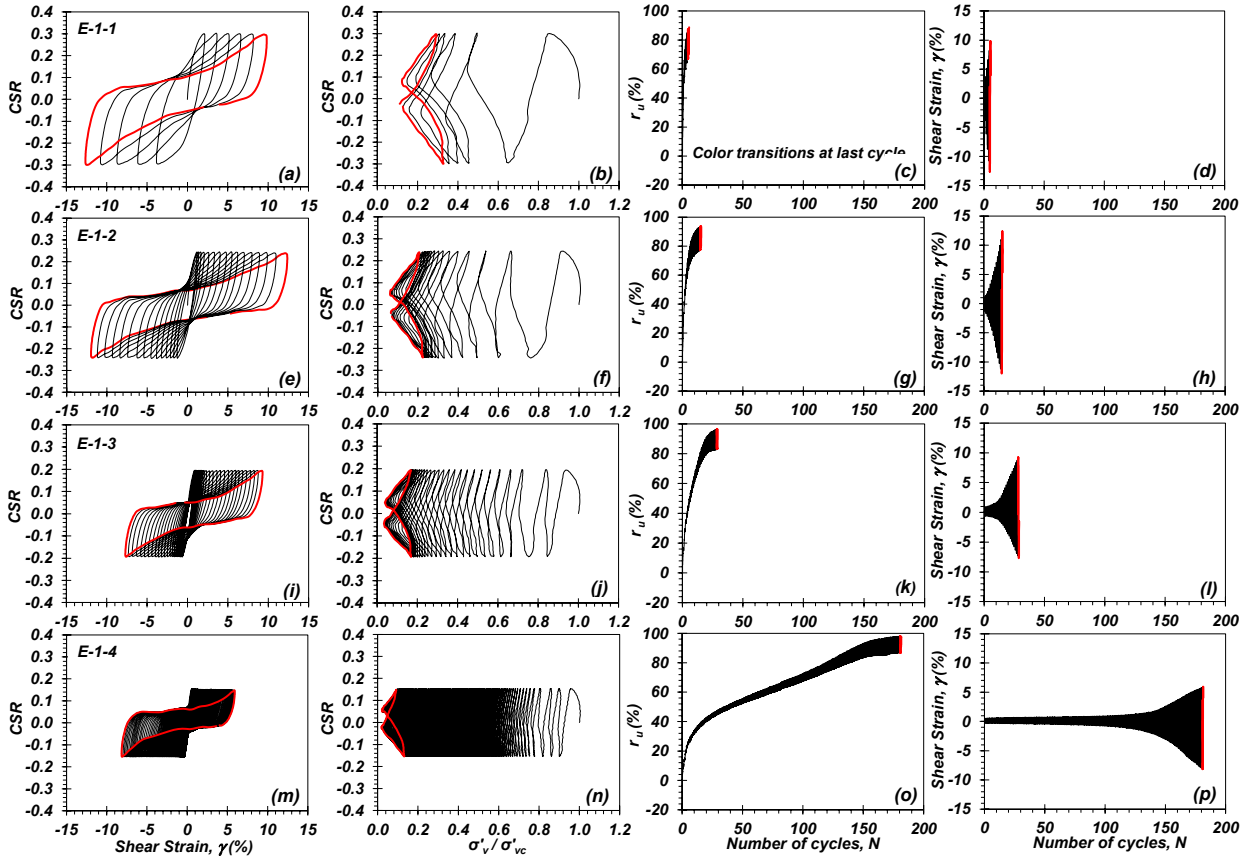

Figure S11. Constant-volume, stress-controlled, cyclic response of intact specimens indicating cyclic shear stress-shear strain, *CSR* - γ, hysteresis (a, e, i, and m), effective stress path (b, f, j, and n), generation of excess pore pressure, r_u, (c, g, k, and o), and accumulation of shear strain, γ, with number of loading cycles, N (d, h, l, and p): (a - d) Specimen E-1-1, (e - h) Specimen E-1-2, (i - l) Specimen E-1-3, and (m - p) Specimen E-1-4.

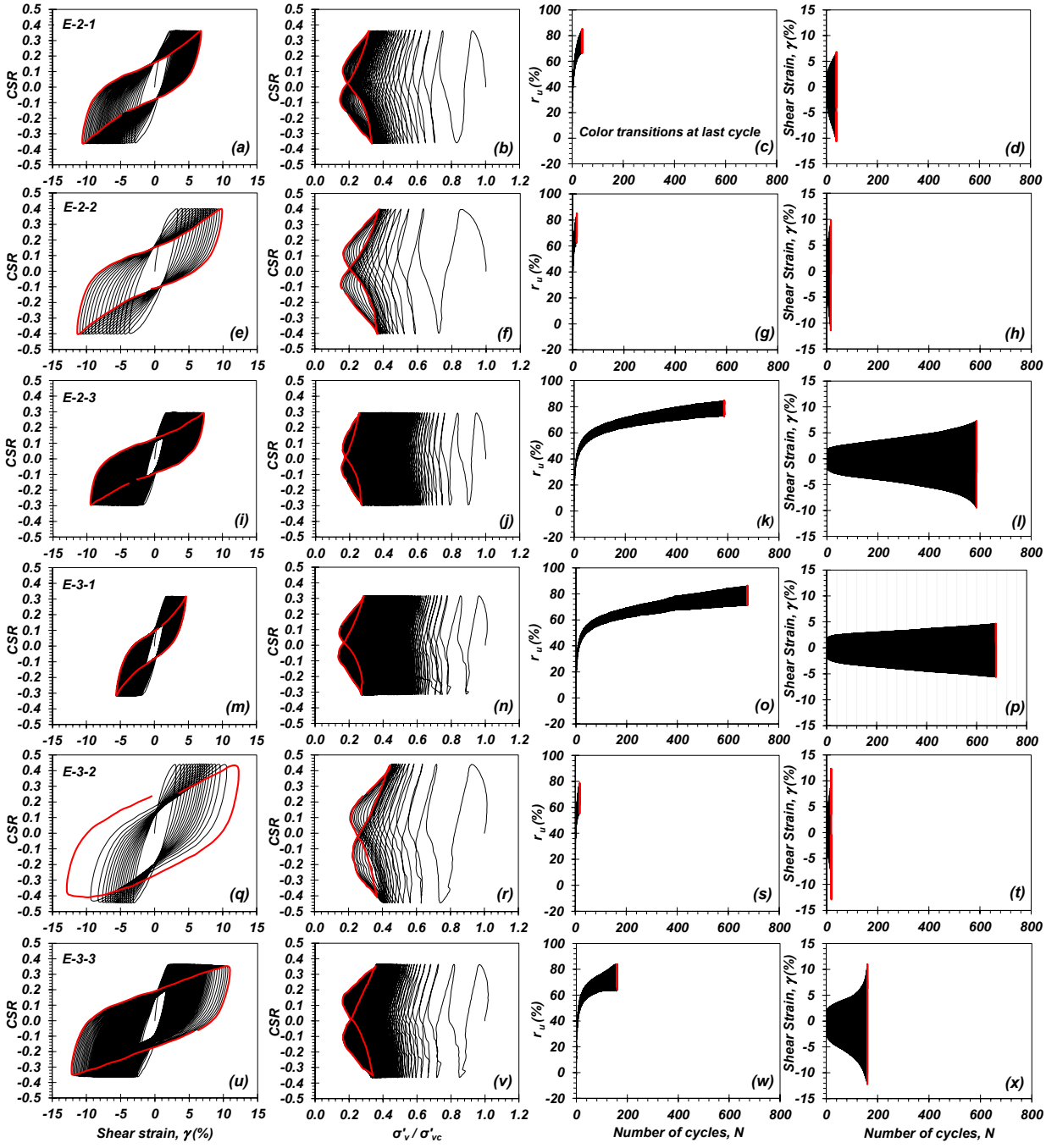

Figure S12. Constant-volume, stress-controlled, cyclic response of intact specimens indicating cyclic shear stress-shear strain, *CSR* - γ, hysteresis (a, e, i, m, q, and u), effective stress path (b, f, j, n, r, and v), generation of excess pore pressure, r_u, (c, g, k, o, s, and w), and accumulation of shear strain, γ, with number of loading cycles, *N* (d, h, l, p, t, and x): (a - d) Specimen E-2-1, (e - h) Specimen E-2-2, (i - l) Specimen E-2-3, (m - p) Specimen E-3-1, and (q - t) Specimen E-3-2, and (u - x) Specimen E-3-3.

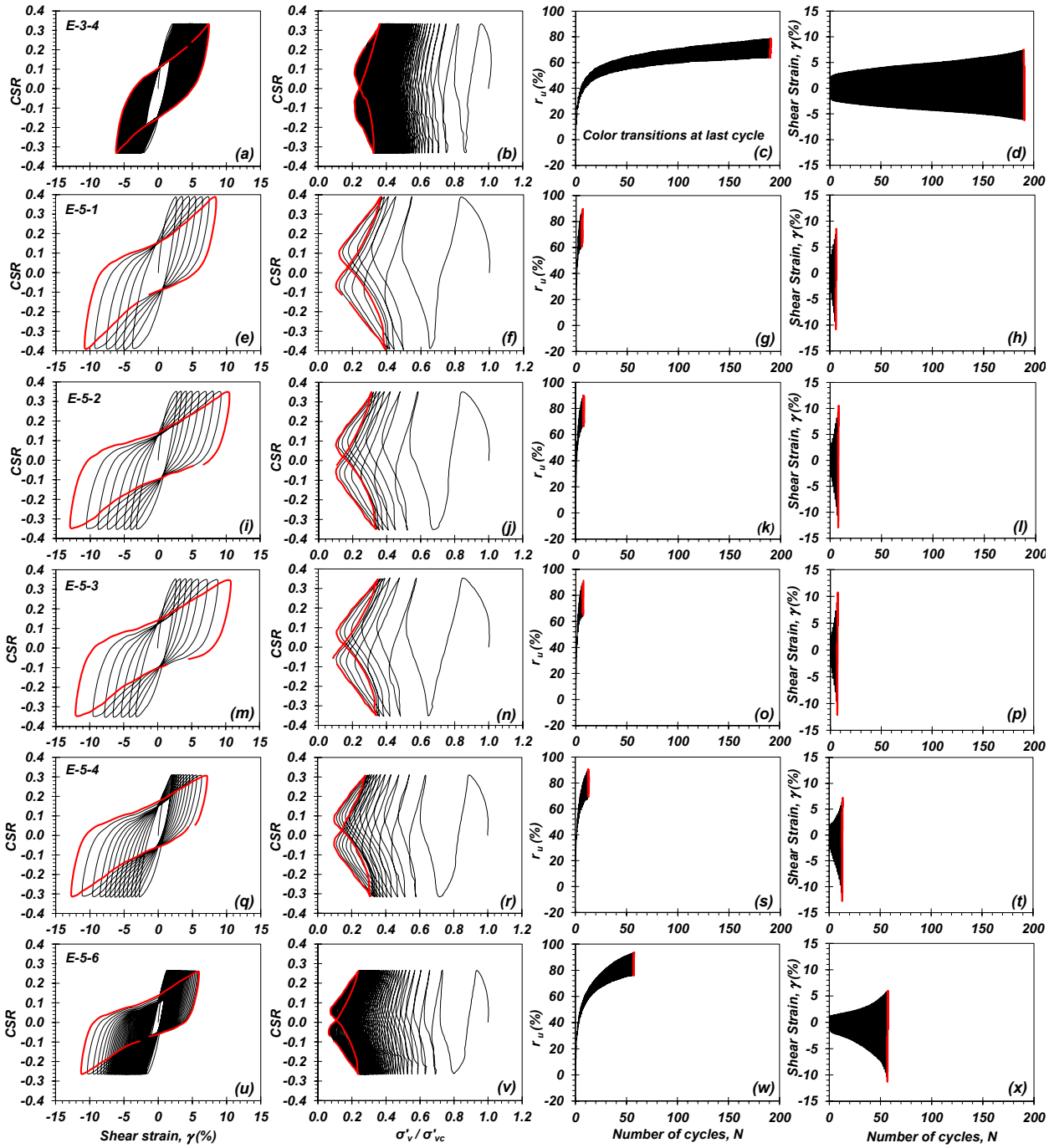

Figure S13. Constant-volume, stress-controlled, cyclic response of intact specimens indicating cyclic shear stress-shear strain, *CSR* - γ, hysteresis (a, e, i, m, q, and u), effective stress path (b, f, j, n, r, and v), generation of excess pore pressure, r_u, (c, g, k, o, s, and w), and accumulation of shear strain, γ, with number of loading cycles, *N* (d, h, l, p, t, and x): (a - d) Specimen E-3-4, (e - h) Specimen E-5-1, (i - l) Specimen E-5-2, (m - p) Specimen E-5-3, (q - t) Specimen E-5-4, and (u - x) Specimen E-5-6.

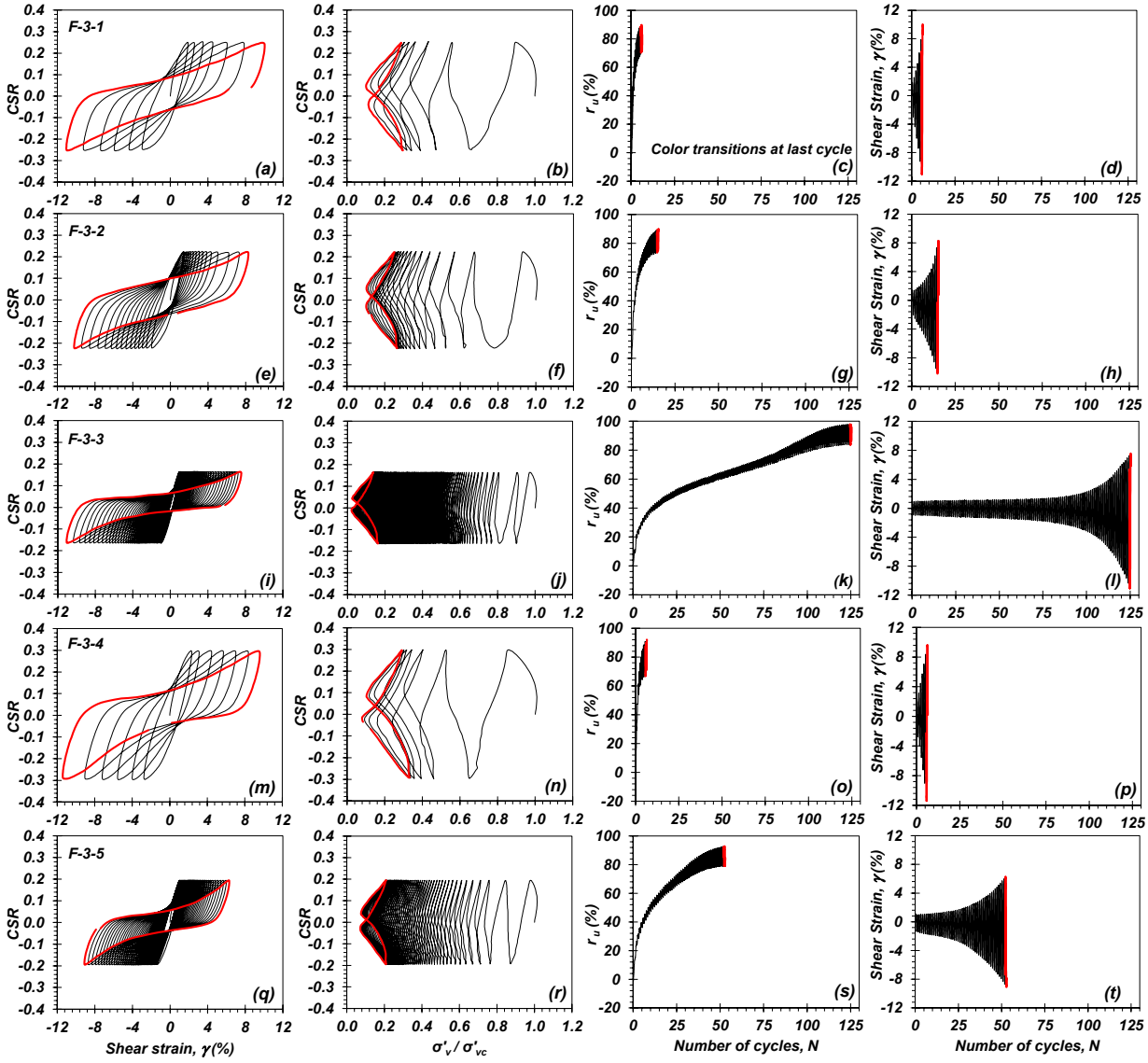

Figure S14. Constant-volume, stress-controlled, cyclic response of intact specimens indicating cyclic shear stress-shear strain, *CSR* - γ, hysteresis (a, e, i, m, and q), effective stress path (b, f, j, n, and r), generation of excess pore pressure, r_u, (c, g, k, o, and s), and accumulation of shear strain, γ, with number of loading cycles, N (d, h, l, p, and t): (a - d) Specimen F-3-1, (e - h) Specimen F-3-2, (i - l) Specimen F-3-3, (m - p) Specimen F-3-4, and (q - t) Specimen F-3-5.

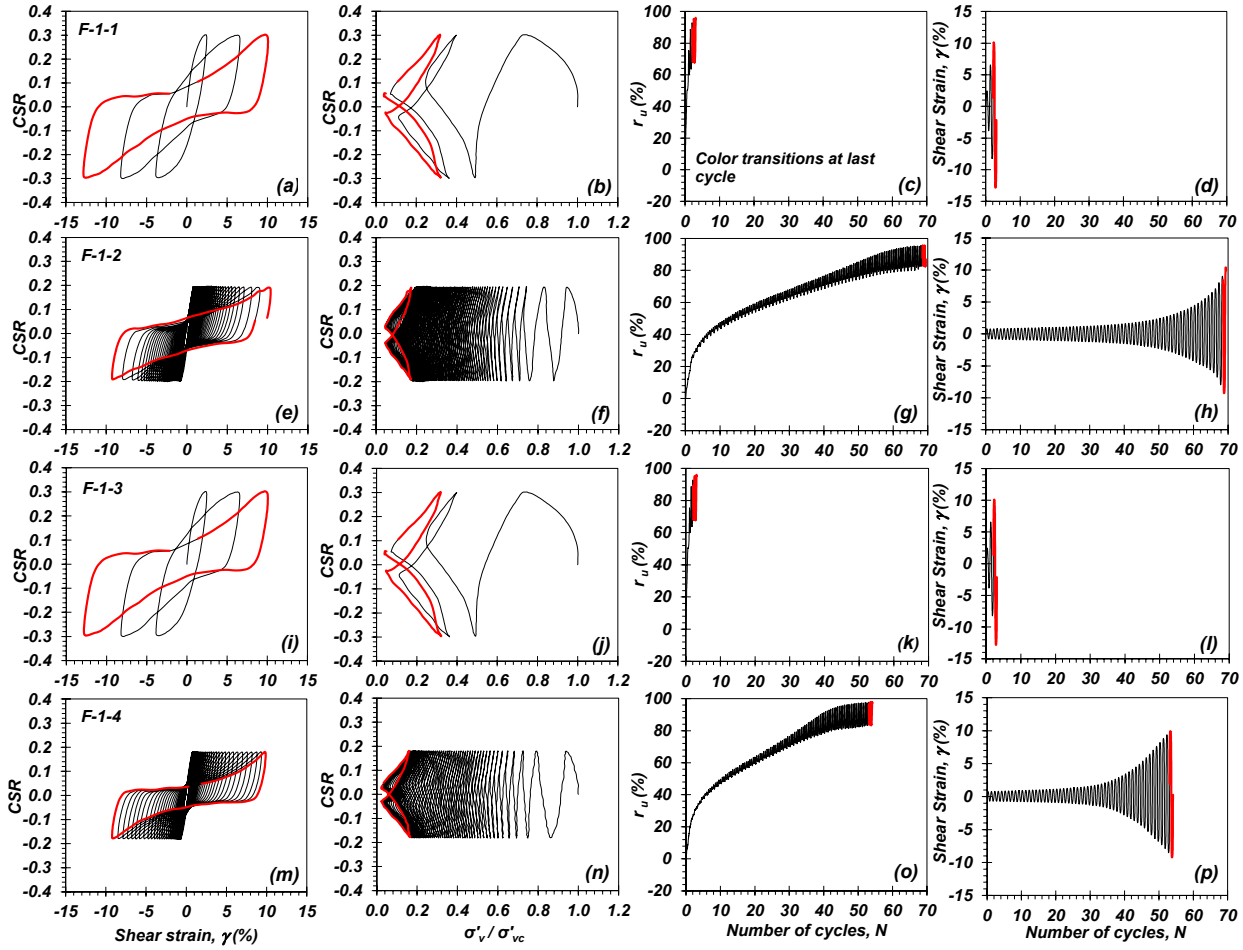

Figure S15. Constant-volume, stress-controlled, cyclic response of intact specimens indicating cyclic shear stress-shear strain, *CSR* - γ, hysteresis (a, e, i, and m), effective stress path (b, f, j, and n), generation of excess pore pressure, r_u, (c, g, k, and o), and accumulation of shear strain, γ, with number of loading cycles, *N* (d, h, l, and p): (a - d) Specimen F-1-1, (e - h) Specimen F-1-2, (i - l) Specimen F-1-3, and (m - p) Specimen F-1-4.

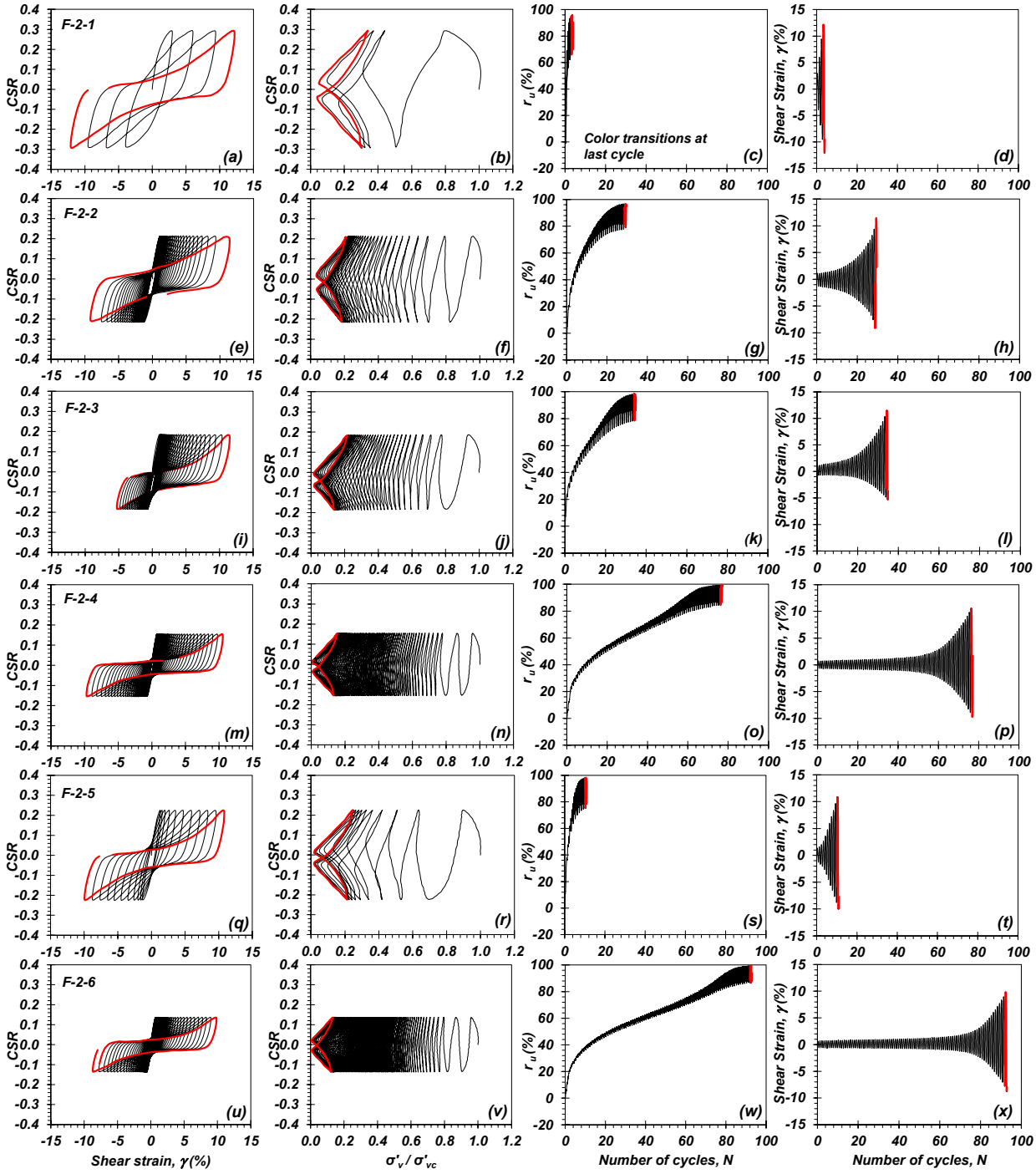

Figure S16. Constant-volume, stress-controlled, cyclic response of intact specimens indicating cyclic shear stress-shear strain, *CSR* - γ, hysteresis (a, e, i, m, q, and u), effective stress path (b, f, j, n, r, and v), generation of excess pore pressure, r_u, (c, g, k, o, s, and w), and accumulation of shear strain, γ, with number of loading cycles, *N* (d, h, l, p, t, and x): (a - d) Specimen F-2-1, (e - h) Specimen F-2-2, (i - l) Specimen F-2-3, (m - p) Specimen F-2-4, (q - t) Specimen F-2-5, and (u - x) Specimen F-2-6.

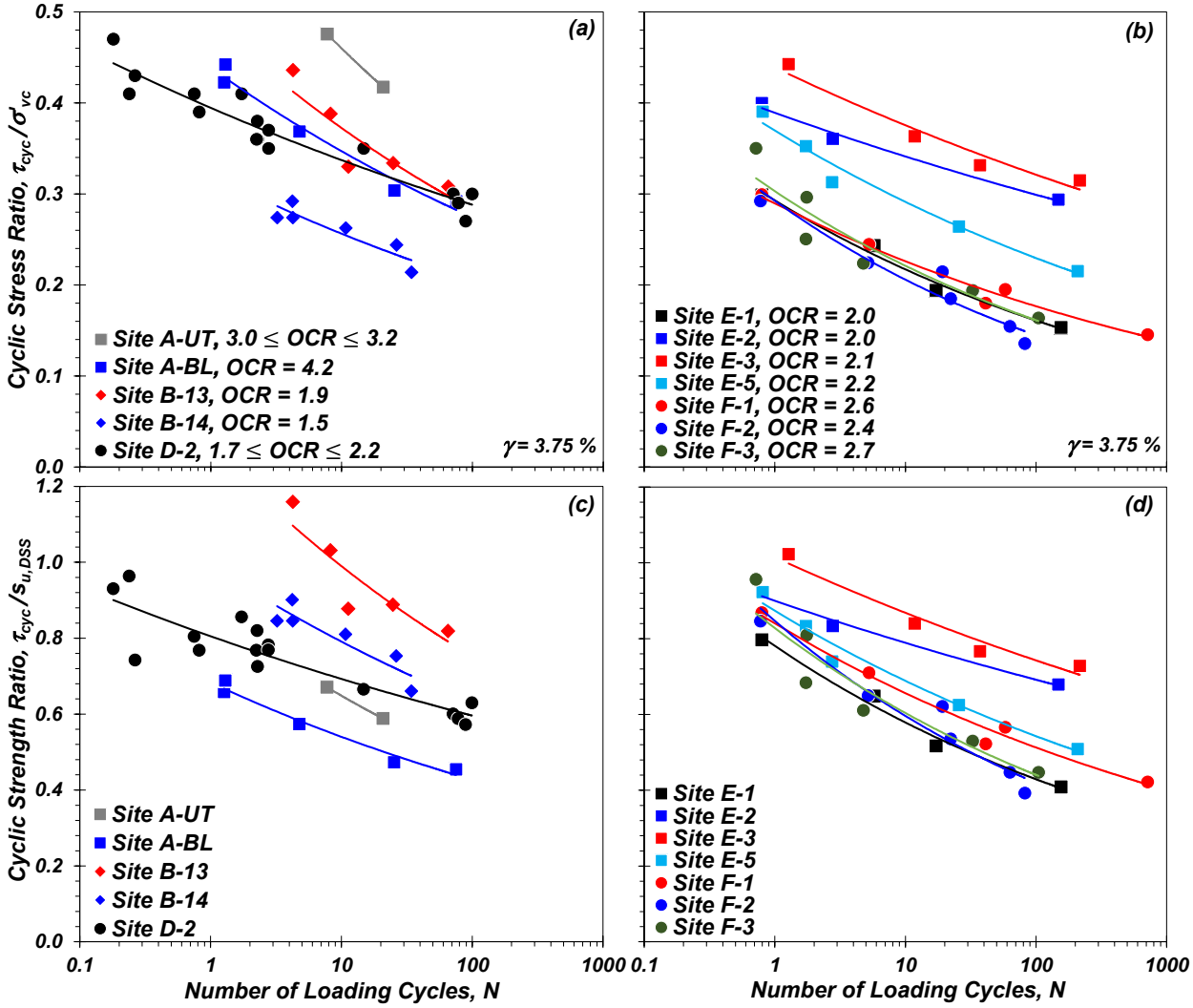

Figure S17. Comparison of the cyclic resistance of intact specimens from Sites A, B, D (a and c), and Sites E and F (b and d) indicating variation of: (a and b) cyclic stress ratio, *CSR*, and (c and d) cyclic strength ratio, $\tau_{cyc}/s_{u,DSS}$, with number of loading cycles, *N* to reach γ_{SA}= 3.75%.

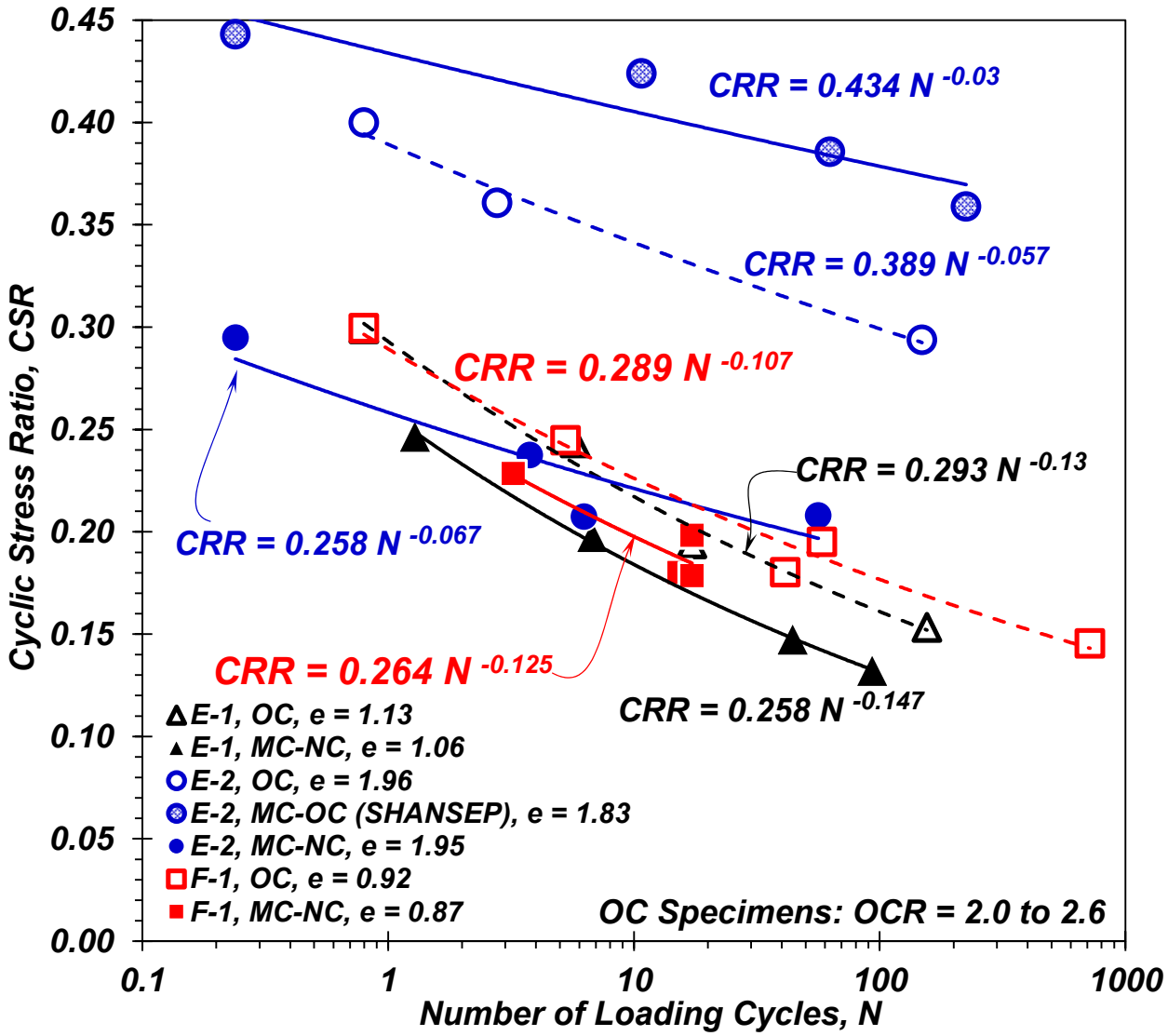

Fig. S18. Variation of the cyclic stress ratio, *CSR*, with number of loading cycles, *N*, for γ= 3.75% derived from constant-volume, stress-controlled, cyclic DSS tests conducted on natural, intact OC, MC-NC, and MC-OC specimens from Sites E and F.

REFERENCES

Andrus, R. D., Mohanan, N. P., Piratheepan, P., Ellis, B. S., and Holzer, T. L. (2007). "Predicting shear-wave velocity from cone penetration resistance." In *Proceeding of 4th Int. Conf Earthquake Geotechnical Engineering*, 1454. New York: Springer.

Armstrong, R. J., and Malvick, E. J. (2016). "Practical Considerations in the use of liquefaction susceptibility criteria." *Earthquake Spectra*, 32(3), 1941-1950.

Becker, D., Crooks, J., Been, K., and Jefferies, M. (1987). "Work as a criterion for determining in situ and yield stresses in clays." *Canadian Geotechnical Journal*, 24(4), 549-564.

Boulanger, R. W., and Idriss, I. M. (2006). "Liquefaction susceptibility criteria for silts and clays." *J. Geotch. Geoenv. Eng.*, (11), 1413-1426.

Bray, J. D., and Sancio, R.B. (2006). "Assessment of the liquefaction susceptibility of fine-grained soils." *J. Geot. Geoenv. Eng.*, 132(9), 1165-1177.

Jana, A., and Stuedlein, A.W. (2021). "Monotonic, Cyclic and Post-Cyclic Response of an Alluvial Plastic Silt Deposit." *J. of Geotech. Geoenv. Eng.* 147(3): 04020174.

Mayne, P. W., Coop, M., Springman, S., Huang, A.-B., and Zornberg, J. (2009). "SOA-1: Geomaterial behavior and testing." *Proc, Proceedings of the 17th International Conference on Soil Mechanics and Geotechnical Engineering*: October 2009, Alexandria, Egypt, Millpress, Rotterdam, the Netherlands, 2777-2872.

Mayne, P., and Peuchen, J. (2018). "Evaluation of CPTU N_{kt} cone factor for undrained strength of clays." *Cone Penetration Testing 2018*, CRC Press. 423-429.

Rix, G.J., Wainaina, N., Ebrahimi, A., Bachus, R.C., Limas, M., Sancio, R., Fait, B., and Mayne, P.W. (2019). Manual on subsurface investigations. *Report No. NCHRP 21-10. 2019*, Transportation Research Board, Washington, D.C.